Robust personalisation of 3D electromechanical cardiac models. Application to heterogeneous and longitudinal clinical databases

Roch Molléro

UNIVERSITÉ CÔTE D'AZUR

informatics mathematics

DOCTORAL SCHOOL STIC

SCIENCES ET TECHNOLOGIES DE L'INFORMATION ET DE LA COMMUNICATION

P H D T H E S I S

to obtain the title of

PhD of Science

of the Université Côte d'Azur

Specialty : Automation, Signal and Image Processing

By

Roch MOLLÉRO

Robust Personalisation of 3D Electromechanical Cardiac Models. Application to Heterogeneous and Longitudinal Clinical Databases.

Thesis Advisors:

Nicholas Ayache, Xavier Pennec, Maxime Sermesant

prepared at INRIA Sophia Antipolis, Asclepios Team

Defended: *19 December 2017*

Jury :

Reviewers:	Martyn Nash	-	University of Auckland
	Irene Vignon-Clémentel	-	Inria (Reo Team)
Examiners:	Bart Bijnens	-	Universitat Pompeu Fabra (Physense)
	Tommaso Mansi	-	Siemens Healthineers
	Philippe Moireau	-	Inria (Medisim Team)
	Hervé Delingette	-	Inria (Asclepios Team)
Supervisors:	Nicholas Ayache	-	Inria (Asclepios Team)
	Xavier Pennec	-	Inria (Asclepios Team)
	Maxime Sermesant	-	Inria (Asclepios Team)

UNIVERSITÉ CÔTE D'AZUR

informatiques mathématiques Inria

ECOLE DOCTORALE STIC
SCIENCES ET TECHNOLOGIES DE L'INFORMATION
ET DE LA COMMUNICATION

THÈSE DOCTORALE

pour obtenir le titre de

Docteur en Sciences

de l'Université Côte d'Azur

Discipline : AUTOMATIQUE, TRAITEMENT DU SIGNAL ET DES IMAGES

Par

Roch MOLLÉRO

Personnalisation robuste de modèles 3D électromécaniques du cœur. Application à des bases de données cliniques hétérogènes et longitudinales.

Dirigée par:
Nicholas AYACHE, Xavier PENNEC, Maxime SERMESANT

préparée à l'INRIA Sophia Antipolis, Équipe ASCLEPIOS

Soutenue: *19 Décembre 2017*

Jury :

Rapporteurs :	Martyn NASH	-	Université d'Auckland
	Irene VIGNON-CLÉMENTEL	-	Inria (Équipe Reo)
Examinateurs :	Bart BIJNENS	-	Universitat Pompeu Fabra (Physense)
	Hervé DELINGETTE	-	Inria (Équipe Asclepios)
	Tommaso MANSI	-	Siemens Healthineers
	Philippe MOIREAU	-	Inria (Équipe Medisim)
Superviseurs :	Nicholas AYACHE	-	Inria (Équipe Asclepios)
	Xavier PENNEC	-	Inria (Équipe Asclepios)
	Maxime SERMESANT	-	Inria (Équipe Asclepios)

Acknowledgments

First, I want to thank Maxime, Nicholas, Xavier and also Hervé for the great scientific supervision during my Ph.D. Thanks Maxime for your dedication and the countless office, lunch or even "before a plane ride" brainstorming discussions which helped shape this Ph.D. Thanks Xavier for all the scientific discussions, mathematical expertise and also the help formalizing papers (and the dreaded "réponses aux reviewers"). Thanks Nicholas for accepting me in the Asclepios lab, creating this amazing work environment and providing a good vision of the field. Thanks finally Hervé for being at every "point these" to ask challenging questions, and being always available to talk about the model. I learnt here that it is never so easy than to know if a specific work or idea is a good direction to explore, but it was really great to be able to rely on the judgement of all of you during the last 3 years. Thanks also for all the good memories we've had outside of work like playing music and snowboarding in Auron, travelling together for meetings and conferences, it was a real pleasure to work with you.

A real thank you to my reviewers Martyn Nash and Irene Vignon Clémentel to carefully read and review my Ph. D. manuscript. Thanks also to Bart Bijnens and Philippe Moireau for being part of the jury, watching my presentation and asking tricky questions to challenge my work. The combined contribution of all of you were perfectly in time for the success of this pre-Christmas defense.

A special thanks to Tommaso, also for being part of the jury but most importantly for recruiting me into the amazing Siemens internship which started my Cardiac Modelling Journey! Thanks also to Alan for the decisive help with OpenCOR and of course the almighty Isabelle for the relentless help through various administrative processes.

A big thank you to everybody that I've met in Asclepios who helped make the lab a great place to work, and with whom I have travelled for both work and leisure, done a lot of skiing, cycling, running, ping-pong and the famous "lifting", played music, and drank a few (international) beers. Thank you to Ján, Bisheh, Kristin, Florian, Chloé, Hakim, Loic C, Mehdi, Nicolas, Hervé L, Vikash, Stephanie, Loic L, Mathieu and Marco. A special thanks to Rocio for the awesome (and quite adventurous) NYE wedding in Mexico! Thanks you to all who were still around until the end of the PhD (and some of you at my defense): Marc-Michel, Thomas D, Sophie, Nina, Raphael, Julian, Shuman, Pawel, Qiao, Clément, Wen, Luigi, Jaume, Tania and Nicolas C!

Finally, a special thanks to my parents and family for supporting me since the beginning, and especially the last 9 years of studies, and to all the cool people I've met in the Cote d'azur area who helped make my time in the area more enjoyable!

Roch

Contents

Chapter 1

Introduction

Contents

1.1 Context

The heart is a very complex and robust organ in the human body, whose function is to create the necessary blood flow through the cardiovascular system. Its malfunction (or *cardiac failure*) is often fatal and is the leading cause of death in the world (more than 32% of all deaths according to the Global Burden of Disease [Feigin 2016]).

To better investigate and help treat cardiac diseases, personalised cardiac models have been developed and investigated for the past 30 years, with the goal of combining anatomical knowledge with multi-modal clinical data to build the most comprehensive virtual model of a patient's heart. Possible applications of these models in patient care are the prediction of changes and outcomes under therapy, better characterization of pathologies, for example by comparing with other patients in a database of personalised models.

These models are made of various components such as a *patient-specific mesh geometry* for the 3D models, an *electromechanical model* which computes the electrical activity and biomechanical forces in the myocardium, and possibly some initial and *boundary conditions*. The interactions between these components lead to the simulation of the cardiac motion, and possibly other aspects of cardiac dynamics such as ventricular pressure and volumes and valve dynamics. Each of these components have many parameters, which all have an impact on the simulation.

To build a good personalised model of a patient's heart, relevant values of these parameters must then be estimated so that the personalised simulation is the most realistic possible. However, the consistent estimation and analysis of these parameters is still a scientific challenge, both due to the complexity of the models and the nature of clinical data:

- Clinical data can be sparse (a few, global measurements) or noisy (due to

imaging resolution) which makes it impossible to estimate exactly all the model parameters.

- In large databases of patients data across different hospitals, the data is usually heterogeneous (the same measurements or images are not available for every case), which makes it hard to compare personalised parameters.

- 3D cardiac model simulations can be quite computationally expensive, so it limits the possibility to use numerically intensive methods in practical applications.

1.2 Objectives

This thesis focuses on the consistent and practical estimation of electromechanical parameters in personalised 3D models and its application for clinical data analysis. The main questions we investigate are:

1. How to quantify uncertainty in personalised simulations due to uncertainty in biomechanical parameters ?

2. Can we jointly use models at multiple scales to speed up some applications, in particular the computationally expensive process of 3D electromechanical model personalisation ?

3. How can we use personalised parameters for the analysis of short term and long-term longitudinal evolution of the cardiac function ?

4. How to perform consistent parameter estimations despite the sparse and heterogeneous nature of clinical data ?

1.3 Main Contributions and Organization of the Manuscript

The main contributions of this work are the following:

- An innovative 0D/3D multiscale approach to 3D cardiac model personalisation, made of a *multifidelity coupling* to approximate outputs of the 3D model from a reduced "0D" model, and a fast and computationally efficient *multifidelity personalisation* algorithm called **Multifidelity-CMA** derived from this coupling.

- The creation of more than **140 personalised 3D simulations** in the context of two longitudinal studies where personalised parameters are used first to model short-term transient effects in digestion, then to analyze long-term evolution of the cardiac function in cardiomyopathies.

- A method called **Iteratively Updated Priors** to automatically select observable directions in the parameter space from a set of measurements, and simultaneously compute *population-based prior probabilities* in these directions to constrain parameter estimation in cases where measurements are missing.

After an introductory chapter (**Chapter 3**), the manuscript is organized along the published and submitted papers during this PhD:

Chapter 3 presents the scientific context of this PhD: we present the structure and dynamics of the heart, and we review the state-of the heart in cardiac modeling and personalisation. We then present the MD-Paedigree project in the context of which this Ph.D. was performed, and the dataset on which the work is based.

Based on [Molléro 2015], **Chapter 4** introduces 3D cardiac electromechanical model personalisation and the impact of *uncertainty in biomechanical parameters* on personalised simulations. First, the uncertainty in the fibre architecture is estimated by sampling *7 representative fibre sets* along the 3 principal directions of fibre variations in an *atlas* of 10 hearts whose fibres were acquired from DTI. These fibre sets are mapped onto new cases and used to compute the resulting uncertainty in personalised simulations through a generic personalisation process. We show *differences in depolarization times* across the myocardium between personalised simulations with the different fibre sets (up to 10ms), and *variability of the personalised parameters* (up to 50% for the *aortic peripheral resistance*). This study shows that given *personalised simulations* which fit the same measurements, both the *personalised parameter values* and other outputs of the simulations can be very different depending on the values of other parameters. This first means that personalised parameter values cannot be interpreted without taking into considerations the values of other parameters and their uncertainty. In addition, we found that the personalisation algorithm used in this study (the Unscented Transform) required a careful manual initialisation, possibly different for each case and set of parameters. Overall, this study outlines the need for a more consistent approach and more efficient tools to parameter estimation in a possibly large database of cases.

Motivated by the need for an efficient personalisation algorithm for 3D simulations, we present in **Chapter 5** a 0D / 3D multifidelity approach, published in [Molléro 2017b], which tackles the burden associated with the computational complexity 3D simulations. We introduce an original *multifidelity coupling* between a 3D cardiac model and a simplified "0D" version of this model, which enables to get reliable (and extremely fast) approximations of the global behavior of the 3D model using 0D simulations. Then we use this multifidelity approximation to speed-up an efficient optimisation algorithm called CMA-ES, leading to a fast and computationally efficient *multifidelity personalisation method* for the 3D model called **Multifidelity-CMA**. We compare our method to classic optimisation methods in terms of gains in CPU time and Optimization Time, and show that the method is particularly fast and computationally efficient. We finally use this method to build 121 3D personalised simulations in less than 2.5 days, witout manual supervision, fine-tuning of the algorithm or precomputation.

In **Chapter 6 and 7** we build and use more than 140 personalised 3D simulations in two studies on the longtitudinal analysis and modeling of the cardiac function:

- In **Chapter 6** (published in [Molléro 2017c]), we build a data-driven model of cardiovascular parameter evolution during digestion, from a clinical study involving more than 80 patients. We present a method for longitudinal parameter estimation in 3D cardiac models, which we apply to 21 patient-specific heart geometries at two instants of the study, for 6 parameters (two fixed and four time-varying parameters). From these personalised hearts, we then extract and validate a law which links changes of cardiac output and heart rate under constant arterial pressure to the evolution of these parameters, enabling fast simulation of hearts during digestion for future patients.

- In **Chapter 7** (published in [Molléro 2017a]) we tackle for the first time in this thesis the problem of non-uniqueness in parameter estimation when some parameter directions cannot be estimated (they are not *observable*), which is an obstacle to get relevant personalised parameters for clinical applications. We introduce the estimation of electromechanical parameters as a *Maximum A Posteriori* (MAP) estimation with prior probabilities on the estimated values, which we apply to 84 different cases. We show that the use of priors reduces considerably the variance of the estimated parameters, in particular because it promotes specific values during estimation when parameter values are not unique. This enables a better conditioning of the parameters for statistical analysis of the cardiac function, which we illustrate on the longitudinal analysis of paediatric cardiomyopathies, where the personalised parameters suggest an improvement of the cardiac function under therapy.

Finally, **Chapter 8** addresses the question of *which parameters can be estimated* given a set of measures (the problem of parameter *observability*). We present an algorithm called **Iteratively Updated Priors**, which performs successive personalisations of the database, in which the prior probability of a personalisation is set from the distribution of personalised parameters in the previous iteration. We show that the algorithm performs the optimisation of a cost function over the whole database with a *sparse regulariser* on the *number of dimensions of the personalised parameter set*. At convergence, estimated parameters of the population lie on a linear subspace of reduced and possibly *sufficient* dimension, in the sense that for each case of the database there is a *unique* parameter value for which the simulation fits the measurements. Since the resulting *population-based priors* represent the population statistics in this subspace, they can also be used to perform consistent parameter estimation for cases where measurements are possibly different or missing, which we illustrate with the 0D model on a database of 811 cases. Finally we argue that through the selection of subspaces of reduced and possibly sufficient dimensions, the algorithm can help find a space of *maximal dimension in which*

parameters are completely observable from a dataset, possibly providing a complete framework to tackle the problem of observability in personalisation.

Chapter 9 summarizes the main contributions of the thesis and presents the perspectives of this work.

Chapter 2

Introduction (French)

Contents

2.1 Contexte

Le cœur est un organe complexe et robuste du corps humain, dont la fonction est de créer et maintenir le flux sanguin à travers le système cardiovasculaire. Son dysfonctionnement (ou *insuffisance cardiaque*) est souvent mortel, et constitue la première cause de mortalité dans le monde (plus de 32% de tous les décès selon le *Global Burden of Disease* [Feigin 2016]).

Pour mieux comprendre et traiter les maladies cardiaques, des *modèles cardiaques personnalisés* ont été développés depuis 30 ans. L'objectif est de combiner les connaissances anatomiques avec des données cliniques multimodales, pour construire le modèle virtuel le plus complet du cœur d'un patient. Les applications cliniques possibles de ces modèles sont la prédiction des changements sous l'effet du traitement, et une meilleure caractérisation des pathologies en comparant à d'autres patients dans une base de données de modèles personnalisés.

Ces modèles sont constitués de différents composants tels qu'un *maillage personalisé* de la géométrie du coeur du patient pour les modèles 3D, un *modèle électromécanique* qui calcule l'activité électrique et les forces biomécaniques dans le myocarde, et éventuellement certaines *conditions aux limites*. Les interactions entre ces composants conduisent à la simulation du mouvement cardiaque, et éventuellement Ã d'autres aspects de la dynamique cardiaque tels que la pression ventriculaire et la dynamique des valves. Chacun de ces composants a de nombreux paramètres qui ont tous un impact sur la simulation.

Pour construire un bon modèle personnalisé du cœur d'un patient, des valeurs pertinentes de ces paramètres doivent être estimées, afin que la simulation personnalisée soit la plus réaliste possible. Cependant, l'estimation et l'analyse cohérentes de ces paramètres reste à ce jour un défi scientifique, à la fois en raison de la complexité des modèles et de la nature des données cliniques:

- Les données cliniques peuvent être assez limitées (quelques mesures globales de volumes ou de pression) ou comporter du bruit (dans le cas de l'imagerie), ce qui rend impossible l'estimation exacte de tous les paramètres du modèle.
- Dans les grandes bases de données de patients, les données sont généralement hétérogènes (les mêmes mesures ou images ne sont pas disponibles pour chaque cas), ce qui rend difficile la comparaison entre patients des paramètres personnalisés.
- Les simulations de modèles cardiaques 3D peuvent être relativement coûteuses en temps de calcul, ce qui limite la possibilité d'utiliser certaines méthodes numériques complexes pour des applications pratiques.

2.2 Objectifs

Cette thèse se concentre sur l'estimation pratique et cohérente des paramètres électromécaniques dans les modèles 3D personnalisés, et les applications à l'analyse de données cliniques. Les principales questions que nous étudions sont:

1. Comment quantifier l'incertitude dans les simulations personnalisées due à l'incertitude des paramètres biomécaniques ?
2. Est-il possible d'utiliser conjointement des modèles à plusieurs échelles pour accélérer certaines applications, en particulier l'estimation de paramètres pour la personnalisation des modèles 3D ?
3. Comment utiliser des paramètres personnalisés pour l'analyse de la fonction cardiaque et son évolution longitudinale à court et à long terme ?
4. Comment effectuer des estimations de paramètres cohérentes malgré des données cliniques hétérogènes ou limitées ?

2.3 Principales contributions et organisation de la thèse

Les principales contributions de ce travail sont les suivantes:

- Une approche multi-échelle 0D / 3D innovante pour la personnalisation du modèle cardiaque 3D, faite d'un *couplage multi-échelle* pour approcher les sorties du modèle 3D à partir d'un modèle réduit "0D", et d'un algorithme de *personnalisation multi-échelle* rapide, flexible et efficace en temps de calcul appelé **Multifidelity-CMA**.
- La création de plus de **140 simulations 3D personnalisées** dans le cadre de deux études longitudinales où les paramètres personnalisés servent à modéliser les effets transitoires à court terme de la digestion, puis à analyser l'évolution à long terme de la fonction cardiaque dans des cardiomyopathies.

- Une méthode appelée **Iteratively Updated Priors** pour sélectionner automatiquement des directions observables dans l'espace des paramètres à partir d'un ensemble de mesures, et calculer des probabilités *a priori* empiriques (*population-based priors*) dans ces directions, pour contraindre l'estimation des paramètres dans les cas où des paramètres du modèles ne sont pas observables.

Après un chapitre introductif (**Chapitre 3**), le manuscrit est organisé autour des articles publiés et soumis au cours de ce doctorat:

Le **Chapitre 3** présente le contexte scientifique du doctorat: nous présentons la structure et la dynamique du coeur, et passons en revue l'état de l'art de la modélisation cardiaque et de la personnalisation. Nous présentons ensuite le projet MD-Paedigree dans le contexte duquel ce doctorat a été effectuée, ainsi que les données considérées au cours de ce travail.

Basé sur [Molléro 2015], le **Chapitre 4** introduit la personnalisation 3D du modèle électromécanique cardiaque et l'impact de l'*incertitude dans les paramètres biomécaniques* sur des simulations personnalisées. L'incertitude dans l'architecture des fibres est d'abord estimée en échantillonnant *7 ensembles représentatifs de fibres* le long des 3 directions principales des variations de fibres, dans un *atlas* de 10 coeurs dont les fibres ont été acquises par DTI. Ces ensembles de fibres sont transférées sur de nouveaux cas et utilisés pour calculer l'incertitude qui en résulte dans les simulations personnalisées, via un processus de personnalisation simple. Nous montrons les différences dans les *temps de dépolarisation* à travers le myocarde entre les simulations personnalisées avec les différents ensembles de fibres (jusqu'à 10ms), et la *variabilité des paramètres personnalisés* (jusqu'à 50% de sa valeur pour la *résistance aortique périphérique*). Cette étude montre qu'étant donné des *simulations personnalisées* qui reproduisent les mêmes mesures, à la fois les *valeurs des paramètres personnalisés* et d'autres aspects de ces simulations peuvent être très différents en fonction des valeurs des autres paramètres (non personnalisés). Cela signifie en particulier que les valeurs des paramètres personnalisés ne peuvent être interprétées sans tenir compte des valeurs des autres paramètres et de leur incertitude. De plus, nous avons pu constater dans cette étude que l'algorithme de personnalisation utilisé dans cette étude (*Unscented Transform*) nécessite une initialisation manuelle spécifique, possiblement différente pour chaque cas et ensemble de paramètres. Dans l'ensemble, cette étude souligne la nécessité d'une approche plus robuste et d'outils plus efficaces pour l'estimation des paramètres dans une base de données potentiellement plus large.

Motivé par la nécessité d'un algorithme de personnalisation efficace pour le modèle 3D, nous présentons dans le **Chapitre 5** une approche multi-échelle 0D / 3D, publiée dans [Molléro 2017b], qui aborde le probleme de la complexité en temps de calcul des simulations 3D. Nous introduisons un *couplage multi-échelle* original entre un modèle cardiaque 3D et une version simplifiée "0D" de ce modèle, ce qui permet d'obtenir des approximations fiables (et extrêmement rapides) du comportement global du modèle 3D en utilisant des simulations 0D. Nous utilisons ensuite cette approximation multi-échelle pour accélérer un algorithme d'optimisation efficace ap-

pelé CMA-ES, conduisant à une méthode de *personnalisation multi-échelle* rapide et efficace pour le modèle 3D appelé **Multifidelity-CMA**. Nous comparons notre méthode aux méthodes classiques d'optimisation en termes de gains en temps de CPU et en temps d'optimisation, et montrons que la méthode est particulièrement rapide et efficace. Nous utilisons enfin cette méthode pour construire 121 simulations personnalisées en 3D en moins de 2,5 jours, sans supervision ni initialisation manuelle de l'algorithme.

Dans les **Chapitres 6 et 7**, nous construisons et analysons plus de 140 simulations 3D personnalisées dans le cadre de deux études sur l'analyse longitudinale et la modélisation de la fonction cardiaque:

- Dans le **Chapitre 6** (publié dans [Molléro 2017c]), nous construisons un modèle de l'évolution des paramètres cardiovasculaires pendant la digestion, basé sur une étude clinique impliquant plus de 80 patients. Nous présentons une méthode pour l'estimation longitudinale des paramètres du modèle cardiaque 3D, que nous appliquons à 21 patients à deux instants de l'étude, pour 6 paramètres (deux paramètres fixes et quatre paramètres variables dans le temps). A partir de ces cœurs personnalisés, nous extrayons et validons une loi qui relie les changements de débit et de fréquence cardiaque sous pression artérielle constante à l'évolution de ces paramètres, permettant une simulation rapide de la digestion pour de futurs patients.

- Dans le **Chapitre 7** (publié dans [Molléro 2017a]) nous abordons pour la première fois le problème de la non-unicité dans l'estimation de paramètres lorsque certaines directions de paramètres ne peuvent être estimées (ells ne sont pas *observable*), qui est un obstacle à l'estimation de paramètres personnalisés consistants pour des applications cliniques. Nous estimation les paramètres électromécaniques via un *Maximum A Posteriori* (MAP), que nous appliquons à 84 cas. Nous montrons que l'utilisation de probabilités a priori réduit considérablement la variance des paramètres estimés, notamment parce qu'elle favorise des valeurs spécifiques lorsque les valeurs des paramètres ne sont pas uniques. Ceci permet un meilleur conditionnement des paramètres pour l'analyse statistique de la fonction cardiaque, que nous illustrons sur l'analyse longitudinale de cardiomyopathies pédiatriques, où les paramètres personnalisés suggèrent une amélioration de la fonction cardiaque avec le traitement.

Enfin, le **Chapitre 8** aborde la question de *quels paramètres peuvent être estimés* étant donné un ensemble de mesures (le problème de *l'observabilité des paramètres*). Nous présentons un algorithme appelé **Iteratively Updated Priors**, qui effectue des personnalisations successives de la base de donnée, dans laquelle la probabilité a priori d'une personnalisation est établie à partir de la distribution de paramètres personnalisés dans l'itération précédente. Nous montrons que l'algorithme effectue l'optimisation d'une fonction de coût sur toute la base de données avec un terme de *régularisation parcimonieuse* sur le *nombre de dimensions du jeu de paramètres personnalisés*. À convergence, les paramètres estimés de la population se trouvent

sur un sous-espace linéaire de dimension réduite et éventuellement *suffisante*, au sens que pour chaque cas de la base de données il existe un vecteur *unique* de paramètres pour laquelle la simulation reproduit les mesures. Puisque les *probabilités à priori empiriques* qui en résultent représentent les statistiques de population dans ce sous-espace, ils peuvent également être utilisés pour effectuer une estimation cohérente des paramètres dans le cas où les mesures sont différentes ou manquantes pour certains cas, ce que nous démontrons sur une base de données de 811 cas. Enfin, nous soutenons que grâce à la sélection d'un sous-espace de dimension réduite et suffisante, l'algorithme conduit à trouver un espace de dimension maximale dans laquelle les paramètres sont complètement observables (étant donné un ensemble de données). Cela fournit donc potentiellement un cadre complet pour gérer le problème de l'observabilité dans la personnalisation.

Le **Chapitre 9** résume les principales contributions de la thèse et présente les perspectives de ce travail.

Chapter 3

Scientific Context: Structure and Function of the Heart, State of the Art in Computational Modeling and the MD-Paedigree Project

Contents

3.1 Structure and Dynamics of the Heart

The heart is a biological pump within the human body which creates the necessary blood flow to ensure the oxygen supply to the different organs. It consists of two parts (See Figure 3.1), the *right heart* and the *left heart* which contain two chambers each: an *atrium* and a *ventricle*. After going through the *systemic circulation* where it provided oxygen to the various organs, the blood reaches the right atrium and is pushed into the right ventricle, then it is ejected into the *pulmonary circulation* toward the lungs during contraction. Going through the pulmonary circulation, the blood lowers its concentrations in carbon dioxide ($C0_2$) and increases its concentration in oxygen (O_2) through gas exchanges in the lungs. Then the blood arrives into the left atrium, is pushed into the left ventricle, then ejected again into the *systemic*

circulation. The main difference between systemic and pulmonary circulations is the blood pressure, lower in the pulmonary circulation to enable gas exchanges between the blood and the air through the lungs, and higher in the systemic circulation to enable the propagation of the blood into a long circulatory system.

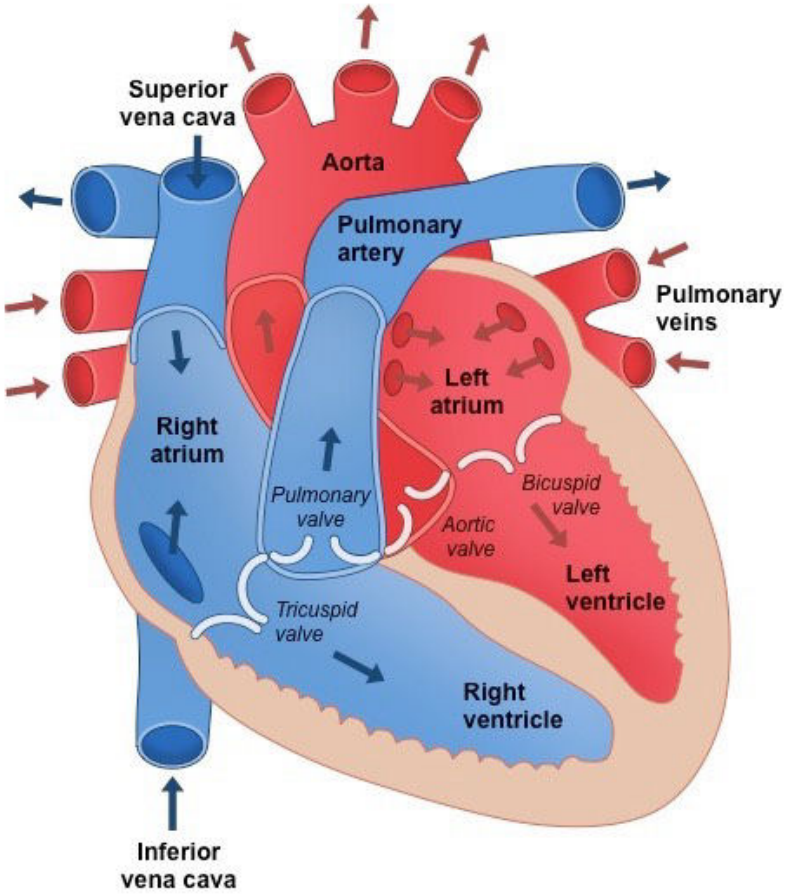

Figure 3.1: Heart anatomy showing in particular the two parts of the heart synchronously pumping blood into the two different parts of the circulatory system: in **blue** is the blood with a low concentration of oxygen going from the organs to the lungs, in *red* is the blood full in oxygen which goes from the lungs to the organs. *(image from ib.bioninja.com.au)*

The constant blood flow is ensured by the periodic contraction of the myocardium, which is the muscular tissue of the heart. This muscle contraction is caused by a series of intertwined physical phenomenons leading to the build-up of the contractile force within the myocardium. First, an electrical wave propagates from the *sino-atrial (SA) node* in the atrium, provoking the *atrial systole*. Then the wave propagates into the whole myocardium approximately 120ms later (a duration called the *Atrio-ventricular delay*) through the *Atrio-Ventricular (AV) node* the

Bundle of His and the system of *Purkinje Fibres* in the ventricles (See Figure 3.2), provoking the *systole*.

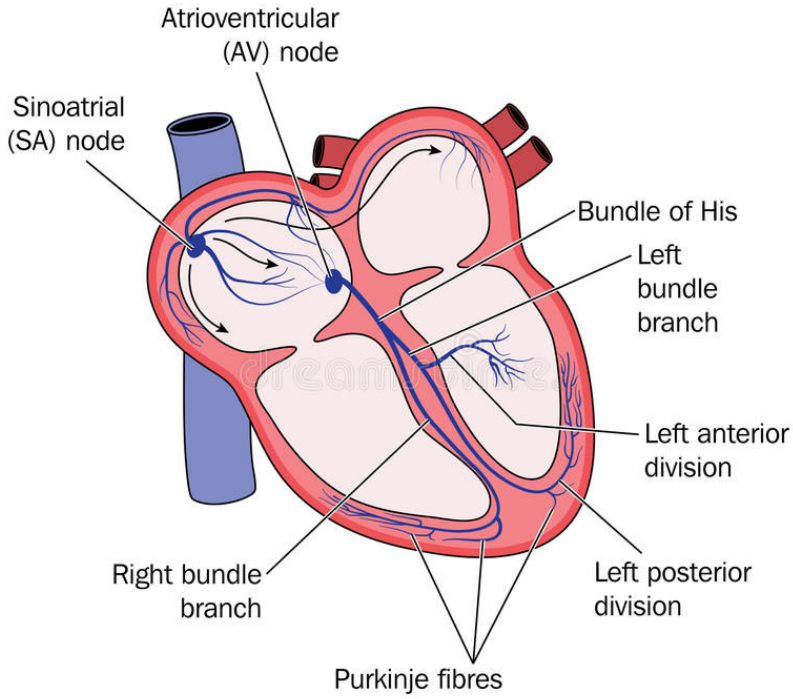

Figure 3.2: Components of the cardiac electrical system which leads to the propagation of the *depolarization wave* across the whole myocardium. *(Image from http://www.dreamstime.com/)*

During the systole, the electrical wave leads to a *depolarization* of the myocardial cells which creates, through complex ion exchanges within the sarcomeres and the binding of the *actin* and *myosin* protein filaments, the buildup of contractile forces within the individual myocytes. This depolarization lasts around 200 to 400 ms, after which a *repolarization wave* leads to the unbinding of the filaments and the *relaxation* of the contractile forces, a phase called the diastole.

At the organ level, the myocardial tissue is organized along fibres whose direction vary from the inner part (the endocardium) to the outer part (the epicardium) of each ventricle. The local contraction of the myocardial tissue leads to the contraction of both atrium, then both ventricles, and the ejection of the blood into the arteries. The resulting *cardiac cycle* is usually described with 4 *cardiac phases*, illustrated in Figure 3.3:

- *Filling*, when the ventricle fills in with blood coming from the atrium. First it fills passively, then the atrium actively fills the ventricle with blood during *atrial systole*.

- *Isovolumetric contraction*, which occurs when the ventricle starts contracting. The atrioventricular valve closes and the ventricular blood pressure rises quickly.

- *Ejection*, when the blood pressure becomes higher than the arterial pressure, leading to the opening of the arterial valve and the ejection of blood in the arteries.

- *Isovolumetric relaxation*, when the myocardial forces drop and the ventricular pressure becomes lower than the arterial pressure. The arterial valve close and the ventricular blood pressure lowers quickly.

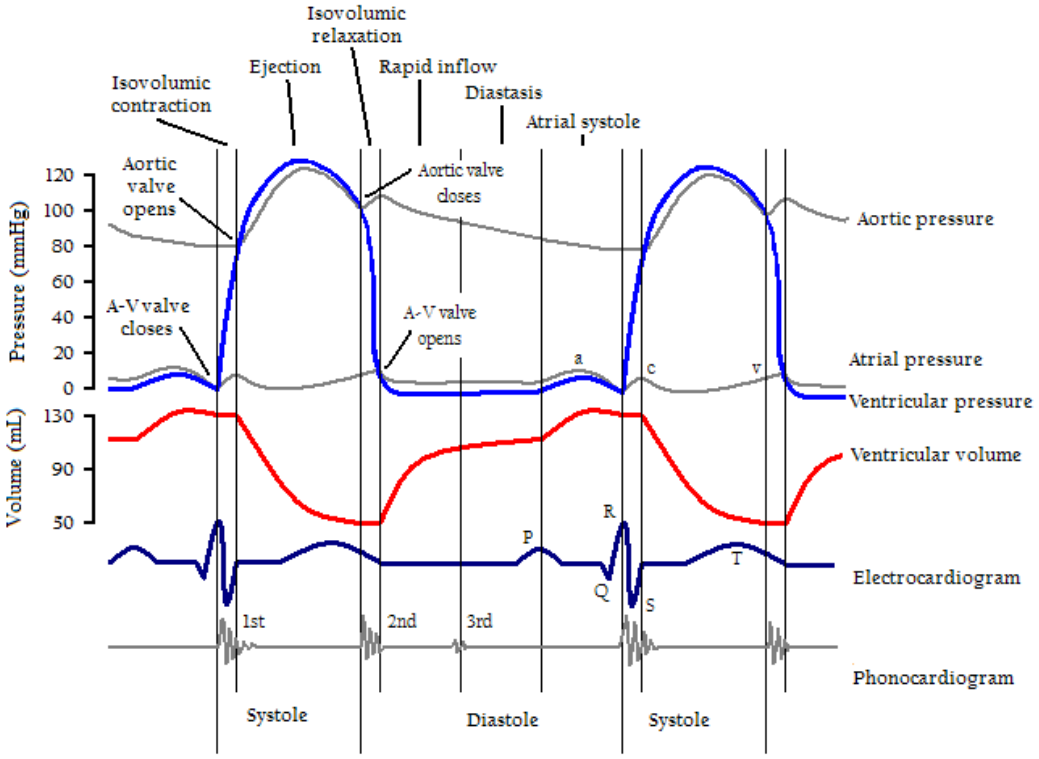

Figure 3.3: Cardiac cycle. *Image from Wikipedia.*

3.2 Computational Cardiac Modeling

Computational modeling of cardiac physics has been an active area of research for the past 30 years. It has led to an extremely wide variety of *multiphysics* and *multiscale* models describing multiple aspects of cardiac dynamics at multiple scales, and methods to apply these models to the analysis of real clinical

data. Here we provide an non-exhaustive overview of different approaches in modeling and parameter estimation. More references can be found in the reviews of [Chabiniok 2016, Clayton 2011, Lopez-Perez 2015, Trayanova 2011].

3.2.1 Multiphysics and Multiscale Modeling

Models can be roughly classified around *which aspects of cardiac physiology* they model, and *at which scale*.

- **Models of cardiac cell** describe the transmembrane currents and *action potential* during the depolarisation of a single cell, either through the modeling of possibly many cellular ionic processes involved [Hodgkin 1952, Ten Tusscher 2004] or with a more phenomenological approach [FitzHugh 1961, Mitchell 2003, Aliev 1996].

- **Models of electrical propagation** study the propagation of the electrical wave within the myocardium in 2D or 3D cardiac tissue [Clayton 2008]. Reaction-diffusion equations coupled with cardiac cells models [Relan 2010] are the most common approach, in particular to study mechanisms of fibrillation [Gray 1998, Panfilov 1998] and tachycardia [Gray 1995]. There are also more phenomenological approaches such as the Eikonal model [Sermesant 2007].

- **Mechanical and Electromechanical models** describe the active contractile forces (activated by the depolarisation) and the passive elastic properties of the myocardium, leading to the contraction and deformation of the myocardium. As classified in [Chabiniok 2016] very large variety of model of forces exists with different properties: hyperelastic [Humphrey 1990] or viscoelastic [Holzapfel 2001], orthotropic [Costa 2001, Nash 2000], isotropic [Yang 1991] or transversly-isotropic [Huyghe 1991, Guccione 1991] depending on the modeling of myocardial fibers and laminar sheets. Many models compute separately the electrophysiology and the mechanical forces [Kerckhoffs 2003, Sermesant 2006], but the most complete approaches model the coupled interaction of electrical activity and mechanical deformation [Nash 2004, Nickerson 2005].

- **Models of fluid dynamics** describe the dynamics of blood flow in the ventricle or the arteries, from zero-dimensional approaches [Thomas 1992] to computational fluid dynamics (CFD) and the computation of the Navier-Stokes equations [Nordsletten 2011, Oertel 2011]. Such models can be coupled to lumped parameter models of the heart and the circulatory system as boundary conditions [Vignon-Clementel 2006, Esmaily Moghadam 2013].

- **Models of cardiovascular circulation** describe the blood circulation in various part of the cardiovascular system [Westerhof 1969]. It can involve a complete closed-loop lumped parameter network (LPN) [Arts 2005, Mihalef 2017, Pant 2016] of the circulatory system. Such models can also be coupled with 3D models for some parts of the system such as the ventricle [Kerckhoffs 2007] or the arteries.

- Finally, the representation of myocardial and arterial geometries can be based on various types of **discretisation**: surface meshes [McLeod 2013, Frangi 2002], volumetric tetrahedral meshes [Bestel 2001, Marchesseau 2010] or meshless approaches such as the Smoothed Particle Hydrodynamics (SPH) [Lluch 2017].

3.2.2 Personalisation and Parameter Estimation

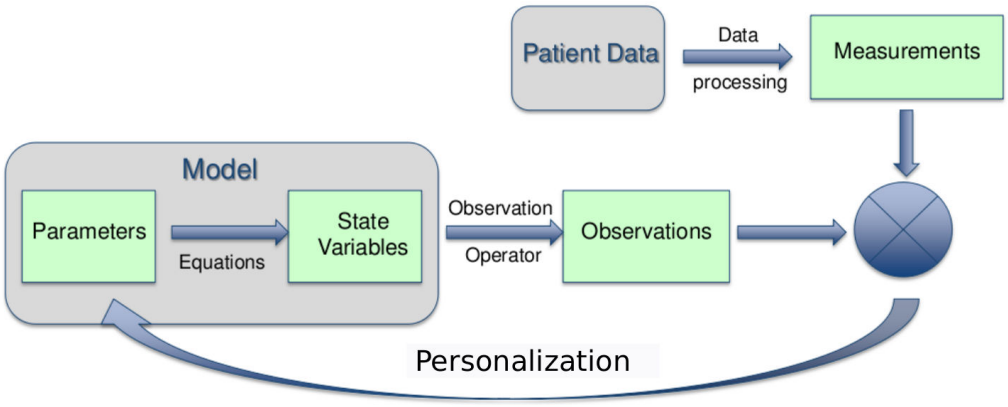

Figure 3.4: Personalisation of a cardiac model. *Image from [Marchesseau 2013b].*

Personalisation is the process of building a simulation which is as similar as possible to the patient's heart (See Figure 3.4). In the case of a 3D model it often includes the *extraction of a patient-specific geometry* from the imaging data through *segmentation*, which includes various types of approaches and techniques for which large reviews can be found in [Peng 2016, Petitjean 2011, Suinesiaputra 2014]. Then, relevant parameters values of the cardiac model have to be estimated so that some of its outputs in the simulation correspond to some measurements. Methods to estimate relevant model parameters can be classified into the following (non mutually exclusive) classes:

- *Sequential methods* update the parameters during the simulation. The key idea is to define a set of *observations* extracted by from the simulation, and repeatedly compare the trajectory of these observations to the data in order to retrieve the unknown parameters. Filtering methods and their *reduced-order* versions are common sequential methods used in the cardiac community, such as the Kalman Filter [Marchesseau 2013c, Moireau 2008], the Unscented Kalman Filter [Pant 2017, Xi 2011, Moireau 2011] or the Extended Kalman filter [Liu 2009].

- *Variational methods* consist in computing and optimising an error criterion over the whole simulation, by alternating successive phases of simulations and updates of the parameters. To that end, *adjoint methods* [Delingette 2012, Sundar 2009] performs a gradient descent through the computation of an adjoint model. This can lead to a fast optimisation because the adjoint model incorporates knowledge of the internal dynamics of the model. On the other hand such methods require to recompute the derivatives of a

possibly complex system of equations if the governing equations of the model are changed.

- *Gradient-free methods* can be seen as a sub-class of *variational methods*, where the criterion is optimised without knowledge on the internal dynamics of the model. This includes algorithms based on local quadratic approximations such such as BOBYQA [Seegerer 2015] and sequential quadratic programming (SQP) [Wang 2009, Schmid 2008], or also genetic algorithms [Khalil 2006]. In general, these methods have the advantage to be parallelisable but they can be sensitive to the initialisation.

- *Data-driven methods* consists in learning a statistical model of the relationship between the parameters and the outputs through the precomputation of many simulations within the parameter space. Such methods include Principal Orthogonal Decomposition (POD) [Boulakia 2011, Yang 2017], polynomial regression [Zettinig 2014] and polynomial chaos expansion (PCE) [Neumann 2014a, Konukoglu 2011], or more recently reinforcement learning [Neumann 2016]. Such methods are usually faster than sequential methods, but may require a careful selection of the parameter space and a possibly high number of precomputed simulations to best approximate the non-linearities of the model.

3.3 Collaborative Context: The MD-Paedigree Project

3.3.1 Presentation of the Project

This Ph.D. was funded and performed in the context of the European project **MD-Paedigree** of the *FP7-ICT programme*, which is self-described as *a clinically-driven and strongly VPH-rooted* (for Virtual Physiological Human) *project which pursue improved interoperability of paediatric biomedical information, data and knowledge by developing reusable and adaptable multi-scale models for more predictive, individualised, effective and safer paediatric healthcare.*

Through this Ph.D., Inria Sophia-Antipolis was mainly involved in two workpackages of this project: *paediatric cardiomyopathies* (CMP) and *cardiovascular disease risk in obese children* (CVD). The long-term vision of all VPH projects is to promote the use of models in clinical practice and for a better understanding of cardiac diseases. On the short term it is also designed to enable the cooperation between clinicians from various centers on current areas of clinical research. In particular the goal of the *paediatric cardiomyopathies* workpackage was to study and characterize various types of rare or *idiopathic* (for which the the cause is unknown) cardiomyopathies, affecting (possibly very young) children. In the *cardiovascular disease risk in obese children* workpackage, the goal was to study the mechanisms of cardiovascular diseases development in relation to obesity in children and adolescents.

The main clinical and technical partners in these workpackages in addition to **Inria Sophia Antipolis** were, first on the technical and modeling side:

- **Siemens Healthineers**, formerly **Siemens Healthcare** which is the branch of **Siemens AG** developping medical technologies.

and on the clinical side:

- **Ospedale Pediatrico Bambino Gesù** (OPBG), a children's hospital located in Rome, Italy.
- **University College of London** (UCL) in coordination with the **Great Ormond Street Hospital for Children** (GOSH), both located in London, United Kingdom.
- **Deutsche Herzzentrum Berlin** (DHZB), a medical research centre specialized in cardiovascular disease and cardiopulmonary transplantation located in Berlin, Germany.

A main focus of the project was to build a comprehensive database of cases with detailed clinical data available for many patients. To that end, patients underwent a large variety of protocols with different imaging modalities such as *2D and 3D echocardiography*, *cine MRI* and *4D flow MRI*. In addition, protocols were made to include multiple *follow-up timepoints* where similar acquisition protocols were performed again, in order to study the evolution of the disease from the original *baseline timepoint* (at enrollment of the patient).

3.3.2 3D Modeling Workflow and Parameter Estimation

On the modeling side, the goal was to build personalised models of patients from this database at various timepoints, in particular with the idea that personalised parameter values could give additional information for the analysis of diseases. Here is the modeling workflow to build a 3D simulation from cine MRI:

Geometrical modeling

From MRI, a biventricular tetrahedral mesh of the patient's heart morphology (around 15 000 nodes) is generated, and the boundaries of both the endocardium and epicardium were tracked along the cardiac cycle. This was done by the **Siemens Healthineers** team with a combination of the methods described in [Wang 2013a] and [Jolly 2011] (Figure 3.5).

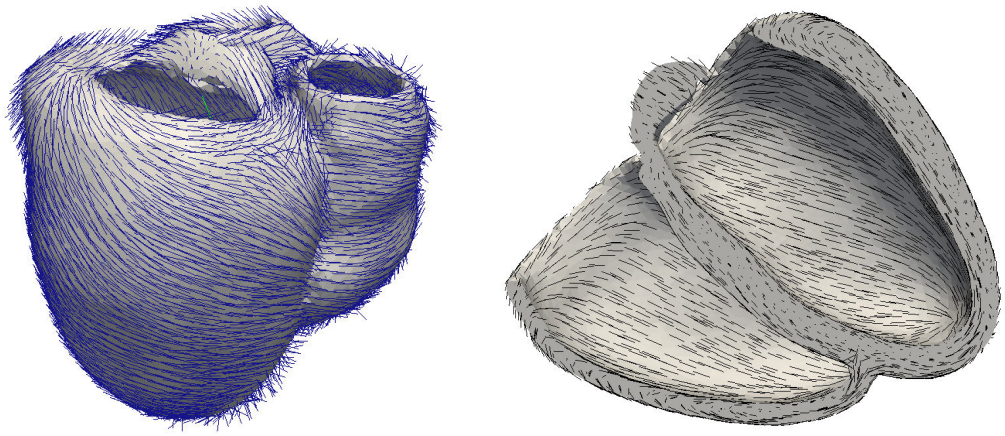

Figure 3.5: Biventricular mesh with myocardial fibres.

On this mesh, we define a *myocardial fibre direction* at each node of the mesh. This is done either from an fibre atlas, in particular in **Chapter 4**, or from the rule-based model of [Streeter 1979], by varying the elevation angles of the fibres across the myocardial wall, from $\alpha_1 = -80$ degrees on the epicardium to $\alpha_2 = 80$ degrees on the endocardium (except in **Chapter 6** where α_1 is an estimated parameter).

Electrophysiological Modeling

Two different methods were used to compute the depolarization and repolarization times across the myocardium:

- In **Chapter 4**, a *personalised Mitchell-Schaeffer* is used as implemented in [Zettinig 2014]. Conductivity values and the *Action Potential Duration* (APD) across the myocardium are personalised as in [Neumann 2014b, Seegerer 2015] from measurements in the ECG.
- In the rest of the manuscript, depolarization times across the myocardium were computed with the Multi-front Eikonal method [Sermesant 2007]. The APD is set from the Heart Rate with classical values of the restitution curve and default values of conductivity are used as in [Pernod 2011].

Mechanical modeling: the BCS model

Our 3D cardiac electromechanical model is based on the implementation of the Bestel-Clement-Sorine (BCS) model [Chapelle 2012] by [Marchesseau 2010, Marchesseau 2013a] in SOFA[1]. The model uses the following items as an input:

- The 3D tetrahedral biventricular mesh.
- The set of myocardial fibres directions, defined at each node of the mesh.

[1] www.sofa-framework.org

- The set of depolarisation and repolarisation times at each node.

Myocardial forces are then computed at each node of the mesh and at each time step, as the combination of an *active contraction force* in the direction of the fibre, and a *passive anisotropic hyperelasticity* driven by the Mooney-Rivlin strain energy (see Fig 3.6a). A haemodynamic model implements the 4 phases of the cardiac cycle. It describes the pressure in the cardiac chambers with global values and the aortic pressure from a Windkessel model [Westerhof 2009] (see Fig 3.6b). The myocardial motion, ventricular volumes and pressures are then computed at each time step of the cardiac cycle.

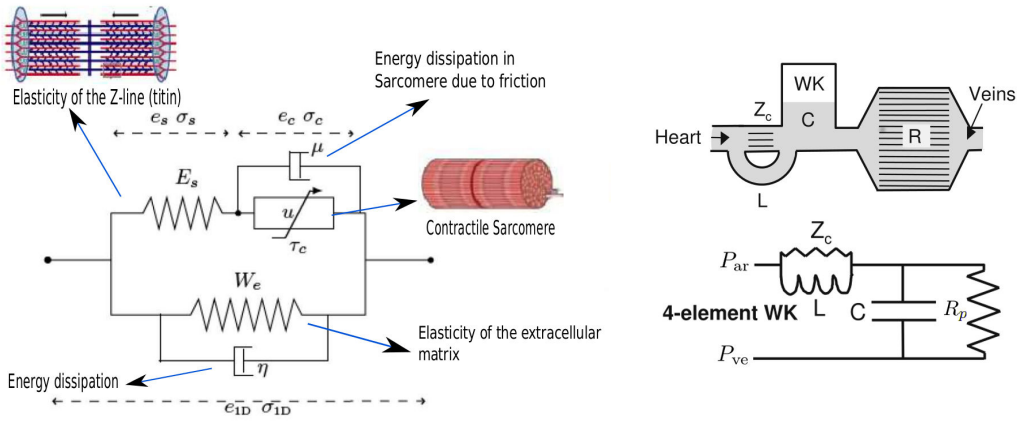

Figure 3.6: **Left:** Rheological model (from [Marchesseau 2013a]) and interpretation of the BCS model, detailed in Section 3.4.1. **Right:** Schema and rheological model (from [Westerhof 2009]) of the windkessel model, detailed in Section 3.4.2.

We report the complete equations of the BCS model and the Windkessel model in the **APPENDIX** (Section 3.4) of this chapter and refer to [Marchesseau 2010, Marchesseau 2013a] for the details of the implementation in the software *SOFA*. In this thesis, we considered various sets of parameters of this model for personalisation:

- For the passive elasticity: in **Chapter 4** we estimate the *bulk modulus* K while c_1 and c_2 are set to a constant value (see Equation 3.4). Then in the subsequent chapters, we set $c_2 = c_1$ and $K = 80c_1$, which we found empirically to give a better mechanical behaviour of the model, and only estimate c_1.

- For the active contractile force: we estimate in all chapters the *contracility* σ_0 (in Equation 3.1). In **Chapter 4** we also estimate the viscosity μ (Equation 3.3), then it is set to a constant value in the subsequent chapters instead of being estimated.

- For the haemodynamics: in **Chapter 4**, we estimate the *aortic peripheral resistance* R_P. In the subsequent chapters we also estimate the *aortic compliance* C and the *venous pressure* P_{ve} (See Equation 3.6) which we found

to be important parameters for modeling the aortic pressure. Alternatively, in **Chapter 8**, we estimate for practical reasons $\tau = R_p C$ in the 0D model. Estimating R_p and C is equivalent to estimate R_p and τ.

The variety of parameter sets considered for personalisation reflects the challenge of finding relevant parameters to be estimated during personalisation, which is a topic of this PhD. After a parameter estimation based on the sensitivity analysis of [Marchesseau 2013a] in **Chapter 4**, we focused on parameters which enable to fit the measurements and data available in the MD-Paedigree project (see Section 3.3.3). Finally in **Chapter 8**, a method was developed to help automatically select the most relevant parameters (and combination of parameters) according to a specific dataset, possibly providing a complete framework to tackle this parameter selection challenge.

3.3.3 A Database of 137 cases for 3D modeling

Due to the large number of patients and acquisition protocols, the data within the project was quite heterogeneous and the same measurements were not available for every patient. In particular in many cases, the cine MRI was available but either the heart rate or pressure measurements were missing. In this work we focused on building a homogeneous database of *complete acquisitions*, which is defined as an acquisition for which all the following data was available:

- The *biventricular mesh* from the cine MRI.
- The *heart rate*, either from the properties of the MRI acquisitions (in the *DICOM* file), or reported by the clinician.
- The *diastolic pressure*, reported by the clinician.
- The *aortic pressure*, reported by the clinician.
- The *stroke volume*, extracted from the tracking or reported by the clinician.

Across the project and the two workpackages, this led to a database of **137 *complete acquisitions*** on which we performed 3D modeling, from three various cohorts:

- The `CVD-UCL` cohort is a group of patients who participated to a clinical study (published in [Hauser 2016]) to assess the cardiovascular response after the ingestion of a high-energy high-fat (142g) meal after fasting for 12h. In particular a short axis cardiac cine MRI sequence was acquired, as well as measurements of the stroke volume, systolic, diastolic and mean cuff pressures before and at several time points within 1h30 of the ingestion of the meal.
- The `CVD-OPBG` is a cohort of mostly overweight patients (80% of the patients have a *Body Mass Index* (BMI) greater than 26) from OPBG.

- The CMP cohort is the aggregated group, from the three clinical centers, of children with cardiomyopathies which are between 0 and 19 years old.

We report here the number of *complete acquisitions* available in each cohort:

Cohort	3D modeling
CVD-UCL	**43**
CVD-OPBG	**36**
CMP	**58**
Total	**137**

The data was not available from the beginning of this Ph.D., but was progressively gathered throughout the project. All the subsequent studies are thus not based on the full dataset of *complete acquisitions*. In the following we then specify at the beginning of each chapter which part of this dataset is used in the presented study.

3.4 APPENDIX: Mechanical Equations of the BCS model and Haemodynamics

As described in [Marchesseau 2013a] our 3D electromechanical model is based on the Bestel-Clement-Sorine model (BCS) of sarcomere contraction as extended by [Chapelle 2012], in conjunction with a Mooney-Rivlin energy for the passive hyperelasticity (see Fig 3.6a). Hemodynamics are represented through global values of pressures and flows in the cardiac chambers, and coupled to the mechanical equations with the Windkessel model of blood pressure for the aortic pressure (see Fig 3.6b).

3.4.1 The BCS model: Active Contraction and Passive Material

The BCS model describes the sarcomere forces as the sum of an active contraction force in the direction of the fibre, in parallel with a passive isotropic visco-hyperelastic component (see Fig 5.1.b). It is compatible with the laws of thermodynamics, and allows to model physiological phenomena at the sarcomere scale which translate at the macroscopic scale (such as the Starling Effect).

The active force in the sarcomere is modeled by the filament model of [Huxley 1957], which describes the binding/unbinding process of the actin and myosin in the sarcomere at the nanoscopic scale. At the mesoscopic scale, it results [Caruel 2014] in a differential equation which relates the active stress τ_c, stiffness k_c and strain e_c of the filament within the sarcomere:

$$\begin{cases} \dot{k_c} = -(|u|_+ + |u|_- + \alpha|\dot{e_c}|)k_c + k_0|u|_+, \\ \dot{\tau_c} = -(|u|_+ + |u|_- + \alpha|\dot{e_c}|)\tau_c + \dot{e_c}k_c + \sigma_0|u|_+, \end{cases} \tag{3.1}$$

where α is a constant related to the cross-bridge destruction during contraction, k_0 is the maximum active stiffness and σ_0 is the maximum contraction (simply called

contractility in this thesis). The values of $|u|_+$ and $|u|_-$ are respectively the rate of build-up k_{ATP} and decrease k_{RS} of the force during contraction and relaxation, which depends on the depolarisation and repolarisation times T_d and T_r of the sarcomere:

$$u = \begin{cases} k_{\text{ATP}} & \text{when } T_d \leq t \leq T_r \\ -k_{\text{RS}} & \text{otherwise} \\ |u|_+ = \max(u, 0), & \\ |u|_- = -\min(u, 0). & \end{cases} \tag{3.2}$$

This active force is applied in the direction of the fibre through the visco-elastic component, made of a spring E_s and a dissipative term μ (see Fig 5.1.b). As derived in [Caruel 2014], the resulting stress $\sigma_{1\text{D}}$ in the fibre direction is given by:

$$\begin{cases} \sigma_{1\text{D}} = E_s \dfrac{e_{1\text{D}} - e_{\text{c}}}{(1 + 2e_{\text{c}})^2}, \\ (\tau_c + \mu \dot{e_c}) = E_s \dfrac{(e_{1\text{D}} - e_{\text{c}})(1 + 2e_{1\text{D}})}{(1 + 2e_{\text{c}})^3}, \end{cases} \tag{3.3}$$

where $e_{1\text{D}} = \underline{\tau_1} \cdot \underline{\underline{e}} \cdot \underline{\tau_1}$ is the strain in the fibre direction τ_1 ($\underline{\underline{e}}$ is the Green-Lagrange strain tensor).

Finally for the passive component the isotropic Mooney Rivlin model of hyper-elastic material is used, driven by the following strain energy:

$$W_e = c_1(I_1 - 3) + c_2(I_2 - 3) + \frac{K}{2}(J - 1)^2, \tag{3.4}$$

where I_1, I_2 and J are the invariants of the Cauchy-Green deformation tensor, c_1, c_2 and K are the parameters of the material.

3.4.2 Haemodynamics and the Windkessel Model

To model the influence of blood dynamics during the cardiac circle, the mechanical equations are coupled with a basic circulation model implementing the 4 phases of the cardiac cycle. For a given ventricle, if we note P_{at} the pressure in the atrium, P_{ar} the pressure in the artery and P_{V} the pressure in the ventricle, the phases are the following:

- *Diastolic Filling*: when $P_{\text{V}} \leq P_{\text{at}}$, the atrial valve is open and the ventricle fills up with blood.
- *Isovolumetric contraction*: when contraction starts, P_{V} rises. $P_{\text{at}} \leq P_{\text{V}} \leq P_{\text{ar}}$ and all the valves are closed.
- *Systolic Ejection*: when $P_{\text{V}} \geq P_{\text{ar}}$, the arterial valve opens and the blood is ejected into the artery.
- *Isovolumetric relaxation*: when the contractile forces disappear, P_{V} finally decreases. $P_{\text{at}} \leq P_{\text{V}} \leq P_{\text{ar}}$ again and all the valves are closed.

We use the haemodynamic model introduced by [Chapelle 2012] which links the blood flow q to the ventricular, atrial and arterial pressures with the following equations:

$$q = \begin{cases} K_{\text{at}}(P_{\text{V}} - P_{\text{at}}) & \text{for } P_{\text{V}} \leq P_{\text{at}} \\ K_{\text{iso}}(P_{\text{V}} - P_{\text{at}}) & \text{for } P_{\text{at}} \leq P_{\text{V}} \leq P_{\text{ar}} \\ K_{\text{ar}}(P_{\text{V}} - P_{\text{at}}) + K_{\text{iso}}(P_{\text{ar}} - P_{\text{at}}) & \text{for } P_{\text{V}} \geq P_{\text{ar}} \end{cases} \tag{3.5}$$

Here the atrial pressure $P_{\text{at}}(t)$ (cardiac preload) is imposed at a constant value $P_{\text{at\_lower}}$ except for a *pressure bump* up to $P_{\text{at\_upper}}$ at the beginning of cardiac cycle, to account for the contraction of the atrium before the ventricular contraction. Finally the pressure of the artery P_{ar} (cardiac afterload) is modeled with the 3-parameters Windkessel model [Westerhof 1969] and coupled to the ventricular outflow q through the equation:

$$R_p C \dot{P}_{\text{ar}} + P_{\text{ar}} - P_{\text{ve}} = (R_p + Z_c)q + R_p Z_c C \dot{q}, \tag{3.6}$$

where Z_{C} and R are the *proximal and distal (peripheral) resistances*, C is the *arterial compliance* and P_{Ve} is the *venous pressure*.

3.4.2.1 Implementation

The passive Mooney Rivlin energy is discretised on the 3D mesh with the MJED (Multiplicative Jacobian Energy Decomposition) method described in [Marchesseau 2010], and the BCS fibre stress and stiffness are computed at each node, separately from the positions and velocities. This allows a fast assembly and a good conditioning of the system of mechanical equations. A Rayleigh damping is then added to account for the viscous global dissipation and finally, the ventricular pressure is computed using a prediction-correction approach, performed after solving the first system of mechanical equations. This efficient algorithm and all the details of the mechanical equations and their 3D discretizations are fully discussed in [Marchesseau 2013a].

Chapter 4

Propagation of Myocardial Fibre Architecture Uncertainty on Electromechanical Model Parameter Estimation: a Case Study

Contents

*This chapter presents a joint work by the teams at **INRIA Sophia-Anpolis**, **Siemens Healthineers** and **Ospedale Pediatrico Bambino Gesù**, performed at the beginning of the project MD-Paedigree to evaluate the influence of unknown parameters on the estimation of personalised parameters. First, uncertainty in myocardial fibre orientation is quantified from 7 representants sampled from a fibre atlas and propagated in a generic personalisation pipeline, applied to the personalisation of a case from the CMP cohort. We then evaluate the resulting variability in 7 personalised simulations and personalised parameter sets. Due to the lack of constraints during parameter estimation, we can observe at the end of the study that the resulting uncertainty in estimated values is extremely large. For example the uncertainty*

on the aortic peripheral resistance can be up to 50% of its value, which appears incompatible with physical considerations. This outlined the need for more consistent approaches to parameter estimation, which we develop in the sequel of this thesis. This work was presented at the FIMH conference in 2015 [Molléro 2015].

4.1 Introduction

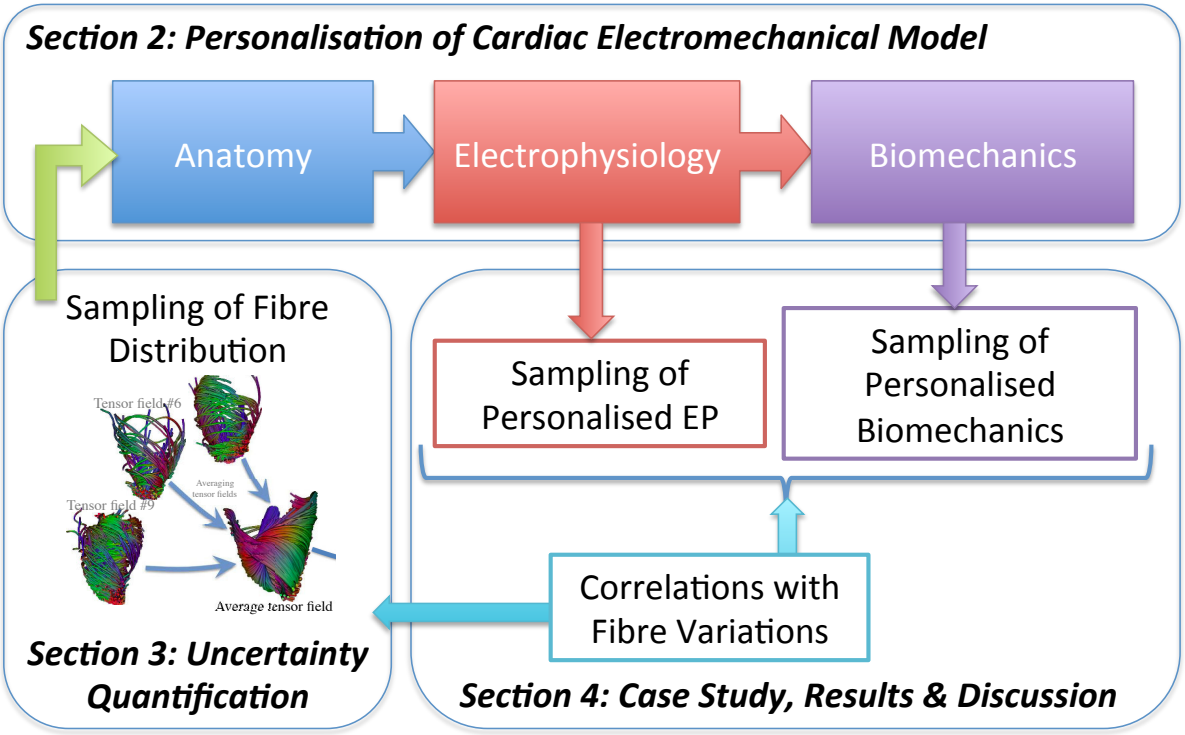

Figure 4.1: Global scheme of fibre variability propagation along a personalisation pipeline.

Cardiac modeling aims at understanding cardiac diseases (such as heart failure, dissynchrony or tachycardia), helping diagnosis and predicting cardiac response to therapy (e.g. cardiac resynchronization therapy, or radiofrequency ablation). In order to impact clinical practice, generic models have to be adjusted to a given patient, which is personalisation [Marchesseau 2013a, Zettinig 2014]. This is still a challenging part, and often computationally demanding, therefore most of the approaches are deterministic. However there are several sources of uncertainty, both due to the data and the models [Neumann 2014a, Konukoglu 2011]. In this work we present the propagation of the uncertainty coming from the lack of knowledge on cardiac fibres for a given patient. Indeed, it is still difficult to obtain measurements on the fibre architecture for a given patient *in-vivo*, therefore we have to rely on prior knowledge. In order to propagate this uncertainty, it has first to be quantified. This

was done by computing statistics on a small population of healthy hearts (details in Section 4.3). Then the personalisation pipeline has to be efficient enough so that a sampling of this uncertainty can be propagated. Finally we obtained a sampling of the distribution of the parameters and personalised simulations (see Figure 4.1).

We illustrated this method on a paediatric dilated cardiomyopathy case (details in 4.4.1). From a clinical standpoint, it is very difficult to predict the dramatic evolution of such rapidly-evolving case, even with advanced imaging. The aim of the project is to test if parameters derived from biophysical models could help predicting the outcome of such cases.

4.2 Personalisation of the Cardiac Electromechanical Model

4.2.1 Robust Segmentation of Myocardium from MRI

Patient-specific heart morphology is obtained from short-axis cine magnetic resonance images (MRI). To that end, a robust, data-driven machine learning approach is employed [Wang 2013a] to estimate surface meshes of the left endocardium, left outflow tract, left epicardium, right endocardium, right outflow tract and right inflow tract. Each surface is estimated using marginal space learning and probabilistic boosting trees, constrained by a shape model learned from a database of hundreds of cases, thus ensuring inter-patient point correspondence. Next, each surface is tracked over the entire cine sequence using a combination of tracking by detection and tracking by registration. Finally, the surface meshes at mid-diastole are selected to generate a closed surface of the biventricular myocardium, which is transformed into a tetrahedral volume mesh for simulation[1].

4.2.2 Personalised Cardiac Electrophysiology Model

Cardiac electrophysiology (EP) is modeled using the approach presented in [Zettinig 2014]. Cardiac transmembrane potentials are calculated according to the mono-domain Mitchell-Schaeffer (MS) model as it offers a good compromise between model observability and fidelity. In this study, we are mostly interested in two parameters: the time during which the ion channels are closed τ_{close}, which captures action potential duration and is directly linked to the QT duration; and tissue diffusivity c, which determines the speed of the electrical wave propagation and is directly linked to the QRS duration. We model fast regional diffusivity for the left c_{LV} and right c_{RV} endocardium to mimic the fast conducting Purkinje network, and slower diffusivity $c_{\text{myo}} \leq c_{\text{LV}}, c_{\text{myo}} \leq c_{\text{RV}}$, for the myocardium. Transmembrane potentials are calculated using LBM-EP, a Lattice-Boltzmann method, which is coupled to a boundary element method approach to calculate the 12-lead cardiac electrocardiogram (ECG) resulting from the cardiac potentials [Zettinig 2014]. The model is finally personalised like in [Neumann 2014b, Seegerer 2015]. BOBYQA, a

[1] http://www.cgal.org – computational geometry algorithms library

constrained gradient-free optimization method is used to estimate tissue diffusivity and τ_{close} such that computed QRS duration, QRS electrical axis (EA) and QT duration match the measurements.

4.2.3 Personalised Cardiac Mechanical Model

The cardiac mechanical model is based on the Bestel-Clement-Sorine (BCS) model [Chapelle 2012]. This model describes the heart as a Mooney Rivlin material, and model the stress along the cardiac fibres according to microscopic scale phenomena. Particularly, this model is compatible with the laws of thermodynamics and is able to model the Starling Effect. In this pipeline, it integrates a circulation model representing the 4 phases of the cardiac cycle (aortic pressure modeled by a 4-parameter Windkessel model), and takes the depolarization times and the action potential durations in each point of the mesh as an input to compute the mechanical contraction and relaxation of the myocardium.

As in [Marchesseau 2013a], we only personalise the most influential and independent parameters which are the *contractility* σ_0, the *viscosity* μ, the *bulk modulus* K and the *aortic peripheral resistance* R_p. The calibration is performed following [Marchesseau 2013a]: after performing 9 simulations using some specific parameter values that lies in a range of acceptable values, an algorithm runs and finds in one iteration the set of parameters that best fit the observations using the Unscented Transform Algorithm. In our case, the observations are the minimal LV volume and the time between the two moments the LV is at 50% of its contraction volume, both calculated from the cine MRI.

4.3 Population-Based Uncertainty Quantification of Fibres

4.3.1 Variability Estimation in Atlas Space

One often characterize the variability of a random vector by its mean and covariance matrix since these two first moments completely characterize the Gaussian distribution. However, in more than a few dimensions, the covariance matrix is too large to be computed robustly from only a few data observations. An alternative is to draw just a few samples from the population distribution, either by choosing randomly a number of points from the data observations, or more rationally by selecting a few points that describe the main subspace of variation in the data, for instance through *Principal Component Analysis* (PCA). Within this subspace one could describe the variability using a minimal number of points thanks to the so-called sigma-points at the vertices of a minimal simplex, originally designed for the Unscented-Kalman Filter [Julier 1997]. However, it is often empirical observed that using symmetric points on all axes is significantly more accurate for underlying symmetric distributions. This is the approach we took in this study to quantify the variability of the fibre architecture.

We used $N = 10$ ex-vivo DTI acquisitions of healthy human hearts, registered in the atlas space [Lombaert 2011]. Both left and right ventricles images were generated with this atlas but due to the lower resolution of the right ventricle we chose to use this atlas only for the left ventricle part. On the right ventricle, we instead use a single DTI heart acquisition with high resolution done by Johns Hopkins University (JHU) [Helm 2005]. Therefore we have no variability estimation of the fibres for the right ventricle.

To compute the mean DTI over the population and quantify the variability, we work in the Log-Euclidean space [Arsigny 2009] rather than the standard Euclidean space. The mean DTI is $\bar{D} = \exp\left(\frac{1}{N}\sum_{i=1}^{N}\log(D^{(i)})\right)$ and the data matrix of centred observations is $X = [vect(\log D^{(1)} - \log \bar{D}) \dots vect(\log D^{(N)} - \log \bar{D})]$. The PCA is obtained by diagonalising the large covariance matrix $\Sigma = XX^{\top}/(N-1)$ or more efficiently we chose to compute the singular-value decomposition (SVD) of the data matrix $X = U\Lambda V^{T}$, where the $N \times N$ diagonal matrix Λ encloses the square root of the eigenvalues of Σ. We choose to only study the first 3 eigenmodes $U_{i=1,2,3}$, because they already explain 59% of the variation of the log-tensors seen in the population. For each mode i, we compute two symmetric images representing the range of variation along the mode at plus or minus one standard deviation s_i as: $M_{i,\pm}(x) = \exp\big(\log(\bar{D}(x)) \pm s_i U_i(x)\big)$.

4.3.2 From Atlas to Patient Space

In order to relate the atlas space to the geometry of our target patient, we register the mesh of our patient to the mask of both the atlas (for the LV) and the JHU heart (for the RV) with a three-steps framework. First, the mask of the patient is aligned with the mask using a rigid landmark based registration method. Correspondences between the atlas and the target heart are manually checked. Secondly, we perform a similarity registration with five coarse levels and one fine level, each of which are composed of 10 iterations. Finally, we perform a diffeomorphic registration using diffeomorphic demons algorithm with 15x10x5x5 iterations (from coarsest to finest levels), a Gaussian smoothing factor of 2 in the regularization phase, and an interpolation for the moving image done with B-splines [Vercauteren 2009]. We then get the full diffeomorphic transformation for each one of our two initial atlases to the target patient mask.

We apply the transformation found in the previous step to the mesh of the patient. For each of the vertices, if the correspondence lies within the RV we use the JHU DTI-image whereas we use the mean or the sampled images of the Lombaert atlas if it lies within the LV. We take the mean (in the Log-Euclidean space) of the tensors of the 5-nearest voxels. The tensor value is then reoriented using the Finite Strain method, and the fibre orientation is taken as its first eigenvector [Peyrat 2007]. The results of the fibres personalisation are 7 sets of fibres shown in Figure 4.2.

4.4 Propagation of Fibre Uncertainty on a Case Study

4.4.1 Clinical Background

The patient is a 16 years old male who had no family history of cardiac disease. After being admitted at the hospital for chest pain, evidence of *reduced ejection fraction* and *dilated left ventricle* led to a first diagnosis of myocarditis. A detailed echocardiographic examination performed 3 month later showed evidence of markedly increased trabeculae of the left ventricular apical and lateral walls, possibly suggesting the presence of *left ventricular non-compaction*. The MRI study did not confirm this diagnosis but only the *idiopathic dilated cardiomyomathy*. After 9 month of follow-up in the clinic, the patient was put on the national heart transplant list due to worsening conditions. The patient is now doing well at follow-up after transplant, and the pathology and histology testing at the hospital confirmed the diagnosis of *idiopathic dilated cardiomyopathy*.

4.4.2 Goodness of Fit and variability after Personalisation

For each of the 7 tested fibre architectures we personalised EP and EM parameters as described in Sec. 4.2.2. High goodness of fit between observations and simulations were achieved for all instances : for the ECG, the maximum obtained errors after personalisation are 0.2 ms for QRS, 2.9 ms for QT and 0.3° for EA, which is well below 1% of the measured values for QRS (96 ms) and QT (413 ms), and below 1% of the maximum possible error (180°) for EA (5°), respectively. Similarly in terms of mechanics, the error between simulated and measured minimal volume and the time at 50% contraction are below 3%.

After this step, we can observe the spatial variability of EP depolarisation times and end-diastolic strain between modes in Figure 4.2. Although the main features of the ECG are the same, variations in local depolarization times can be up up to 10ms from one set of fiber to the mean fiber set due to the difference in current propagation. Interestingly we can notice for some of the sets a correlation between the peaks and zones of the variations of the depolarization times and the variations of fibre orientation which would be interesting to further study.

4.4.3 Uncertainty on the Model Parameters and Discussion

Table 4.1 shows the values of the parameters after calibration for the mean fibre model, and their relative variation for each fibre set (Mx and Px are the two fibre sets representing the mode x as described in Section 4.3, for x = 1, 2 or 3).

For the EP parameters, we first note that c_{RV} varies the most although the fibres are fixed on this ventricle. This might be explained by the large changes in *direction of depolarisation* on the LV due to changes in fibre orientation, which would require the conductivity of the RV to vary as well to *match the same EA*. Logically, τ_{close} varies very little, since it is directly linked to the QT duration, that is not much affected by fibre orientation. Finally, one should notice the observed variabilities

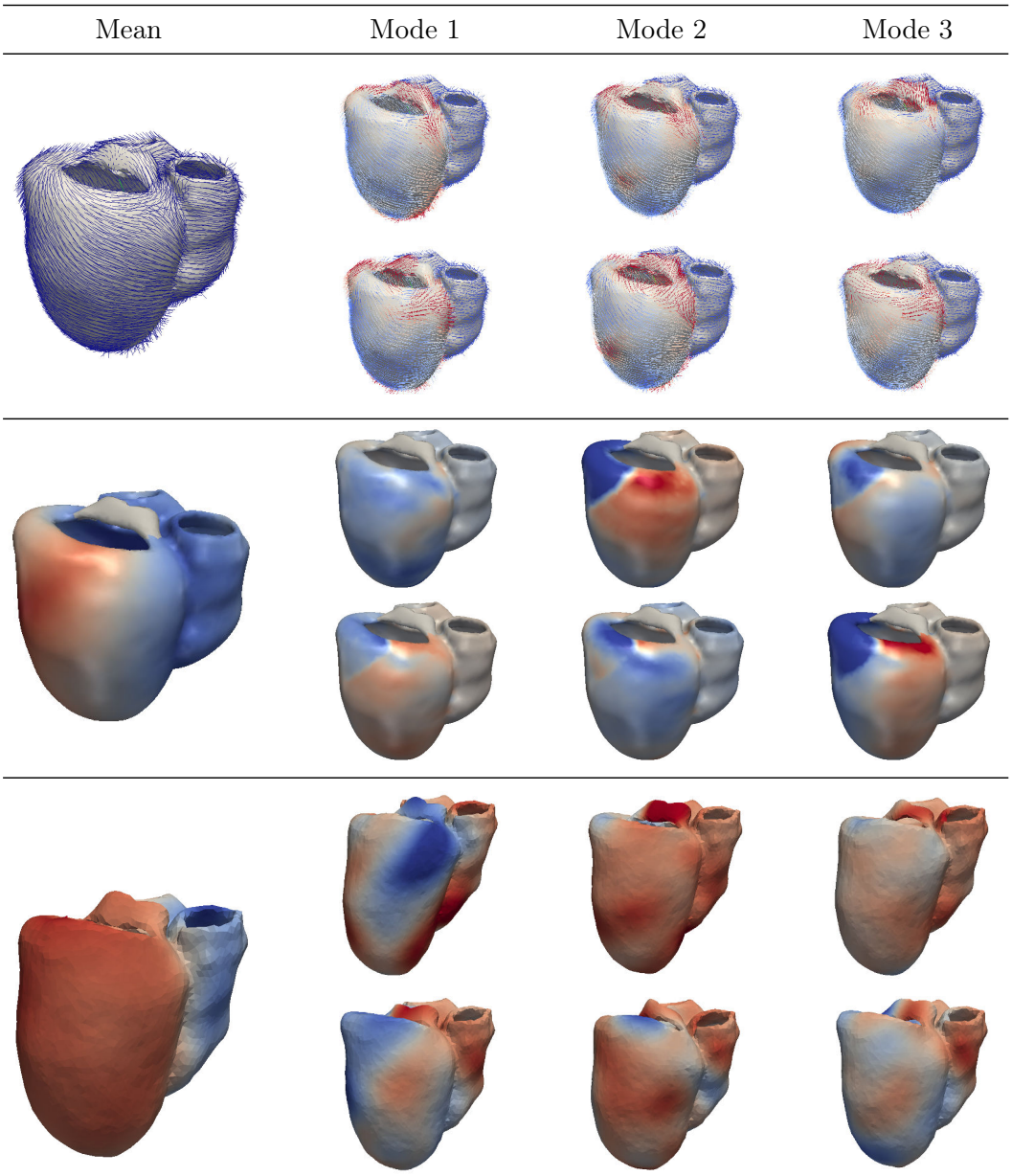

Figure 4.2: **Top left**: Mean fibres. **Top right**: modes of variation plus (top) / minus (bottom) s_i coloured by angular variation w.r.t. the mean (from 0° blue to 20° red). **Middle left**: Mean depolarisation times after EP personalisation; from blue (early) to red (late≈100 ms). **Middle right**: Variation from mean depolarisation times colouring from blue (-10 ms) to grey (0 ms) to red (+10 ms). **Bottom left**: Local strain at end-systole range from blue (high) to red (low). **Bottom right**: Variation for each different fibre modes after mechanical personalisation (blue: more contraction, red: less than on mean fibre).

with the *intrinsic uncertainty* due to the parameter estimation process (which was for instance quantified as high as 45% for c_{RV} in some cases) [Zettinig 2014].

About the mechanical parameters, we can easily explain the variations of R_p and σ_0. It's indeed well known that the fiber architecture has a strong influence on the stroke volume and when we fix all the parameters, we see that the ejection fraction is *maximal for the mean fibre*, with the *largest variations along the mode 2*. To achieve the same level of ejection fraction with a less efficient set of fiber, the aortic peripheral resistance must be lowered and the contractility increased, which is what we observe for all the modes, (and in a larger range for the mode 2). The variations of K and μ are more challenging to interpret directly. They impact directly the slopes of contraction and relaxation phases, thus ensuring the fitting of the time at 50% contraction.

Table 4.1: Variability in estimated EP and EM model parameters after personalisation.

Parameter	c_{myo}	c_{LV}	c_{RV}	τ_{close}	σ_0	μ	K	R_p
Unit	mm^2/s	mm^2/s	mm^2/s	ms	Pa	Pa s	Pa	$\mathrm{Pa\,m^3\,s}$
Mean	1.21e3	4.70e3	1.83e4	2.09e2	4.74e6	2.29e5	2.01e7	1.9e7
P1	-17.2%	-14%	-14.7%	-0.48%	+2.71%	-5.84%	-5.21%	-26.7%
M1	+11.5%	+10.6%	+6.06%	+0.14%	+4.2%	-8.54%	-11.4%	-30.9%
P2	-0.82%	+2.34%	+24.2%	-0.14%	+2.4%	-20.1%	+4.86%	-54.6%
M2	+3.28%	+2.55%	-30.9%	-0.14%	+0.86%	-2.02%	+10.6%	-35.8%
P3	+3.28%	+7.02%	-11.4%	-0.14%	+3.75%	-2.87%	-7.64%	-34.4%
M3	-0.82%	-7.66%	+9.06%	-0.57%	+0.75%	-12.6%	-0.98%	-20.7%

4.5 Conclusion

In this chapter we detailed how a quantified uncertainty on myocardial fibres could be propagated along an efficient model personalisation pipeline. We presented the need to comprehensively quantify the influence of the parameters on the final output, and reversely to quantify their uncertainty when personalising models in order to fit clinical data. Atlases with mean and principal modes of variations are a good way to hierarchically represent the main directions of variability on quantities with many parameters such as vector or scalar fields. We used that method for the uncertainty on local fibre orientation in each point of the heart, and assessed the variations of personalised parameters according to those uncertainty. Interestingly, if we have prior knowledge on some parameters of the heart, this method could reciprocally give us information on the fibre set with the highest probability.

Finally, several aspects of this pipeline could be further improved for a more general assessment of the uncertainty, in particular with a better personalisation from clinical data (evolution of regional volumes, the whole flow curve) and an

extension of the Atlas method to regional parameters such as conductivity or stiffness maps.

Chapter 5

Multifidelity-CMA: A Multifidelity Approach for Efficient Personalisation of 3D Cardiac Electromechanical Models

Contents

The study [Molléro 2015] presented in ***Chapter 4*** *led to the conclusion that both a more consistent personalisation framework (which possibly integrates uncertainty quantification), and a more handy and efficient tool for parameter estimation were required to perform consistent personalisations of a possibly large database of patients in the context of MD-Paedigree. In both cases, the computational complexity of 3D simulations (15 minutes in average but possibly up to 1 hour) is an obstacle. In this chapter we develop a reduced "0D" model of our 3D model, then build a multiscale coupling to approximate outputs of 3D simulations from 0D model simulations. Then, we use this coupling to build an efficient personalisation algorithm called* ***Multifidelity-CMA*** *for the 3D model. A preliminary version [Mollero 2016] of this work was presented at the MICCAI conference in 2016. The complete method, presented here, was published in* Biomechanics and Modeling in Mechanobiology *in August 2017 [Molléro 2017b]. In both papers the method was applied to the complete collection of* complete acquisitions *from the 3 cohorts available at the time of submission.*

5.1 Introduction

Electromechanical models of the heart simulate the physical behavior of a patient's heart, in order to perform advanced analysis of the cardiac function. They are of increasing interest to help clinicians in their daily practice [Kayvanpour 2015, Baillargeon 2014, Smith 2011]. In particular, recent works have been successful in predicting haemodynamic changes in cardiac resynchronization therapy [Sermesant 2012], ventricular tachycardia inducibility and dynamics [Chen 2016], as well as in detecting and localising infarcts [Duchateau 2016] using 3D personalised models.

After building the patient's heart mesh geometry, the simulated heartbeat has to match clinical data, such as ejected blood volume and pressure measurements, or more detailed information about regional motion and abnormalities available from imaging modalities such as 3D echocardiography or cine MRI. This is done by finding adequate simulations settings (boundary conditions, loading constraints) and values of model parameters such as myocardial stiffness and contractility [Xi 2011, Chabiniok 2012]. This phase of parameter estimation is usually referred to as the *personalisation* of the cardiac model [Marchesseau 2013c] and results in a *personalised cardiac model* [Wang 2012] made of a *patient-specific heart geometry* [Schaerer 2006] and *patient-specific biomechanical parameters.*

A wide variety of 3D computer heart models exists in the literature, which describe the anatomy and physiology of the heart at various scales. For example the 3D mesh describing the heart geometry can be made of very different numbers of nodes, and the cellular electromechanical phenomena underlying the build-up

of myocardial forces can either be described with a large number of equations, or simplified equations. We refer to the two comprehensive reviews of [Chabiniok 2016] and [Clayton 2011] for a large discussion of various models of different scales, types and implementations. The scale and precision (also known as fidelity) of the model is chosen according to the study and the available data. In general, the time required to compute a simulation increases with its level of detail. The simulation of a 3D heartbeat using some of the most complex 3D models can take up to several hours of computation on computers with hundreds of cores [Panthee 2016]. This means that for applications where many simulations need to be repeatedly performed (e.g. parameter estimation), computational time becomes a real issue.

The joint use of low-fidelity models to approximate a high-fidelity model and lower the computational burden has been investigated by the *multifidelity modeling* community since [Kennedy 2000]. As described in [Peherstorfer 2016], a *model-management method* usually handles and feeds the outputs of a *low-fidelity model* (e.g. a simplified model, a regression model or a projection-based model) to an underlying *application-specific method* (e.g. an optimisation algorithm) as surrogates to the high-fidelity model outputs. The method also optionally decides when to recompute simulations of the high-fidelity model to guarantee the accuracy of the low-fidelity approximation.

Here we present an original 0D/3D multifidelity approach for the personalisation of 3D cardiac models (Fig. 5.1). First, from our 3D cardiac model, we derived and implemented a simplified "0D" model which is faster by 4 orders of magnitude. This was performed as proposed in [Caruel 2014], by approximating the geometry of the ventricle as a sphere and assuming spherical symmetry and homogeneity of the electromechanical behavior.

Then, we introduce a *multifidelity coupling* in order to approximate 3D model simulations from 0D model simulations. To this end, we build a parameter mapping which converts parameters of the 3D model into parameters of the 0D model, based on a few representative 3D simulations in the parameter space (called the *sigma-simulations*). Outputs of the 3D model are then approximated from 0D model simulations, thus enabling a reduction of the computational burden when a large number of 3D simulations outputs are required.

Finally, we present a *multifidelity personalisation method*, built by adapting an efficient optimization algorithm called CMA-ES [Hansen 2006] to use approximations of the 3D simulations obtained through the *multifidelity coupling* instead of the real 3D simulations. This leads to a fast and computationally efficient personalisation method for the 3D model parameters.

A preliminary version of this work was described in [Mollero 2016]. Here we propose a significantly extended methodology for the *multifidelity coupling*. First, the *sigma-simulations* selection is performed so that additional computational gains are possible when some estimated parameters have the same equations and values in both models. Then, a more robust, non-linear, parameter mapping is used. An additional step is finally introduced to correct the possible errors arising during the estimation of 0D model parameters. We also present an improved methodology for

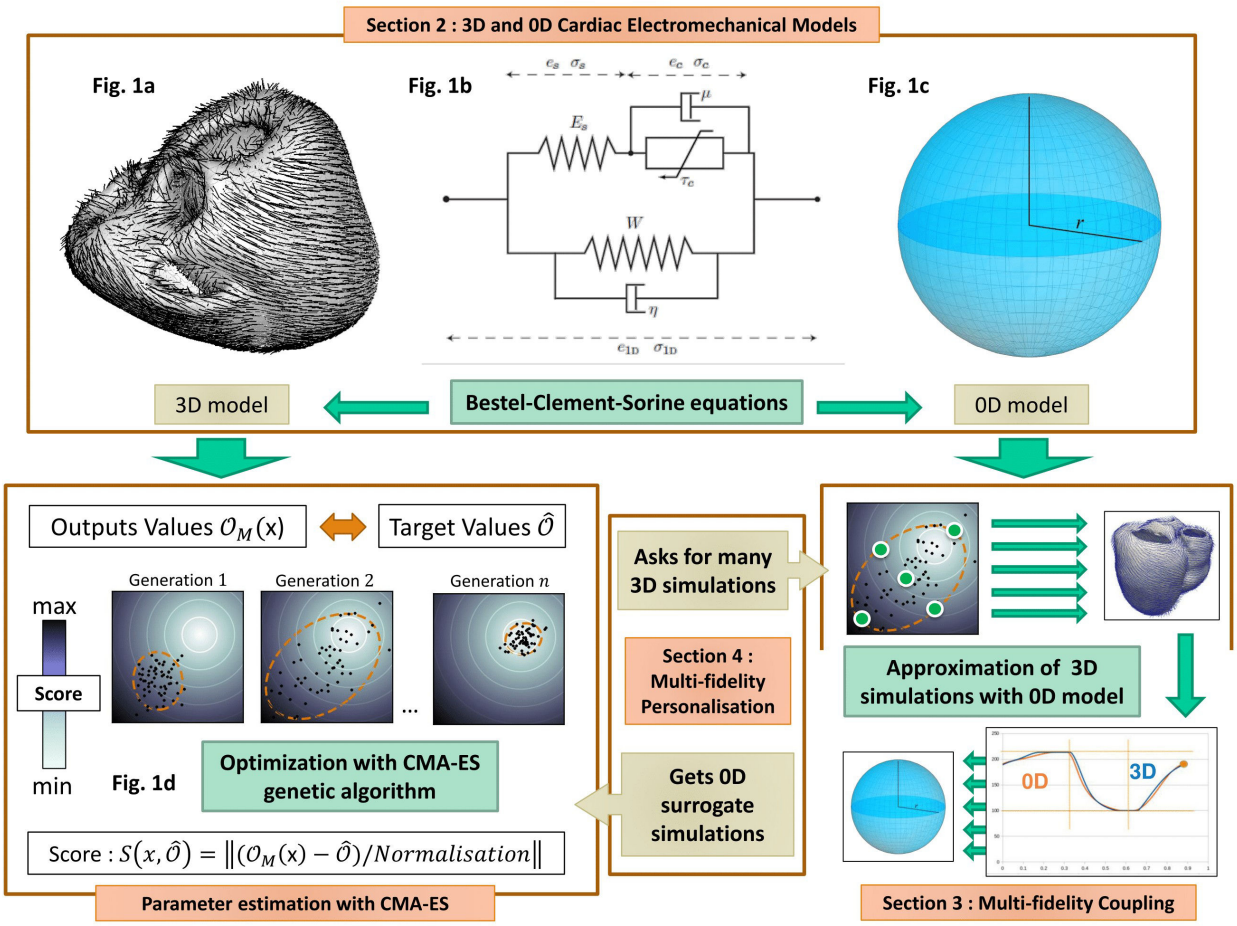

Figure 5.1: 3D and 0D cardiac models (1.a, 1.b and 1.c). Our *multifidelity personalisation method* performs *parameter estimation* in the 3D model using CMA-ES (1.d), based on 0D simulations obtained through the *multifidelity coupling* between the models.

the *multifidelity personalisation method* which enables the use of a single coupling for many iterations of CMA-ES. This is done while simultaneously ensuring that the approximation is accurate enough for the optimisation algorithm, resulting in an overall estimation which is 5 times faster than in [Mollero 2016] on average.

In terms of results, we present extended results and discussions for both the *multifidelity coupling* and the *multifidelity personalisation method*. The approximation accuracy of the coupling is compared to an hypersurface interpolation method and the personalisation method is compared to BOBYQA [Powell 2009], a commonly used derivative-free optimization algorithm. This leads to an extended discussion on the computational aspects of our method in a parallel environment. This work is illustrated on a personalisation problem involving 5 parameters and 3 outputs, and we demonstrate results on a database of *121 different geometries and clinical values*, which we believe to be one of the largest cohort of personalised cardiac cases to date. This personalisation took around 2.5 days on our cluster.

Lastly our 0D model equations are encoded in the CellML format [Cuellar 2003] and made available for download from the Physiome Model Repository[1] [Yu 2011]. Python scripts to perform parameter estimation in the 0D model will be released within 1 month of publication, from the same location.

5.2 Multi-fidelity Cardiac Modeling and Personalisation Framework

In this work we use both a 3D electromechanical model which can simulate the behaviour of complex patient-specific heart geometries, and a reduced "0D" version of this model which can be summarized in a few equations. Both models rely on the same mechanical laws but simplifying assumptions are made on the geometry of the 0D model to derive its equations. We also introduce the *personalisation framework* for the parameters of both models.

5.2.1 The 3D Cardiac Model

Our 3D cardiac eletromechanical model is an implementation of the Bestel-Clement-Sorine (BCS) model ([Chapelle 2012]) by [Marchesseau 2010, Marchesseau 2013a] in SOFA[2], an open-source simulation software. The model uses the following items as an input:

- A 3D tetrahedral biventricular mesh, either synthetically created or derived from segmented MRI images.

- A set of myocardial fibres directions, defined at each node of the mesh. Here we use synthetic fibres from the rule-based of [Streeter 1979].

- A set of depolarisation and repolarisation times at each node of the set computed from an electrophysiology model. Here we use the Eikonal model as described

[1] https://models.physiomeproject.org/e/470

[2] www.sofa-framework.org

in [Sermesant 2012].

Myocardial forces are then computed at each node and at each time step from the equations of the BCS model. Then the myocardial motion (mesh nodes velocities) as well as ventricular volumes and pressures are computed at each time step of the cardiac cycle from these forces (As described in Section 3.4). With myocardial meshes made of around 15 000 nodes and a time step of 5 ms, a single beat of 0.9s takes 15 minutes to compute on average on a single-core (Intel(R) Core(TM) i7-4600U [2.10GHz]).

5.2.2 The 0D Cardiac Model

As described in [Caruel 2014], it is possible to derive the equations of a fast *0D model* of the heart, which relies on the same BCS equations. This is done by making the following simplifying assumptions on the geometry, the electrical activation and the properties of the material:

1. The ventricle has a spherical shape.
2. The material is incompressible.
3. The electrical activity is synchronous and homogeneous over the sphere.

With these assumptions of spherical symmetry, myocardial forces and motion are also spherically symmetric and can be entirely described by the inner radius r of the ventricle. Deformation and stress tensors can also be reduced to a simple form (see [Caruel 2014]), which leads to a system of a dozen equations (see APPENDIX).

We implemented the equations into C code and solve the system of equations using an explicit *Forward Euler* method with a temporal discretisation of 0.01 milliseconds. This leads to the simulation of around 15 beats per second. We also encoded the 0D model in the CellML format [Cuellar 2003], which is an open standard based on the XML markup language to store and exchange computer-based mathematical models. This model can be downloaded from the Physiome Model Repository[3] and easily exploited through the software OpenCOR [Garny 2015].

5.2.3 Parameter Estimation Framework for Cardiac Models

After building the model, parameter estimation is usually the first step to analyse clinical data with a model. It consists in finding parameter values for which the simulation with the model reproduces available values and quantities in the data, such as pressure or volume measurements. In particular when the geometry is patient-specific, this phase is called cardiac model *personalisation* [Marchesseau 2013c, Kayvanpour 2015].

Formally, we consider a cardiac model M, a set of simulated quantities called the *outputs* $\mathscr{O}$ and a subset $\mathscr{P}_{\mathrm{M}}$ of varying parameters of the model (while the other parameters are supposed fixed). Given a vector of these parameters $x \in \Omega_{\mathrm{M}}$, we

[3] https://models.physiomeproject.org/e/470

note $\mathscr{O}_{\mathrm{M}}(x)$ the values of the outputs $\mathscr{O}$ in the simulation of M with parameter values x. The goal of personalisation is to find parameter values $x* \in \Omega_M$ for which the outputs values $\mathscr{O}_{\mathrm{M}}(x*)$ best match some target values $\widehat{\mathscr{O}}$.

This is an inverse problem, which can be tackled by different methods (see the review of [Chabiniok 2016]). We propose here a parameter estimation framework (Fig 5.1.d) through derivative-free optimization, using an efficient genetic algorithm called CMA-ES [Hansen 2006].

5.2.3.1 Robust Optimisation With the Genetic Algorithm CMA-ES

We define the *score* $S(x, \widehat{\mathscr{O}})$ of some parameter values x as the L_2 distance between $\mathscr{O}_{\mathrm{M}}(x)$ and $\widehat{\mathscr{O}}$, normalised by the Hadamard (coordinate-by-coordinate) division $\oslash$ with a vector $\mathscr{N}$, in order to compare outputs with different units:

$$S(x, \widehat{\mathscr{O}}) = \|(\mathscr{O}_{\mathrm{M}}(x) - \widehat{\mathscr{O}}) \oslash \mathscr{N}\|.$$

We then perform a derivative-free optimisation with the genetic algorithm *CMA-ES*, which aims at minimising this score S. The algorithm (which stands for Covariance Matrix Adaptation Evolution Strategy) asks at each iteration n for the scores of m points $x_i \in \Omega_{\mathrm{M}}$ (a *generation*), drawn from a multivariate distribution with covariance I_n^c and mean I_n^m. Then, it combines bayesian principles of *maximum likelihood* with *natural gradient descent* on the ranks of the points scores in the generation to update both I_n^c and I_n^m.

The CMA-ES algorithm has many advantages in this context. First, it can explore a large and unbounded parameter space while still performing a local search at each iteration, and has shown very good results on problems involving hundreds of parameters to optimise [Geijtenbeek 2013]. Second, because the updates of the I_n^c and I_n^m only depend on the score ranks, it is very robust to outliers in the generation, in particular to parameter values for which the simulation diverges (in which case we give an arbitrary high score to these parameters).

Also, since each score comes from an independent simulation, this algorithm is well suited to parallel environments. We can either decide to set a very high population size m and do many parallel simulations (in this case the algorithm can converge in a few iterations), or a lower population size and rely instead on many iterations of the algorithm for convergence.

5.2.3.2 Application to the 0D model

Because the 0D model is extremely fast (15 beats per seconds), parameter estimation is also very fast with the 0D model. For example with a population size of 50 points per generation it takes less than 50 generations and 3 minutes on a 4-core computer (with parallel computation of the simulations within each generation) to make most of the problems with sets of up to 10 outputs and parameters converge.

In our current implementation, 29 outputs can be extracted from the pressure, volume and flow curves and 25 parameters of the 0D model can be estimated. Python

Table 5.1: Sets of *3D model parameters* and *global outputs* in the example.

Global outputs $\mathscr{O}$	*Parameters of the 3D model* $\mathscr{P}$
Stroke Volume SV	*Contractility* σ_0
Mean Aortic Pressure MP	*Stiffness* c_1
Diastolic Aortic Pressure DP	*Peripheral resistance* R_p
	Aortic Compliance C
	Venous Pressure $P_{\mathbf{ve}}$

scripts to automatically perform the parameter estimation will be released within 1 month after the publication, available for download from the Physiome Model Repository[4].

5.2.3.3 Application to the 3D model

It is possible to apply directly this framework to the 3D model, but the computational burden can become an issue because of the time required to compute the 3D simulations. Indeed, either we set a small population size, but we need many iterations of CMA-ES (of around 15 minutes each). Or we set a high population size but is the number of parallel CPUs used at the same time which may become prohibitive. In Section 5.4, our *multifidelity personalisation method* lowers this computational burden by replacing the outputs values of 3D simulations with approximations computed from 0D simulations through a *multifidelity coupling* between the two models, as explained in Section 5.3.

5.3 Multi-fidelity Coupling: Approximating Global Outputs Values of the 3D Model

We present here a *multifidelity coupling* between the 3D and the 0D model. We will call *global outputs* of the models quantities which can be computed from the simulations of both models, such as the total ejected blood volume (stroke volume) or the minimal (diastolic) aortic pressure.

We consider a set of N_1 parameters of the 3D model $\mathscr{P}_{3\mathrm{D}}$, a set of global outputs $\mathscr{O}$, and a set of parameter values $x_i \in \Omega_{3D}$ of the parameters $\mathscr{P}_{3\mathrm{D}}$. The goal is to get approximations of the values $\mathscr{O}_{3\mathrm{D}}(x_i)$ by performing 0D simulations and only a few 3D simulations.

We will illustrate the method on the following problem: a set of 5 parameters $\mathscr{P}_{3\mathrm{D}}$ of the 3D model, and a set of 3 outputs $\mathscr{O}$ listed in Table 5.1. We want to approximate the output values for $m = 30$ simulations with parameters x_i, drawn from a multivariate distribution (as in a CMA-ES iteration).

[4]https://models.physiomeproject.org/e/470

5.3.1 Global Strategy: Building a Mapping Between 3D and 0D Mechanical Parameters

Because they rely on the same equations, both models display many similar trends in their *global outputs* values when some parameters vary. For example, if a 3D simulation and a 0D simulation have the same stroke volume, the stroke volume variations with changes in the haemodynamic parameters (such as the aortic peripheral resistance) are very similar in both models.

However some parameters do not behave exactly the same, and are not always even in the same range of values. This is especially the case of **mechanical parameters** such as the 3D and 0D dampings which rely on different equations. But even for parameters from the same equations in both models (such as σ_0 and c_1) the values might be very different in 0D and 3D simulations with similar outputs, due to the different assumptions.

Formally, there is no trivial function which can convert the $x_i \in \Omega_{3D}$ into values $y \in \Omega_{0D}$ of 0D model parameters $\mathscr{P}_{\text{0D}}$, for which the global outputs values $\mathscr{O}_{\text{0D}}(y)$ and $\mathscr{O}_{\text{3D}}(x)$ are the same (or at least close). The idea of the *multifidelity coupling* is to find 0D model simulations which are similar to a few selected 3D simulations, then **build a parameter mapping ϕ between the parameters of both models**. We use the following strategy:

1. First we perform a few representative 3D simulations within the domain of interest (called the *sigma-simulations* with parameters $X_i \in \Omega_{3D}$).
2. Then, for each 3D sigma-simulation with parameter values $X_i \in \Omega_{3D}$, we estimate parameter values $Y_i \in \Omega_{0D}$ of a *coupled 0D simulation* which approximates the outputs $\mathscr{O}$ of the 3D sigma-simulation .
3. From those 3D model parameters X_i and 0D model parameters Y_i we derive a *parameter mapping* ϕ which converts 3D parameters into 0D parameters.
4. Finally, we approximate the global outputs values $\mathscr{O}_{\text{3D}}(x)$ of all the 3D simulations $x_i \in \Omega_{3D}$, from the 0D simulations with parameters $\phi(x_i) \in \Omega_{0D}$. This is done by adding a correction term ψ which is learnt, to avoid numerical errors in the previous steps.

The overall process is illustrated in Fig 5.2. In the sequel, we first discuss the selection of representative *sigma-simulations* (Sec. 5.3.2), then the computation of *coupled 0D simulations* (Sec. 5.3.3), then the *parameter mapping* ϕ (Sec. 5.3.4) and the *correction term* ψ (Sec. 5.3.5). Finally we give numerical results of the multifidelity approximation in Sec. 5.3.6.

5.3.2 Sigma-Simulations: Performing Representative 3D Simulations Within the Domain of Interest

We consider a subset $\mathscr{P}'_{\text{3D}} \subset \mathscr{P}_{\text{3D}}$ of $N_2 < N_1$ parameters which cannot be converted directly into 0D model parameters. In order to assess the global outputs

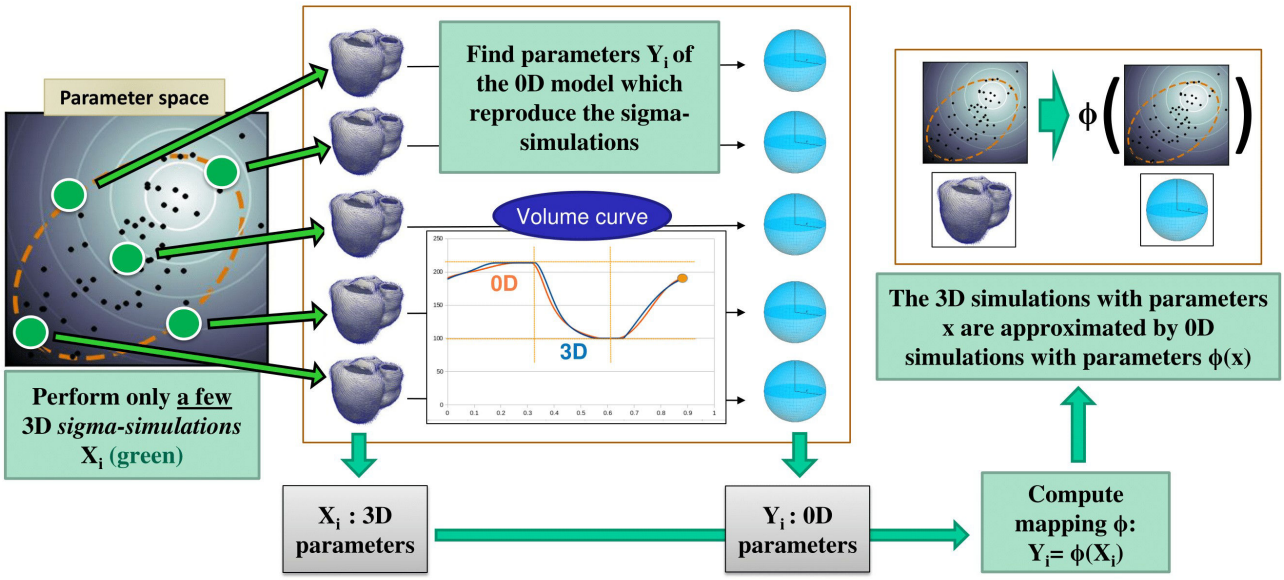

Figure 5.2: Multi-fidelity coupling: After performing a few 3D *sigma-simulations*, we find *coupled 0D simulations* for each of those simulations. Then we build a *parameter mapping* which converts parameters of the 3D model into parameters of the 0D model, in order to approximate 3D simulations outputs with the outputs of 0D simulations.

variations to these parameters in the set of $x_i \in \Omega_{3D}$, we perform a few selected simulations in the domain Ω_{3D}.

To this end, we perform PCA on the set of $x_i \in \Omega_{3D}$, which gives N_1 eigenvectors of the set. Then we extract the N_2 eigenvectors $\vec{d_k}$ which display the maximal variations of the parameters $\mathscr{P}'_{3D}$. This is done by sorting the eigenvectors by the norm of their projection of the subspace made by the coordinates corresponding to the parameters $\mathscr{P}'_{3D}$, and selecting the N_2 largest.

One *sigma-simulation* is then performed at the center (X_0) of the domain of interest Ω_{3D} and pairs are performed equidistant of X_0 in each of the N_2 extracted directions ($X_k^+ = X_0 + d_k$ and $X_k^- = X_0 - d_k$ for $k = 1..N_2$). This gives a total of $2N_2 + 1$ representative simulations in the domain.

In our example, the three haemodynamics parameters R_p, C and $P_{\mathbf{ve}}$ have the same values and the same equations in both models, so we can use the same values directly in the two models. On the other hand, the *contractility* σ_0 and the *stiffness* c_1 do not have the same values in both models so we need to assess how their variation is going to impact the global outputs. We then extract the $N_2 = 2$ directions for which the variations of σ_0 and c_1 are maximal, and perform a total of $2N_2 + 1 = 5$ sigma simulations with parameters X_0, X_1^+, X_2^+, X_1^- and X_2^-.

Table 5.2: *Coupling outputs*, *Coupled 3D parameters*, *Coupled OD parameters* which are estimated and *Directly Mapped Parameters* in the example of Fig 5.3.

Coupling outputs $\mathscr{O}$
Maximal Volume **Vmax**
Minimal Volume **Vmin**
Mean Aortic Pressure **MP**
Diastolic Aortic Pressure **DP**

Coupled 3D parameters $\mathscr{P}'_{0D}$
Contractility σ_0
Stiffness c_1

Directly Mapped Parameters
Peripheral resistance R_p
Aortic Compliance C
Venous Pressure $P_{\mathbf{ve}}$

Coupled 0D parameters $\mathscr{P}_{0D}$
Contractility σ_0
Stiffness c_1
Resting Radius r_0

5.3.3 Coupled 0D Simulations: Reproducing Global Outputs of the 3D Sigma-Simulations with 0D Simulations

Then for each sigma-simulation with parameters X_i, $i = 1..2N_2 + 1$ and output values $\mathscr{O}_{3D}(X_i)$, we want to find a corresponding 0D simulation which has similar global outputs values. To this end, we consider another set $\mathscr{O}'$ of global outputs called the *coupling outputs*, and a set of 0D parameters $\mathscr{P}'_{0D}$ called the *coupled 0D parameters*.

We then find values Y_i of the parameters $\mathscr{P}'_{0D}$ for which the *coupling outputs* values $\mathscr{O}'_{0D}(Y_i)$ of the 0D model simulations are the closest from the *coupling outputs* values $\mathscr{O}'_{3D}(X_i)$ of the 3D model sigma-simulations, with all other parameters being the same in both models. This is what we call a *coupled 0D simulation*.

This is done by performing, for each 3D sigma-simulation $k = 1..N_2$, an independent parameter estimation of the 0D model parameters $\mathscr{P}_{0D}$ using the method presented in Section 5.2.3. The target values $\widehat{\mathscr{O}'}$ for the coupling outputs $\mathscr{O}'$ are their values in the corresponding 3D sigma-simulation.

In our example, since we want to approximate outputs from the volume and pressure curves (see Table 5.1), we need to approximate these curves with the 0D model. We then chose a set of 4 *coupling outputs* $\mathscr{O}'$ from these curves, and a set of 3 *coupled 0D parameters* $\mathscr{P}_{0D}$ of the 0D model to estimate, both listed in Table 5.2.

After performing the 5 parameter estimations for the 5 sigma-simulations, we found 5 *coupled 0D simulations* with parameters Y_i, $i = 1..5$ which have similar *coupling outputs* values, which we report in Table 5.3. We also display the pressure and volume curves of the 3D sigma-simulations and *coupled 0D simulations* in Fig 5.3.

It is worth noting there is no guarantee that we can find a set of parameters for which the 0D simulation has exactly the same global outputs values as the 3D simulation. In fact, we can observe in Table 5.3 that some coupling outputs do not have the same values in a 3D sigma-simulation and the 0D corresponding coupled simulations. We will see in a subsequent section how this obstacle can be overcome.

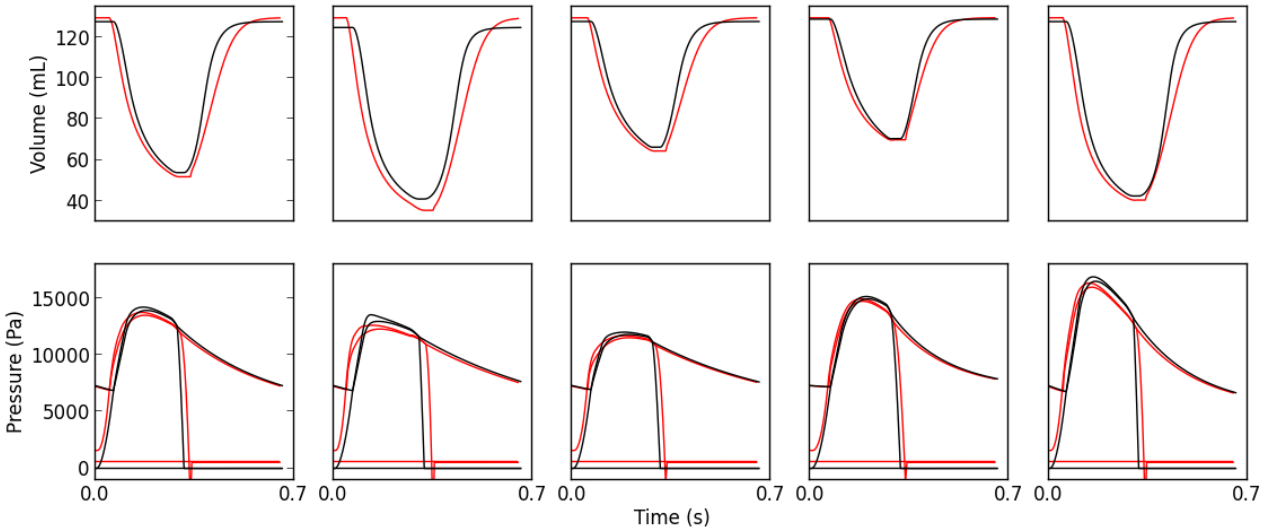

Figure 5.3: Comparison between the volume (top) and pressure (bottom) curves of the sigma-simulations simulated with the 3D model (red), and the corresponding *coupled 0D simulations* (black). The 5 columns correspond respectively to the sigma-simulations with parameters X_0, X_1^+, X_2^+, X_1^- and X_2^-.

Table 5.3: *Coupling outputs* values for the 3D sigma-simulations with parameters X_i and the corresponding *coupled 0D simulations* with parameters Y_i

	Vmax (ml)	Vmin (ml)	MP (Pa)	DP (Pa)
X_0	129	51.8	10278	7290
X_1^+	129	35.5	10034	7590
X_2^+	129	64.4	9556	7614
X_1^-	129	69.8	10743	7906
X_2^-	129	40.4	10761	6664
Y_0	128	53.9	10318	7310
Y_1^+	125	41.0	10107	7679
Y_2^+	128	66.3	9591	7634
Y_1^-	129	70.4	10759	7910
Y_2^-	128	42.5	10806	6683

We point out that there are many possibilities to choose the sets of *coupling outputs* $\mathscr{O}'$ and *coupled 0D parameters*. For example, another possibility would have been to use directly the set of outputs to approximate $\mathscr{O}$. This would have lead to 0D and 3D simulations with the same stroke volume, but not necessarily the same minimal and maximal volumes. In general the sets of $\mathscr{O}'$ and $\mathscr{O}$ have to be related so that it is possible to calculate the values of the outputs $\mathscr{O}$ from the values of the *coupling outputs* $\mathscr{O}'$.

Similarly, there are many possibilities to choose the sets of *coupling 0D parameters*. Here we could also have set the resting radius in the 0D model to a value

for which the "resting volume" is the same than in the 3D model, then estimate only the *stiffness* and *contractility* of the 0D model. Empirically, it seems to be a good thing to use more parameters to avoid ending in a local minimum during the parameter estimation of the *0D simulations*.

5.3.4 Parameter Mapping: A Function to Convert 3D Model Parameters into 0D Model Parameters

We now have a corresponding *coupled 0D simulation* with parameters $Y_i \in \Omega_{0D}$ for each sigma-simulation with parameters $X_i \in \Omega_{3D}$. The second idea of the coupling is to build a mapping ϕ between the 3D and 0D model parameters using the X_i and Y_i. This mapping will then be used to approximate global outputs values $\mathscr{O}_{3\text{D}}(x_i)$ of the 3D simulations with parameters x_i, from the values $\mathscr{O}_{0\text{D}}(\phi(x_i))$ of the 0D simulations with parameters $\phi(x_i)$.

The parameters $X_i \in \Omega_{3D}$ were chosen in a specific way in Section 5.3.2: one (X_0) is at the center of the x_i and there are two equidistant of X_0 (X_k^+ and X_k^- for $k = 1..N_2$) for each of the N_2 axis, which are orthogonals from each other. However, the Y_i were independently estimated for each sigma-simulation so there is no such relationship.

For the mapping ϕ we use here a degree 2 hypersurface which interpolates the Y_i in the points X_i. In dimension 1 this is equivalent to finding a degree 2 polynomial which interpolates three specific points. In higher dimension (N_2 in our case), there is a straightforward formula because of the specific organisation of X_i along orthogonal axis:

$$\begin{cases} c_k = (x - \vec{X_0}) \cdot \frac{\vec{d_k}}{||\vec{d_k}||^2}, k = 1..N_2 \\ \vec{F_k^+} = \frac{(Y_k^+ - Y_0) + (Y_k^- - Y_0)}{2}, k = 1..N_2 \\ \vec{F_k^-} = \frac{(Y_k^+ - Y_0) - (Y_k^- - Y_0)}{2}, k = 1..N_2 \\ \phi(x) = Y_0 + \sum_{k=1}^{N_2} c_k \cdot (c_k \cdot \vec{F_k^+} + \vec{F_k^-}). \end{cases} \tag{5.1}$$

This formula leads to $\phi(X_i) = Y_i$ for all the $i = 1..2N_2 + 1$ sigma-simulations, so the parameters of the 3D sigma-simulations are mapped to the parameters of the *coupled 0D simulations* of the previous section. We will then use this mapping to approximate global outputs of 3D simulations with parameters x_i from 0D simulations with parameters $\phi(x_i)$.

5.3.5 Approximating Global Outputs: Correcting Bias

Ideally in the computation of *coupled 0D simulations* in Section 5.3.3, we find 0D simulations with the same coupled outputs values than the 3D sigma-simulations i.e. $\mathscr{O}'_{3\text{D}}(X_i) = \mathscr{O}'_{3\text{D}}(Y_i)$. As illustrated in Table 5.3, this is not always the case and the *coupled outputs* values can be different between the *coupled 0D simulations* and the sigma-simulations. This also means that the direct approximation of the sigma-

simulations output values $\mathscr{O}_{3D}(X_i)$ by the values $\mathscr{O}_{0D}(Y_i)$ through the mapping has a bias due to this difference.

In order to correct this approximation bias, both for the output values of the sigma-simulations and all the subsequent 3D simulations with parameters x_i, we build a new degree 2 hypersurface ψ between the parameters of the sigma-simulations X_i and the bias. The formula is exactly the same as in Equation 5.1 where the Y_i are replaced by the bias values $(\mathscr{O}_{3D}(X_i) - \mathscr{O}_{0D}(Y_i))$.

The final *approximating function* $\mathscr{C}_{\phi,\psi}$ used to approximate the $\mathscr{O}_{3D}(x_i)$ is then given by the following formula:

$$\mathscr{C}_{\phi,\psi}(x_i) = \mathscr{O}_{0D}(\phi(x_i)) + \psi(x_i) \approx \mathscr{O}_{3D}(x_i), \tag{5.2}$$

and interpolates in particular the *global outputs* values $\mathscr{O}_{3D}(X_i)$ of the sigma-simulations.

5.3.6 Approximation Results

Results are given here for the approximation of the *global outputs* values $\mathscr{O}_{3D}(x_i)$ of the 30 simulations with parameters x_i. We compute the mean absolute error made on the approximation of the 3 global outputs $\mathscr{O}$, first with the biased approximation with $\mathscr{O}_{0D}(\phi(x_i))$ (MAE_{Biased}), then with the corrected approximation with $\mathscr{C}_{\phi,\psi}$ ($MAE_{\text{Corrected}}$). Results are reported in Table 5.4.

We observe a good approximation of the output values compared to the range of values to be approximated, and that the *corrected approximation* makes a better approximation of the outputs values than the *biased approximation*. This means the hypersurface ψ indeed corrects errors due to the differences between the *coupled 0D simulations* and the 3D sigma-simulations.

Table 5.4: Error in the approximation of the global outputs values $\mathscr{O}_{3D}(x_i)$ with the various methods.

Global Output	SV (ml)	DP (Pa)	MP (Pa)
Range	38.23	3010	2254
$MAE_{\text{Corrected}}$	1.59	56.4	137
MAE_{Biased}	4.58	62.8	140
$MAE_{\text{Hypersurface}}$	2.09	511	408
$MAE_{\text{Hypersurface-11}}$	0.25	174	93

Finally, we compare our method to an interpolation with a degree 2 hypersurface ($MAE_{\text{Hypersurface}}$). To this end we use the same formula than Equation 5.1, where the Y_i are replaced by the output values $\mathscr{O}_{3D}(X_i)$. We see in particular that our method performs better on all the outputs ($MAE_{\text{Corrected}} < MAE_{\text{Hypersurface}}$), in particular on the pressure values. This is because the sigma-simulations are computed only in the directions of maximal variations of the parameters σ_0 and c_1 (see

Section 5.3.2). There is then a few directions of the parameter space in which the variations of global output values could not be evaluated by the interpolation.

In order to compare more fairly to an interpolation method, we computed the sigma-simulations in all the directions of the domain by selecting all the eigenvectors in Section 5.3.2, leading to $2 \cdot N_1 + 1 = 11$ sigma-simulations. We performed the degree 2 interpolation from these 11 sigma-simulations and report the results ($MAE_{\text{Hypersurface-11}}$). The degree 2 hypersurface performs better than our method on the stroke volume and the mean pressure but not on the diastolic pressure.

We conclude that the approximation using the coupling of the 0D and 3D models gives competitive approximation results compared to the classical regression methods, and with the lowest computational cost. This is because the variations of some outputs (which rely on the same equations in both models) can be directly approximated in some directions of the parameter space, without having to compute 3D simulations in these directions. Here in particular, the pressure outputs variations due to changes in the haemodynamic parameters C, R_p and P_{ve} are correctly predicted with the coupling (especially the Diastolic Aortic Pressure (DP) variations), even though no sigma-simulation was computed in the directions of maximal variation of these parameters (Section 5.3.2). As a consequence, only 5 sigma-simulations are required to approximate all the outputs values within the parameter space with the coupling, while the hypersurface interpolation needs 11 sigma-simulations to achieve similarly accurate results.

5.4 Multi-Fidelity Optimization for Efficient 3D Cardiac Model Personalisation

Here we present our *multifidelity personalisation method* for the 3D model. We suppose a parameter estimation with CMA-ES was set up over N_1 parameters $\mathscr{P}$ of the 3D model as described in Section 5.2.3, some global outputs $\mathscr{O}$, some target values $\widehat{\mathscr{O}}$ and a population size m. The idea of the method is to replace the scores of 3D simulations in CMA-ES with *approximate scores* calculated through *multifidelity coupling*.

We illustrate the method with the same set of 5 parameters $\mathscr{P}$ and 3 outputs $\mathscr{O}$ as in Section 5.3 and the same number $m = 30$ for the population size. Target values $\widehat{\mathscr{O}}$ for the optimization are respectively **60 ml** for the Stroke Volume (SV), **7315 Pa** for the Diastolic Aortic Pressure (DP) and **10152 Pa** for the Mean Aortic Pressure (DP). The normalisation coefficients for this problem (in the vector $\mathscr{N}$ defined in Section 5.2.3.1) are **10 ml** for the Stroke Volume (SV), **200 Pa** for the Diastolic Aortic Pressure (DP) and the Mean Aortic Pressure (DP).

5.4.1 Multifidelity-CMA: CMA-ES Optimisation with the Multifidelity Coupling

At each iteration, the algorithm CMA-ES asks for the scores of m simulations of the 3D model, whose parameters x_j are drawn from a multivariate distribution.

A first approach to replace the computation of the 3D simulations by 0D simulations is to perform the coupling described in Section 5.3 for each generation of CMA-ES. This means recomputing sigma-simulations, *coupled 0D simulations* and a parameter mapping for each set of x_j. This was our approach (called *Coupled-CMA*) in [Mollero 2016]. We showed that the optimisation could converge with *approximate scores*, even as fast as with the real scores in some cases. We also personalised 34 hearts with this method, thus exhibiting a practical personalisation method with a lower computational burden than the original CMA-ES algorithm (because only the *sigma-simulations* were computed for each generation instead of the m 3D simulations).

Here we present an improved approach called *Multifidelity-CMA*. Instead of recomputing the coupling for each generation, we approximate scores of 3D simulations of *successive generations of CMA-ES*. Indeed, because the sets of parameters x_j^n and x_j^{n+1} asked by CMA-ES in two consecutive generations n and $n+1$ are usually close, the function $\mathscr{C}_{\phi,\psi}$ computed at the iteration n to approximate 3D simulations with parameters x_j^n, can give a good approximation for 3D simulations with parameters x_j^{n+1} as well.

On the other hand, after a few iterations $n+1..n+p$, the points asked by CMA-ES can be increasingly far from the *sigma-simulations* of the *multifidelity coupling* performed at n. This can lead to approximations of the scores which are increasingly inaccurate, making the optimisation impossible.

We then developed a criterion to evaluate the accuracy of the approximation for a few successive iteration of CMA-ES, then decide at which step a new *multifidelity coupling* has to be computed. This is done by iterating on the following steps:

1. **Coupling step.** At a generation n_0 of CMA-ES, we first perform a *multifidelity coupling*, as explained in 5.3.4. This leads to the computation of the function $\mathscr{C}_{\phi,\psi}$.

2. **Exploration step**. Then, we perform N iterations $n = n_0 + 1..n_0 + N$ of the CMA-ES algorithm, where all the outputs $\mathscr{O}_{3D}(x_j^n)$ of the 3D simulations with parameters x_i^n are approximated by $\mathscr{C}_{\phi,\psi}(x_j^n)$.

3. **Control step.** For each of these N iterations, we compute a *control-simulation*: the 3D simulation whose parameters o_n are the mean of the population parameters x_j^n.

4. **Selection step**. We compute our *criterion* $M(o_n)$ as the *Mahalanobis distance* between the vector of outputs values $\mathscr{O}_{3D}(o_n)$ of the control-simulation and the set of vectors of approximated outputs values $\mathscr{C}_{\phi,\psi}(x_j^n)$.

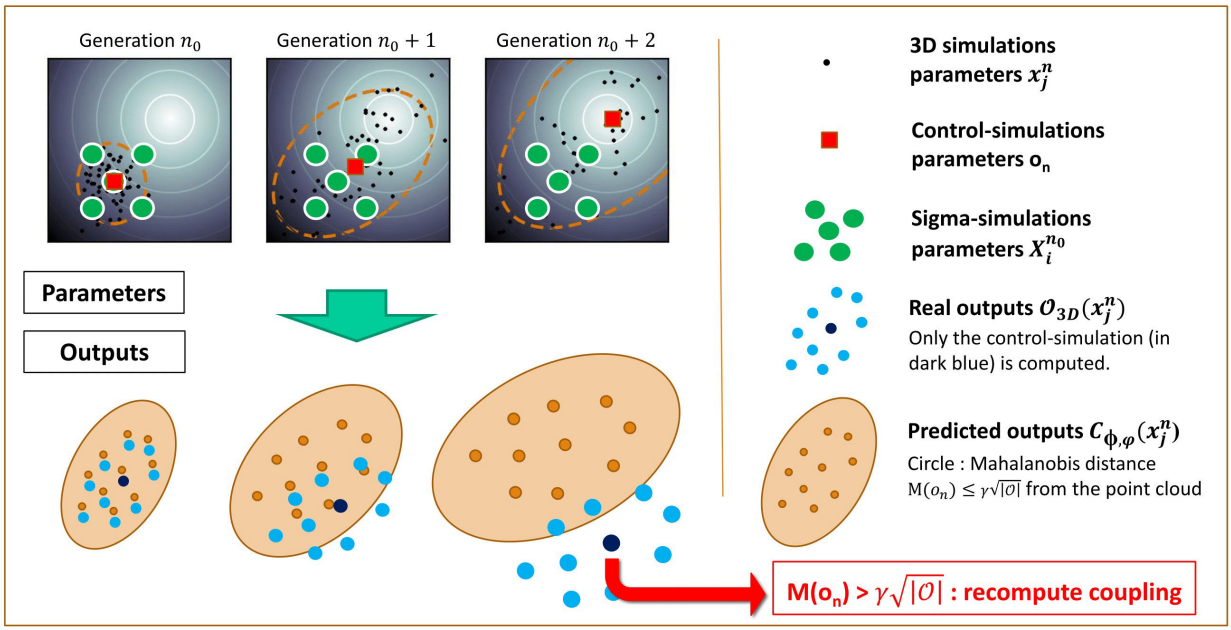

Figure 5.4: Criteria for selecting the generation for the next **coupling step** in the **selection step**: as the 3D parameters of the simulations asked by CMA-ES (in black) are increasingly far from the sigma-simulations (in green) of the coupling, the predicted outputs values with 0D simulations (in orange) are increasingly far from the real outputs values of the 3D simulations. We then recompute the coupling when this distance is too high ($M(o_n) > \gamma\sqrt{|\mathcal{O}|}$).

Finally we select the iteration $n*$ at which the next **coupling step** is performed with the following criteria:

$$n* = \underset{M(o_n) < \gamma\sqrt{|\mathcal{O}|}}{\operatorname{argmin}} \mathcal{O}_{3\mathrm{D}}(o_n)$$

The process is illustrated in Fig 5.4. The Mahalanobis distance $M(o_n)$ is a ratio between the approximation error on the *control-simulation* output values, and the range of *approximate outputs values* for this generation. Roughly, this gives an indication on "how accurate the coupling is" on the *control-simulation*, compared to "how accurate it needs to be" so that CMA-ES can rank the scores accurately.

For example in Fig 5.5, we report for $N = 10$ iterations the scores of the control-simulations o_n which were predicted through the function $\mathscr{C}_{\phi,\psi}$ (in black), and the real scores of these simulations (in blue). Simultaneously, we show the criterion $M(o_n)$ for these N iterations and the upper value (red line) $\gamma\sqrt{|\mathcal{O}|}$ for the criterion ($\gamma = 1.5$ here).

We can see that the score prediction (thus the approximation of the outputs $\mathcal{O}_{3\mathrm{D}}(x_j^n)$ values by $\mathscr{C}_{\phi,\psi}$) is quite accurate for at least the 5 first iterations, and is less accurate for $n \geq 6$. Then, even though the score prediction seems as accurate at the iteration 5 than at the generation 1, $M(o_n)$ is higher. This is because the

prediction error is more important *relatively to the set of* $\mathscr{C}_{\phi,\psi}(x_j^n)$ of the generation, in particular in directions where the set has a lower variance.

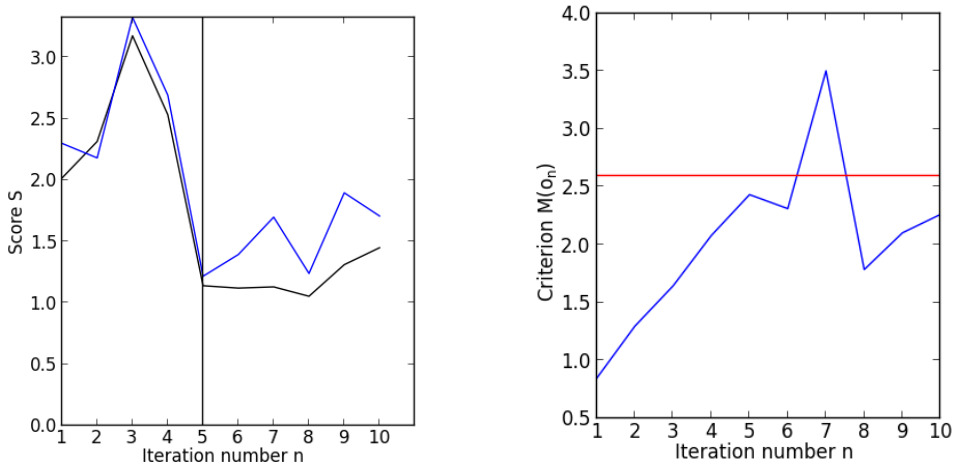

Figure 5.5: Top: real scores (blue) and approximated scores (black) of the N=10 control-simulations. Bottom: Value of the criterion $M(o_n)$ of the control-simulations.

In this example, the iteration 5 was selected to recompute the coupling (black vertical line), which is also the iteration where the control simulation has the minimal score over the 10 iterations. In some cases, later iterations can have a lower score but are not selected because the criterion $M(o_n)$ is too high for this iteration (such as the iteration 7).

The upper bound $\gamma\sqrt{|\mathscr{O}|}$ for the criterion has an important impact on the optimisation behavior. If a high accuracy is imposed (small γ value), then one of the earlier iterations of the **exploration step** is usually selected for the subsequent **coupling step**, even if a later control-simulation has a lower score. This can lead to a slow optimization. On the other with a small accuracy (high γ value) the CMA-ES algorithm can end up in local minima because it performed the optimization on inaccurate values.

Therefore the value of γ characterizes a trade-off between maximising the optimisation gain with a single coupling, and ensuring the approximation errors do not impact the optimisation process. Because of the probabilistic nature of the algorithm and the various non-linearities of the score function, the optimal value of γ seems very dependent on the optimisation problem. We found $\gamma = 1.5$ to give good convergence results in our experiments and the number $n*$ of the iteration selected in the **selection step** is 5.5 in average in our experiments.

5.4.2 Computational Considerations: A Parallelisable Method

The main computational cost in personalisation methods comes from the computation of the 3D simulations. In our implementation, each simulation of one heartbeat

with the 3D model uses one CPU, during a time T_{3D} which depends mostly on the size of the mesh, and the heartbeat duration.

Most of the modern research is performed on computer clusters which can perform many tasks at the same time. In particular in our method, many steps can be parallelised. To compare different optimization methods in a parallel setting, we introduce here two metrics: the classic *CPU Time* which measures the total amount of CPU resources used, and the *Optimization Time* which measures the duration of the optimization in (real) time.

During one complete iteration of *Multifidelity-CMA*, the following steps are parallelised:

1. Computation of the $2N_2 + 1$ 3D sigma-simulations: the simulations are performed in parallel and each one takes a CPU Time T_{3D}. The whole step has then a *CPU Time* of $(2N_2 + 1) \cdot T_{3D}$ and an *Optimization Time* of T_{3D}

2. Computation of the *coupled 0D simulations*: all the parameter estimations are performed in parallel. Each one uses 4 CPUs during fixed time of around 3 minutes. The whole step has a CPU Time of $(2N_2 + 1) \cdot 4 \cdot$ 3 minutes and an *Optimization Time* of 3 minutes.

3. Computation of the N 3D control-simulations: the simulations are performed in parallel and each one takes a CPU Time T_{3D}. The whole step has a *CPU Time* of $N \cdot T_{3D}$ and an *Optimization Time* of T_{3D}

In our example we have 5 sigma-simulation and 10 control-simulation, and the 3D simulation takes 15 minutes. Each iteration of *Multifidelity-CMA* then takes a total *CPU Time* of 5*15+4*5*3+10*15 = 285 minutes and an *Optimization Time* of 33 minutes.

5.4.3 Results: Comparison of Optimization Time, CPU Time for 4 Personalisations Methods

Here we compare the evolution of the *CPU Time* and the score S during optimization on a typical case, with the 4 following optimization methods:

1. The *Multifidelity-CMA* method with 0D/3D coupling.

2. The *Multifidelity-CMA* method where the approximation of outputs is done with a degree 2 hypersurface interpolation relying on 11 sigma-simulations (as explained in Section 5.3.6).

3. The classic CMA-ES method with a population size of $m = 30$.

4. BOBYQA, which is another commonly used gradient-free optimizer for example to solve personalisation problems [Seegerer 2015] or as a baseline to evaluate other personalisation methods [Neumann 2016]. It uses *trust region* method and forms successive quadratic models of the score function which interpolates the points computed during optimization.

Figure 5.6: Comparison of the evolution of the score S (top) and CPU Time (bottom) during optimization for the four methods. BOBYQA is in red, the classic CMA-ES is in blue, Multifidelity-CMA with the hypersurface approximation is in black and Multifidelity-CMA with 0D/3D coupling is in green.

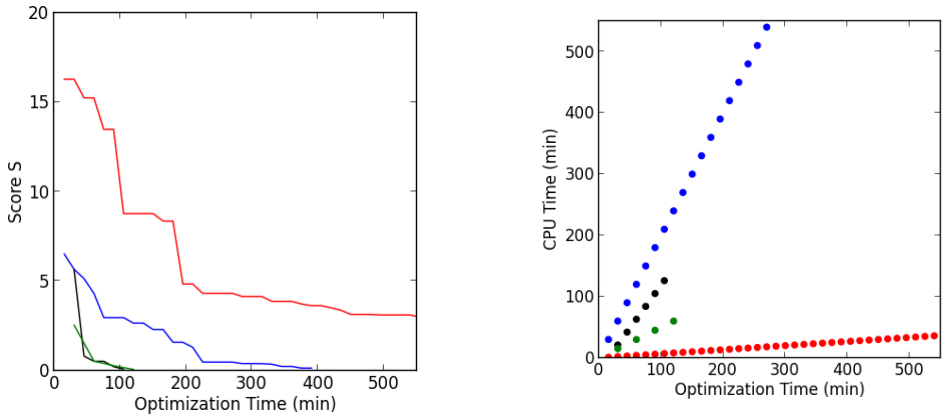

Results are shown in Figure 5.6. We can see that BOBYQA (red) is slow to converge, but has also a low computational cost, both due to the fact that BOBYQA performs only one iteration at a time. The normal CMA-ES (blue) converges faster than BOBYQA, but with a very high computational cost because 30 simulations of the 3D model are computed at each generation.

Finally, both our multifidelity approaches are very fast to converge, however the *Multifidelity-CMA* which uses the 0D/3D *multifidelity coupling* is the one with the lowest CPU Time (because only 5 sigma-simulations per complete iteration is computed instead of 11, as explained in Section 5.3.6).

We conclude than the multifidelity approach of the CMA-ES algorithm leads to considerable improvements in optimization speed, both from the original CMA-ES algorithm and BOBYQA. Finally, the approximation of outputs with a 0D/3D *multifidelity coupling* instead of a generic hypersurface interpolation leads to additional computational gains.

5.4.4 Results: Personalisation of a Database of 121 cases

We finally present results on a large database of 121 cases. For each patient, a biventricular heart mesh geometry (between 10 000 and 15 000 nodes) was built from the available MRI image and the boundaries of the myocardium were tracked in the cine MRI images as described in [Jolly 2011] and [Wang 2013b]. This led to the computation of the volume curve, then the value of the stroke volume. Pressure measurements were also available for each heartbeat.

We applied our **Multifidelity-CMA** method to personalise the whole cohort. The optimization started from a vector x_{start} of parameter values which has the same values for every patient, except for P_{ve}, which is set at the value $DP - 2000Pa$ (see Table 5.6). The algorithms ran for around 2.5 days, and the BOBYQA optimization

was ran on the same problems during this period as well.

We consider a personalisation to be *successful* when a set of parameter values was found with a score lower than $l_1 = 0.1$, and *acceptable* if the score is lower than $l_2 = 1$. This means the personalised simulation matches the target stroke volume within 1 ml and the pressure measurements within 20 Pa for the *successful* case, and within respectively 10 ml and 200 Pa in the *acceptable* case. In other cases the personalisation is said *failed*. We report the number of *successful*, *acceptable* and *failed* cases on this database, for both methods in Table 5.5.

Table 5.5: Results of the personalisation on the database.

Result	Successful	Acceptable	Failed
Multifidelity-CMA	113	6	2
BOBYQA	5	69	47

A high number of cases were successfully personalised (113 among 121 cases) with our method. For the acceptable cases, and one of the failed case, the optimization had converged in a local minima. For the other failed case, the CMA-ES algorithm diverged to extreme parameter values during optimization. For BOBYQA, the convergence was not yet reached in most of the non-successful cases (the score is the lowest in the last iteration).

We finally report the mean and standard deviation of all the estimated parameter values, in Table 5.6, as well as the norm of their relative variation $|\Delta|$ compared to the *starting value* during the optimization. This shows in particular that the stiffness c_1 did not change a lot during the personalisation process. The aortic compliance C and the contractility σ_0 are the parameters which changed the most.

Table 5.6: Statistics of the estimated parameter values and their variations during the personalisation.

	c_1 (kPa)	σ_0 (MPa)	P_{ve} (Pa)	R (MPa.m^3.s)	C (MPa^{-1}.m^{-3})
x_{start}	50.1e^1	68.8	DP-2000	54.1	18.0e^{-3}
Mean	50.5e^1	91.6	4760	68.2	8.17e^{-3}
Std.	0.36e^1	36.5	1340	16.3	2.41e^{-3}
Mean $\|\Delta\|$	4.74%	53.9%	26.2%	35.8%	54.7%

5.5 Discussion and Conclusion

We presented a novel multifidelity approach involving a 3D cardiac electromechanical cardiac model and a simplified 0D model, which relies on the same equations but with simplifying assumptions. We developed an original *multifidelity coupling* between the parameters of both models, which gives a good *multifidelity approximation* of *global output values* in 3D simulations from 0D simulations. We then used

this approximation in an efficient parameter estimation process using the genetic algorithm CMA-ES, in order to have an efficient *multifidelity personalisation method* for the 3D model.

Our *multifidelity coupling* procedure computes a mapping between the parameters of a few representative 3D *sigma-simulations* within the domain, and the parameters of corresponding *coupled 0D simulations* with the same output values. This is done through parameter estimation on the 0D model parameters to compute *coupled 0D simulations* that have the same *global outputs values* than 3D *sigma-simulations*. The parameter mapping is then derived through an interpolation method.

This enables to get fast and accurate approximations of 3D simulations with the 0D model. These approximations are then used in the parameter estimation of 3D model parameters with CMA-ES, to replace 3D simulations while simultaneously controlling the accuracy of the approximation and recomputing a coupling when the accuracy is too low. Ultimately, this results into both an increase of the speed of the 3D parameter estimation process and a decrease of the computational cost.

Our multifidelity approach slightly differs from more classic multifidelity methods [Kennedy 2000, Peherstorfer 2016] where the same parameter values are used as input of both models, and the outputs of the low-fidelity model are corrected *a posteriori* to fit the outputs of the high-fidelity model. Since the parameters of both models are not exactly the same, we had to find a mapping between the *parameters* instead of the *outputs*. This was tractable thanks to the fast parameter estimation in the 0D model.

A first extension of the *multifidelity coupling* would be to use additional shared parameters and equations in both models, to approximate a larger variety of outputs of the 3D model (e.g. flow velocities, timings of valve opening and closing). Since CMA-ES has already been proven successful on complex optimisation problems with a larger parameter space, we expect the personalisation method to scale well. A second extension would be to use the *multifidelity personalisation* to personalise "geometrical" or "local" measurements which are outputs of the 3D model but not of the 0D model (e.g. the septal shortening or the circumferential torsion). Indeed, even though they cannot be approximated through the 0D/3D *multifidelity coupling*, their values can still be locally approximated during personalisation using the hypersurface interpolation.

Finally, the lower-fidelity approximation could be used not only for personalisation but also for other applications that require many simulations, such as parameter sensitivity or uncertainty quantification (with Monte-Carlo methods for example) and also for applications simulations that require the computation of many cardiac cycles. In particular, a case where the multifidelity approach could be useful is when the 3D model is coupled with a full-body circulation model as boundary conditions. Indeed, studies associated to such models (for example on the influence of physical exercise, increased heart rate and/or pressure loads) usually require many heartbeats to be computed. This can be computationally intensive with the 3D model but, it could be done faster using 0D simulations, through a similar coupling method. In this case where the number of coupled parameters would be high,

additional constraints could be added in the parameter mapping to impose correlations between parameters with different equations or values but a similar behavior.

Compliance with Ethical Standards : Informed consent was obtained from the subjects and the protocol was approved by the local Research Ethics Committee.

5.6 APPENDIX: Reduced Equations of the 0D model

$$
\begin{cases}
\dot{k_c} = -(|u|_+ + |u|_- + \alpha|\dot{e_c}|)k_c + k_0|u|_+ & \text{(a)}\\
\dot{\tau_c} = -(|u|_+ + |u|_- + \alpha|\dot{e_c}|)\tau_c + \dot{e_c}k_c + \sigma_0|u|_+ & \text{(b)}\\
(\tau_c + \mu\dot{e_c}) = E_s\dfrac{(e_{1D} - e_c)(1 + 2e_{1D})}{(1 + 2e_c)^3} & \text{(c)}\\
C = (1 + \dfrac{y}{R_0})^2 & \text{(d)}\\
e_{1D} = \dfrac{C - 1}{2} & \text{(e)}\\
\sigma_{1D} = E_s\dfrac{e_{1D} - e_c}{(1 + 2e_c)^2} & \text{(f)}\\
\sigma_{\text{passive}} = 4(1 - C^{-3})(c_1 + c_2C) & \text{(g)}\\
\sigma_{\text{viscosity}} = 4\eta(1 + C^{-6})\dot{C} & \text{(h)}\\
\Sigma_{\text{sph}} = \sigma_{1D} + \sigma_{\text{passive}} + \sigma_{\text{viscosity}} & \text{(i)}\\
\rho d_0\ddot{y} = P_v(1 + \dfrac{y}{R_0})^2 - \dfrac{d_0}{R_0}(1 + \dfrac{y}{R_0})\Sigma_{\text{sph}} & \text{(j)}\\
q = 4\pi R_0^2(1 + \dfrac{y}{R_0})^2\dot{y} = \begin{cases} K_{\text{at}}(P_V - P_{\text{at}}) & \text{for } P_V \le P_{\text{at}} \\ K_{\text{iso}}(P_V - P_{\text{at}}) & \text{for } P_{\text{at}} \le P_V \le P_{\text{ar}} \\ K_{\text{ar}}(P_V - P_{\text{at}}) + K_{\text{iso}}(P_{\text{ar}} - P_{\text{at}}) & \text{for } P_V \ge P_{\text{ar}} \end{cases} & \text{(k)}\\
R_pC\dot{P_{\text{ar}}} + P_{\text{ar}} - P_{\text{ve}} = (R_p + Z_c)q + R_pZ_cC\dot{q} & \text{(l)}
\end{cases}
$$

Table 5.7: Mechanical equations of the 0D model

5.6.0.1 Mechanical Equations

The list of simplified equations of our 0D model is reported in Table 5.7. Equations (a), (b), (c) and (f) are the same sarcomere and visco-elastic equations than Equations 3.1 & 3.3, which are calculated once for the whole sphere. C in equations (d), (e), (g) and (h) denotes a component of the simplified Cauchy-Green deformation tensor which depends only on $y = R - R_0$. σ_{passive} in equation (g) is the stress due to the passive law and $\sigma_{\text{viscosity}}$ in equation (h) is the stress due to an additional viscous damping η, both expressed as a simple function of C (see [Caruel 2014] for

the full derivations). In equation (i), Σ_{sph} is the sum of all the stresses applied to the sphere. Equation (j) is the resulting equation of motion which, coupled with the haemodynamic model (k) and the windkessel equation (l), gives the full system of 3 equations to be solved at each iteration.

5.6.0.2 Electrophysiology Equations

Assuming synchronous and homogeneous electrical activation (and thus sarcomere force) means that all of the ventricle is depolarised simultaneously. This leads to a rate of ventricular pressure rise during the isovolumetric contraction (resp. isovolumetric relaxation) which is very close to the rate of build-up k_{ATP} (resp. decrease k_{RS}) of the active stress τ_c. However in 3D, this rate is also very dependent on the time for the ventricle to be fully depolarised, which is roughly the QRS duration.

$$
\begin{aligned}
f &= \begin{cases}
\dfrac{t - T_{d,global}}{QRS_{\text{duration}}} & \text{when } T_{d,global} \leq t \leq T_{d,global} + QRS_{\text{duration}} \\
1 & \text{when } T_{d,global} + QRS_{\text{duration}} \leq t \leq T_{r,global} \\
(1 - \dfrac{t - T_{r,global}}{QRS_{\text{duration}}}) & \text{when } T_{r,global} \leq t \leq T_{r,global} + QRS_{\text{duration}} \\
0 & \text{otherwise}
\end{cases} \\
|u|_{+} &= k_{\text{ATP}}.f_{\text{depo}} \\
|u|_{-} &= k_{\text{RS}}.(1 - f_{\text{depo}})
\end{aligned}
\tag{5.3}
$$

Table 5.8: Electrical activation in the 0D model

In order to correct this discrepancy between the models, we adapted the electrical parameter u to take into account the QRS duration. We model the fraction f_{depo} of the ventricle which is currently depolarised as a piecewise linear function of time which depends on $T_{\text{d,global}}$, $T_{\text{r,global}}$ and QRS_{duration}. Then the values of $|u|_{+}$ and $|u|_{-}$ in Equation (a) are adapted to depend on the value of f_{depo} as described in Table 5.8.

Chapter 6

Longitudinal Parameter Estimation in 3D Electromechanical Models: Application to Cardiovascular Changes in Digestion

Contents

After building an efficient personalisation algorithm in ***Chapter 5****, we built personalised simulations of all the cases available in the MD-Paedigree project. We then studied applications of these personalised simulations for longitudinal modeling and analysis of the cardiac function, which we present through two studies, in this chapter, and in* ***Chapter 7****.*

The study in this chapter is a joint work on the `CVD-UCL` *cohort with the* ***Great Ormond Street Hospital for Children****, which was presented at the FIMH conference in 2017 [Molléro 2017c]. For 21 patients, we build personalised simulations of* complete acquisitions *at two instants (before and within 1h30 after ingestion of a high-fat high-calorie meal) and we analyse the trends in personalised parameters evolution in relation to real physiological phenomena during mild exercise. This enables to build a simple multilinear law of cardiovascular parameter changes which we show to be accurate for the fast simulation of the second timepoint.*

6.1 Introduction

The main function of the heart is to create the necessary blood flow through the cardiovascular system, so that the oxygen supply of all the organs meets their needs. When an organ or a part of the body needs more energy (such as the muscles during exercise, or the digestive system during digestion), the heart rate and the blood flow increase because the overall demand in oxygen is higher.

The main changes in the cardiac function leading to an increase of the cardiac output are an increased heart rate, a decreased action potential duration and an increased contractility (positive inotropy). When the cardiac output increase is small (such as digestion or a mild exercise), the systolic pressure usually increases but the diastolic pressure is constant, the latter being a consequence of the dilation of the arteries which lowers the arterial resistance [Laughlin 1999]. Those qualitative changes are well-known, but are rarely quantified in the context of 3D cardiac electromechanical models, in part because most studies only involve personalisations on a single beat only (see [Chabiniok 2016] for a complete review).

A clinical study was performed in [Hauser 2016] to assess the cardiovascular response to a food stress protocol, involving the ingestion of a high-energy meal after fasting for 12h. From the data of this study, we propose a consistent estimation of patient-specific 3D cardiac electromechanical models at two different instants of the protocol (pre-ingestion and t+1h). We first calibrate both the biomechanical parameters which are constant in time (such as the myocardial fibre directions) and time-varying (such as the arterial resistance) from the pre-ingestion measurements and heart motion extracted from the MRI. Then, we re-estimate values of the time-varying parameters (contractility and haemodynamics parameters) to reproduce changes in cardiac output and blood pressure at the second instant.

From these personalised simulations, we analyse the trends of the estimated parameters in relation to known physiological changes during mild exercise [Otsuki 2006, Albert 1952]. Finally, we build a law of evolution of the biomechanical parameters which leads to arbitrary changes of both the simulated cardiac output and stroke volume, while maintaining the same mean and diastolic pressure. The good accuracy of this law, which we validate with cross-validation over the 21 patients, then opens the door to the fast simulation of hearts during digestion in future patients.

6.2 Clinical Study and Data

More than 80 patients participated to a clinical study to assess the cardiovascular response after the ingestion of a high-energy (1635 kcal), high-fat (142g) meal after fasting for 12h, following the stress protocol in [Hauser 2016]. Informed consent was obtained from the subjects and the protocol was approved by the local Research Ethics Committee. An objective of the study was to analyze the evolution of blood flow toward the various organs of the body. In particular, a short axis cardiac cine MRI sequence was acquired before the ingestion, as well as measurements of the

	SP (mmHg)	DP (mmHg)	MP (mmHg)	SV (mL)	CO (L/min)	HR (bpm)
Mean	117.13	60.95	84.16	92.11	6.17	67.65
Std.	9.99	6.45	5.98	19.69	1.34	10.25
Mean Δ (%)	-	-	-	-0.10	**17.58**	**17.76**
Std. Δ (%)	-	-	-	**11.43**	17.74	13.19

Table 6.1: Statistics of the measurements and their evolution Δ between T_1 and T_2 (in percentage of the value at T_1). Systolic, Diastolic and Mean cuff Pressure (SP, DP, MP), Stroke Volume (SV), Cardiac Output (CO) and Heart Rate (HR).

stroke volume, systolic, diastolic and mean cuff pressures at several time points within 1h of the ingestion of the meal. Two instants are considered in particular: T_1 which is before the meal ingestion, and the latest measurement time T_2 around 1h after ingestion, which also corresponds to the peak of the increased cardiac activity.

Overall (see Table 6.1), an increase of both the Heart Rate (HR) and the Cardiac Output (CO) of around 17% was observed. There were no significative changes in the values of the Systolic, Diastolic and Mean cuff pressure (SP, DP, MP) during the 1h process of digestion (beyond the intra-patient variability of the measurements). Finally the Stroke Volume (SV) was constant on average but the measurement showed a high inter-patient variability of the evolution (11%).

Additionally, we tracked the boundaries of the endocardium over the entire cine MRI sequence acquired at T_1, then extracted from this sequence a point at the apex of the left ventricle and one at the top of the left ventricle septum. This was used to calculate the *Septal Shortening* (SS) as the maximal shortening of the distance between these two points during the cycle. It has an average value of -17% and a standard deviation of 3.7% across the population.

6.3 Patient-Specific Cardiac Modeling

6.3.1 3D Electromechanical Cardiac Model

We performed 3D cardiac modeling for 21 of these patients. A high-resolution biventricular tetrahedral mesh of the patient's heart morphology was extracted as in [Molléro 2015] from the pre-ingestion MRI at T_1, made of around 15 000 nodes. On this mesh, a *myocardial fibre direction* can be defined at each node of the mesh (see Fig 6.1a), by varying the elevation angles of the fibre across the myocardial wall from α_1 on the epicardium to α_2 degrees on the endocardium. In this paper, α_2 is set at the default value of 90^o and α_1 is a variable parameters in our experiments.

The depolarization times across the myocardium were computed with the Multi-front Eikonal method [Sermesant 2007]. The APD is set from the Heart Rate with classical values of the restitution curve and default values of conductivities are used as in [Pernod 2011]. Myocardial forces are computed based on the Bestel-Clement-Sorine model as detailed in [Chapelle 2012]. It models the forces as the combination of an active contraction force in the direction of the fibre, in parallel with a passive

(a) Fig 1a: 3D heart geometry with myocardial fiber direction

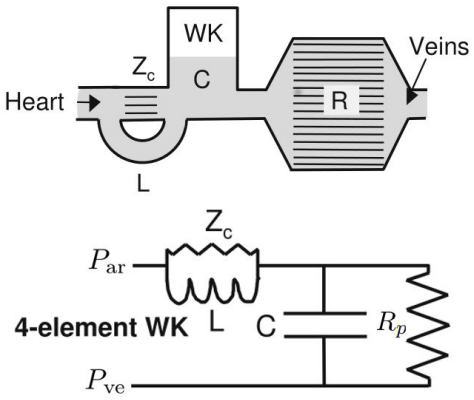

(b) Fig 1b: Schema and rheological model and of the windkessel model (figure from [Westerhof 2009])

anisotropic hyperelasticity driven by the Mooney-Rivlin strain energy. In this paper, we only consider two main parameters of the model: the *contractility* σ_0 and the *stiffness* c_1. Finally for the haemodynamics, the pressure in the cardiac chambers are described by global values, and the mechanical equations are coupled with a circulation model implementing the 4 phases of the cardiac cycle [Marchesseau 2013b].

In particular the pressure of the aortic artery P_{ar} (cardiac after-load) is modeled with a 4-parameter Windkessel model [Westerhof 2009], which describes the evolution of arterial blood pressure with the second-order equation of an electric circuit (see Fig 6.1b). The blood inertia is modeled by the inductance L, the arterial compliance by a capacity C and the proximal and distal (peripheral) resistances respectively by a resistance Z_{C} and R_p (see Fig 6.1b). Finally, the venous pressure P_{ve} models the mean pressure in the venous system. In the following, Z_{C} and L are fixed at a default value (see [Marchesseau 2013b]) while C, R_p and P_{ve} are variable parameters.

6.3.2 Longitudinal Parameter Estimation

After building the heart mesh geometry, *parameter estimation* is the next step in order to have model simulations which reproduce the available data. Considering a set of simulated quantities called the "outputs" O (such as the Stroke Volume or the Mean Pressure for example), and a set of model parameters P, it consists in finding adequate values $\mathbf{x}$ of the parameters such that the output values $O(\mathbf{x})$ in the 3D model simulation fit the "target values" $\widehat{O}$ available in the data. This is done by performing an optimization of the parameter values $\mathbf{x}$ in order to minimize a distance $S(x, \widehat{O}) = ||O(x) - \widehat{O}||_S$ between the simulated values $O(\mathbf{x})$ and the target values $\widehat{O}$ (normalised to compare quantities with different units).

For each patient, we have here measurements of different *varying* quantities at the two instants T_1 and T_2 (such as the stroke volume and the heart rate), so we need to estimate different values for some cardiac model parameters (in particular

the haemodynamic parameters) at these two instants. On the other hand, during the time-scale of the study (1h on average), some parameters of the cardiac model can be considered *constant*. This is the case of the epicardial fibre elevation angle α_1 for example, or the stiffness c_1. In order to have consistent sets of estimated parameters at these two different instants, we need to use the same values for these parameters at these two instants.

To that end, we perform a two-step parameter estimation. First, we estimate values of both the fixed and varying parameters from the data at T_1. Then we reuse the estimated values of the fixed parameters for T_2 and estimate new values for the varying parameters only, from the data at T_2. As summarized in Table, we then have two distinct *Parameter Estimation problems*: the estimation of 6 parameters values in order to fit 4 target output values at T_1 (with the heart rate of the simulations set to its value at T_1). Then the estimation of 4 parameters values in order to fit 3 target output values at T_2 (with the heart rate at T_2).

Estimated Parameters at T_1	Target Outputs at T_1
Stiffness c_1	**Septal Shortening**
Epicardial Fibre Elevation Angle α_1	Stroke volume at T_1
Contractility σ_0	Aortic Diastolic Pressure
Aortic Peripheral Resistance R_p	Aortic Mean Pressure
Aortic Compliance C	
Venous Pressure $P_{\mathbf{ve}}$	
Estimated Parameters at T_2	**Target Outputs at T_2**
Contractility σ_0	Stroke volume at T_2
Aortic Peripheral Resistance R_p	Aortic Diastolic Pressure
Aortic Compliance C	Aortic Mean Pressure
Venous Pressure $P_{\mathbf{ve}}$	

Table 6.2: Estimated Parameters and Target Outputs in the parameter estimations at T_1 and T_2. Constant parameters whose values are reused for the estimation at T_2 are outlined in bold. The heart rate in the simulations for the estimation at T_1 (resp T_2) correspond to the measured value at T_1 (resp T_2).

The optimisation was performed with an extended version of the framework described in [Mollero 2016]: the main algorithm is the CMA-ES genetic algorithm, which asks at each iteration for the score of a high number of 3D simulations. Instead of actually computing all these 3D simulations, we only compute a few within the parameter space ($2N+1$ where N is the number of estimated parameters). Then we build a "low-fidelity" surrogate model [Peherstorfer 2016] from these simulations which allows to approximate the outputs of the 3D simulations for many successive iterations of the algorithm, without performing all the 3D simulations. This robust and efficient "multifidelity optimization" allows a very fast exploration of large parameter sets with a low computational cost. In particular for the two problems at

	c_1 (kPa)	α_1 (°)	σ_0 (MPa)	P_{ve} (mmHg)	R_p (MPa.m^3.s)	C (MPa^{-1}.m^{-3})
Mean	54.2e^1	-58.7	82.6	48.3	47.4	6.23e^{-3}
Std.	27.7e^1	2.94	34.0	12.9	17.2	1.98e^{-3}
Mean Δ	-	-	-1.52%	6.93%	**-14.2**%	-7.30%

Table 6.3: Statistics of the estimated parameters and of the difference Δ between estimated parameters at T_1 and T_2

T_1 and T_2, we performed the optimization for the 21 patients simultaneously and the convergence was reached in around two days.

6.4 Exploitation of Estimated Parameters

6.4.1 Analysis of Parameter Trends in the Population

Across the 21 patients and the two estimations, the average *fit error* on the target output values are 1.9 mL for the Stroke Volume, 1% for the Septal Shortening, and 0.1 mmHg for both the mean and diastolic pressures, with few outliers. As a consequence of this step, we now have a population of 21 personalised patient hearts at two instants. For each parameter, we report in Table 7.1 the mean and standard deviation of its estimated values at T_1 across the 21 patients, as well as the mean of its *evolution* Δ between the instants T_1 and T_2 (difference between the values estimated at T_2 and T_1).

The first remark is that on average, the parameter R_p which models the arterial peripheral resistance decreases by 14%. This was expected and corresponds to findings in [Hauser 2016]. In a clinical setting the peripheral resistance is indeed computed as the ratio between the blood flow and the blood pressure, and a similar relationship can be derived in the model: as shown in Fig 6.2a the ratio (MP-P_{ve})/CO is almost exactly equal to the peripheral resistance R_p in our simulations. Across the population, since the cardiac output CO increases by around 17% but the pressures are constant, the peripheral resistance has to decrease by a close number (14.2% here) on average.

We then notice both an average increase of the venous pressure P_{ve} and decrease of the arterial compliance C. These two trends can be explained as to compensate the decrease of the resistance and avoid a drop in the mean blood pressure. Indeed, in the model, a decrease of R_p leads to a decrease of the "characteristic time" $\tau = RC$ at which the blood pressure decreases from the systolic pressure to the "asymptotic pressure" P_{ve}. A decrease of R_p only leads then to a decrease of the mean pressure. On the other hand, a decrease of C leads to an increase of the "pulse pressure" (difference between systolic and diastolic pressure) since C links an increase of arterial volume to an increase of arterial pressure with the formula $C\Delta P = \Delta V$ (a less compliant aorta has a higher pulse pressure for the same stroke volume). This contributes to the increase of the mean pressure (see Fig 6.2b), and

it is also the case of the increase of P_{ve}. Interestingly, we can note that these two trends (decrease of the arterial compliance and increase of venous pressure) in parameters correspond to actual cardiovascular phenomena which are commonly observed during exercise [Otsuki 2006, Albert 1952].

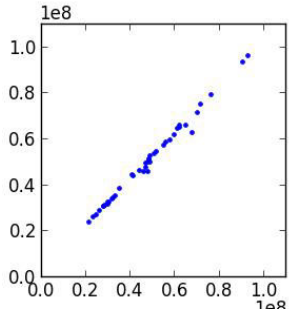

(a) Fig 2a: (MP-P_{ve})/CO as a function of R_p

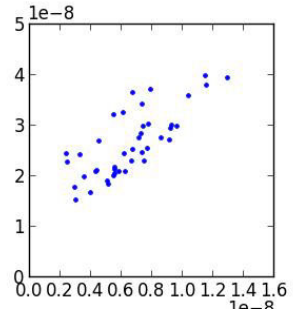

(b) Fig 2b: SV/(MP-DP) as a function of C

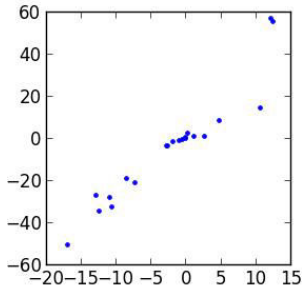

(c) Fig 2c: $\Delta\sigma_0$ (%) as a function of ΔSV (%)

Finally, we can also observe a high correlation between changes in the Contractility σ_0 and changes in the ejected volume, as shown in Fig 6.2c. This is also a known phenomenon in cardiac dynamics, in particular at the core of the Starling Effect.

6.4.2 Parameter Evolution Law

From this data and the estimated parameters, we then build a law f which, from a given simulation, gives *variations of the electromechanical parameters* σ_0, P_{ve}, R_p *and* C which leads to a new simulation with *prescribed changes in heart period (HP) and stroke volume (SV)* while having **same mean and diastolic pressures**: $f(\Delta HP, \Delta SV) = (\Delta\sigma_0, \Delta P_{\text{ve}}, \Delta R, \Delta C)$

This is done by computing a multivariate regression between the changes (in %) in Heart Rate and Stroke Volume and the changes in the estimated parameters values at the two instants T_1 and T_2, for the 21 patients. We report in Table 6.4 the coefficients of this multivariate regression:

Table 6.4: Coefficient of the multivariate regression f

	$\Delta\ \sigma_0$	$\Delta\ P_{\text{ve}}$	$\Delta\ R_p$	Δ C
Δ HP	-0.02	-0.15	1.20	0.51
Δ SV	3.05	0.52	-1.04	1.19

The predicted variations of parameters with the variations of the heart period (ΔHP) are consistent with the mean variations across the population described earlier. Interestingly with the coefficients of the second row (ΔSV), we can also note how the parameters have to change for an increase in Stroke Volume only with constant pressures.

We finally tested the accuracy of this law with a *leave-one-out* approach: for each patient, we computed the regression f from the data and estimated parameters of all the others patients. Then we changed the baseline parameters (at T_1) of this patient with the parameters predicted from f, and simulated the Pressure and Stroke Volume values at T_2. The obtained results were accurate: on average, the target Stroke Volume at T_2 was predicted within 1.9 mL and the mean absolute variations in Diastolic and Mean Pressure were within 2.1mmHG, which is beyond the variability of both the intra-patient and population variabilities.

6.5 Conclusion and Discussion

In this chapter we performed a consistent longitudinal estimation of cardiac model parameters for 21 patient-specific hearts at two different instants within a 1h time span, from clinical data. This was done through two successive parameter estimation problems: we first estimated 6 parameters to fit the simulated Stroke Volume, the Septal Shortening and the Mean and Diastolic Pressures to their values at the first instant. Then we reused the estimated values of the fixed parameters at this step and performed a second estimation of 4 parameters to fit values of Stroke Volume and Pressures at the second instant. This was done in parallel for the 21 hearts in around two days and a maximum of 150 simulations of the 3D model per patient.

From those personalised hearts, we identified relationships between the estimated parameters and the simulated pressure and volume outputs, and linked their evolution between these two instants to classical physiological phenomena. Then we extracted a law which computes changes of electromechanical parameters from changes of stroke volume and heart rate with constant pressure. This law allows in particular to easily simulate the changes observed between the two instants without having to perform the parameter estimation step at the second instant. This was evaluated in a leave-one-out test and showed that it can predict accurately changes in the model parameters.

A first direct continuation of this work would be to quantify (from further data) to what extent this law holds for changes of cardiac outputs which are more important (digestion can be seen as a 'mild' exercise and it is known for example that blood pressure rises during more intense exercises). Finally, for future patients, it could also be interesting to evaluate to what extent the changes in both the Stroke Volume and the Heart Rate can be predicted, and use our law to simulate the predicted heartbeats.

Chapter 7

Longitudinal Analysis using Personalised 3D Cardiac Models with Priors: Application to Paediatric Cardiomyopathies

Contents

In this chapter we present a study which was performed on all the available complete acquisitions *in March 2017 from the* `CVD-UCL` *and* `CMP` *cohorts, which is a joint work with the 3 clinical partners. In a first step we show that performing* Maximum A Posteriori *estimation with prior probabilities leads to less variance in the population of personalised parameters, in particular because specific (and usually unique) values are promoted when there is no uniqueness in parameter estimation. With this approach, the variability in the population only reflects variability in physiological properties of the cases, and the parameters can be used for analysis of the cardiac function. In a second step we project these personalised parameters onto the main axis of a classifier between the* `CVD-UCL` *and the* `CMP` *cohorts, and we show that for the 4 patients of the* `CMP` *cohort where we have a second timepoint, the evolution suggests an improvement of the cardiac function under therapy. This work was presented at the MICCAI conference in 2017 [Molléro 2017a].*

7.1 Introduction

Tridimensional Personalised Cardiac Models are of increasing interest for clinical applications. They compute the myocardial motion under the influence of simulated electromechanics and haemodynamics, in order to simulate a heartbeat. Their equations usually depend on a large number of parameters, so after extracting a patient's heart geometry from clinical imaging, the first step to build a *personalised simulation* is to estimate parameter values for which the simulation matches the measured heartbeat.

Recent works have shown that the *personalised parameter values* can capture intrinsic properties of the heart [Chabiniok 2012]. In particular, the simulations can help predict the possible behavior of the heart to some changes associated to specific conditions (such as exercise or drug treatment), leading to applications in therapy planning [Crozier 2015]. Although these studies are very promising, progress is facing three main obstacles:

- the difficulty to find large homogeneous cardiac databases where the same information is available for all the cases
- the non-uniqueness of the parameter values due to the sparsity of clinical measurements compared to the high number of parameters of the models
- the computational time required to run models (from few minutes to several days for the most complex ones). This can be a burden in the parameter estimation requiring many simulations, and even worse for large databases

Here we present a cardiac modeling study overcoming these difficulties by first building a homogeneous cohort of more than 61 patients including 22 controls and 39 children with various cardiomyopathies. For each case, MRIs were acquired, together with pressure and heart rate measurements, resulting in 84 heart mesh geometry and haemodynamic conditions. On the modeling side, we performed the estimation of 6 parameters to reproduce the stroke volume and pressure measurements. This was performed with prior probabilities on the parameter values, in order to overcome the problem of the parameters uniqueness. Finally, the personalisation for the full cohort was performed in a relatively short time (around 2 days), thanks to a "multi-fidelity" optimization scheme which predicts changes in simulations of the 3D model with a much faster and simpler 0D model.

This led to more consistent parameter values across the 84 cases, on which we studied the relationship to clinical condition and its evolution. In particular, using the follow-up data patients with cardiomyopathy we show that the evolution of parameters naturally suggest and improvement of the heart condition under therapy. Finally we demonstrate that these estimated parameters could also be complementary to the clinical measurements in order to characterise better the difference between healthy and cardiomyopathy cases.

7.2 Clinical Data

We used two different cohorts (C1 and C2) in this study. The two protocols were approved by the local Research Ethics Committees. First 22 volunteers (C1) who participated to a clinical study to assess the cardiovascular response after the ingestion of a high-energy (1635 kcal), high-fat (142g) meal after fasting for 12h, closely following the protocol in [Hauser 2016]. In this study, short axis cardiac cine MRI sequences were acquired before the ingestion and at one or more time points within 1h of the ingestion of the meal, in order to study the evolution of the blood flow in the arteries. After the meal ingestion, both the heart rate and the cardiac output increased by around 15%. However no substantial changes were observed in the mean, diastolic and systolic pressures during digestion (compared to the intra-patient variability of the measurement).

The second cohort (C2) consists in 39 children with various cardiomyopahies, ranging from class I to IV on the Ross and NYHA classifications [Hsu 2009] for heart failure symptoms, from two different clinical centers. The cine MRI was acquired at their enrollment and for 4 of them, at follow-up (after a few months). The most common symptom among this cohort is a dilation of the left ventricle (Dilated CardioMyopathy) with low ejection fraction.

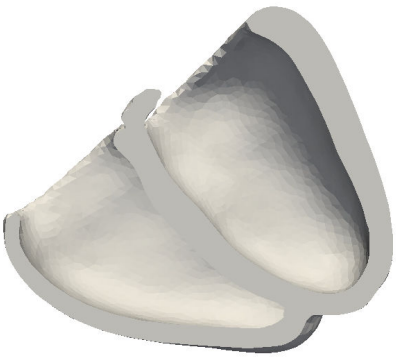

(a) Fig 1a: Typical mesh geometry of a heart in the cohort (C1)

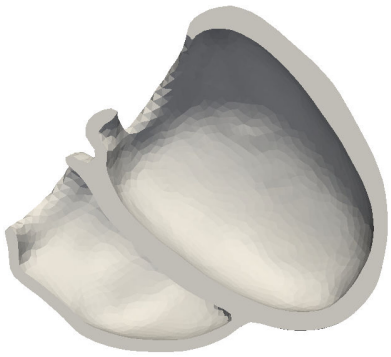

(b) Fig 1b: Mesh geometry of a paediatric heart with Dilated Cardiomyopathy (DCM) in the cohort(C2)

We performed the cardiac modeling of a total of 41 different instants across the 22 volunteers of the first cohort, and at the 39 enrollment times and 4 available follow-up times of the second cohort. This lead to a total of 84 complete set of cine MRI, cuff pressure measurements and heart rates. See Figs.7.1a,7.1b for typical heart geometries from each cohort.

7.3 Personalised Cardiac Modeling

7.3.1 3D Electromechanical Cardiac Model

From each MRI, a high-resolution biventricular tetrahedral mesh of the patient's heart morphology (around 15 000 nodes) is generated as described in [Wang 2013b]. On this mesh, a *myocardial fibre direction* is defined at each node of the mesh by varying the elevation angles of the fibre across the myocardial wall from $\alpha_1 = -80$ on the epicardium to $\alpha_2 = 80$ on the endocardium.

The depolarization times in the myocardium were computed with the Eikonal model using default values of conductivities and the APD was computed from the Heart Rate with classical values of the restitution curve. Myocardial forces are computed based on the Bestel-Clement-Sorine model as detailed in [Marchesseau 2013a]. It models the forces as the combination of an active contraction force in the direction of the fibre, in parallel with a passive anisotropic hyperelasticity driven by the Mooney-Rivlin strain energy. In this paper, we only consider two main parameters of the model: the *contractility* σ_0 and the *stiffness* c_1.

Finally the mechanical equations are coupled with a haemodynamic model which implements the 4 phases of the cardiac cycle, and describes the pressure in the cardiac chambers with global values (see [Marchesseau 2013a] for implementation details). In particular, the pressure of the aortic artery is modeled with a 4-parameter Windkessel model [Westerhof 2009], whose main parameters are *blood inertia* L, the *arterial compliance* C and the *proximal and distal (peripheral) resistances* Z_{C} and R_p. A *venous pressure* P_{ve} has to be set as well. In the following, Z_{C} and L are set at a default value (see [Marchesseau 2013a]), while C, R_p and P_{ve} are estimated parameters.

7.3.2 Parameter Estimation with Priors

A typical *parameter estimation* problem is composed of simulated quantities called the "outputs" O (such as the simulated Stroke Volume and Mean Pressure), and a set of model parameters P. The estimation consists in finding adequate values x of the parameters such that the output values $O(x)$ in the 3D model simulation fit the "observed values" from the clinical measurements $\widehat{O}$ of interest.

This is done by minimizing a cost function (or **score**) $S(x, \widehat{O})$ between the simulated values $O(x)$ and the target values $\widehat{O}$:

$$S(x, \widehat{O}) = ||O(x) - \widehat{O}||^2 + \lambda R(x)$$

where $R(x)$ is a *penalty* (or *regularisation*) term, weighted with λ, that can be formulated as a quadratic form with mean value μ_R and covariance matrix Δ:

$$R(x) = (x - \mu_R)\Delta^{-1}(x - \mu_R)^T$$

In Bayesian Inference, this is equivalent to finding the *maximum a posteriori*

with a Gaussian prior and a Gaussian likelihood.

Finally, since the parameters are positive, it is more meaningful to consider that the logarithm of the parameter values follow a Gaussian distribution rather than the parameter themselves, so the optimisation is performed over the logarithm of the parameters values.

In this paper, we focus on the set of **5 parameters** P: c_1, σ_0, R_p, C and $P_{\mathbf{ve}}$, in order to fit **3 target outputs** to their clinical measurements, which are the *Stroke Volume* **SV** the Aortic *Diastolic Pressure* **DP** and *Mean Pressure* **MP**.

We then performed two different personalisations: first, one (P1) without priors on the parameter values during the optimization (λ=0). This allowed us to have a first assessment of the variability of the parameters and of the values which lead to the best simulations. It was then followed by a second personalisation (P2), with priors on the values of both c_1 and C equipped with diagonal covariance matrix:

$$\mu_R = \begin{bmatrix} \mu_{c_1} \\ \mu_C \end{bmatrix}, \Delta = \begin{bmatrix} \delta_{c_1} & 0 \\ 0 & \delta_C \end{bmatrix} \tag{7.1}$$

We observed in $P1$ that simulations with c_1 around $500\,000\,Pa$ led to good behavior compared to the dynamics observed in echocardiographic images. For the arterial compliance C, we used a prior based on the mean value of $1.8e^{-8}\,S.I.$ as reported in [Laskey 1990].

Therefore $\mu_{c_1} = ln(500\,000) = 13.12$, $\delta_{c_1} = 0.5$ and $\mu_C = ln(1.8e^{-8}) = -17.83$, $\delta_c = 1$.

7.3.3 Efficient Multi-Fidelity Optimization

The optimization in each personalisation problem was performed with a "multifidelity" approach [Peherstorfer 2016] based on our recent work in cardiac model personalisation [Mollero 2016], where the outputs of the 3D model are approximated during the optimization by simulations from a very fast low-fidelity model called "0D model", made of around twenty equations only.

As explained in [Mollero 2016], a small number of 3D "sigma-simulations" can indeed be used to approximate many 3D simulations in a large parameter space. This is done by first finding similar 0D simulations with the same outputs of interest (such as the pressure and stroke volume), then building a mapping between the parameters of the corresponding 3D and 0D simulations.

This multifidelity method was here adapted for the two personalisation problems, where the 0D and the 3D models share the same haemodynamic variables R_p, C and $P_{\mathbf{ve}}$ from the Windkessel model. In this specific case, the variations of pressure and stroke volume with respect to these variables are very similar, and we found to have better approximation results by only computing a mapping between c_1 and σ_0 (as opposed to all the personalised parameter in our original approach) to the 0D model parameters.

As a result, our Multi-Fidelity Optimization Method performs the optimization of 3D parameters based on 0D model approximations which are faster to compute.

Table 7.1: Statistics of the estimated parameters in the estimations (P1) and (P2)

	σ_0 (MPa)	c_1 (kPa)	R_p (MPa.m^3.s)	C (MPa^{-1}.m^{-3})	P_{ve} (mmHg)
Mean (P1)	156	$37.8e^1$	48.0	$6.13e^{-3}$	44.6
Log-Mean (P1)	18.51	12.60	17.62	-18.96	8.62
Log-Std (P1)	0.98	0.66	0.37	0.32	0.44
Mean (P2)	71.1	$4.44e^1$	84.1	$7.29e^{-3}$	32.01
Log-Mean (P2)	18.03	12.98	18.2	-18.77	8.32
Log-Std (P2)	0.41	0.22	0.26	0.25	0.27

It only requires the computation of successive sets of 5 simulations of the 3D model (the sigma-simulations). In particular, the simultaneous personalisation (P1) of the 84 hearts was completed in around 36 hours, and in 48 hours for (P2).

7.4 Results

In Table 7.1 we report the mean of both the estimated values (*Mean*) and logarithmic estimated value (*Log-Mean*), as well as the standard deviation of the logarithm of the estimated values (*Log-Std*).

As expected, we can notice that the standard deviation of all the parameters in the population is reduced between (P1) and (P2). Interestingly, the goodness of fit was not impacted in the personalisation by the use of prior probabilities on c_1 and σ_0 in (P2). Most cases are fitted under 1.2ml for the stroke volume and 0.5 mmHg for the pressure measurements with few outliers. This means that the prior could be stronger in order to further reduce the variability while maintaining simulations which match the clinical measurements.

7.4.1 Application to Longitudinal Analysis of the Cardiac Function

From a clinical point view, an interesting application of the modeling is to characterise the state of the heart function, beyond the information given by the clinical measurements and the imaging. The underlying idea is that some of the estimated parameters values can capture properties of the heart which cannot be directly measured from standard imaging (such as the myocardial stiffness). This additional information on the heart could contribute to the diagnosis, by comparing the estimated parameters with the parameters of other known cases.

To analyse the relationship between the parameter values and the clinical condition, we performed a linear discriminant analysis (LDA) over the parameter values and the heart rate, in order to classify between the two cohorts. This leads to the computation of two vectors w and b such that given a vector X of parameter x, the predicted cohort is C2 if $A^{\mathrm{T}}X + b > 0$, and C1 otherwise.

The vector w corresponds to the most discriminative direction in the population between healthy and cardiomyopathy cases. In this context, this axis could be a candidate to characterise whether the cardiac function at a given time is closest to

a healthy heart, or a heart with cardiomyopathy, based on the parameters values observed in the two cohorts.

For example, we display in Fig 7.2 the projection of the parameters on this vector (x-axis) and a orthogonal direction to w. Most healthy cases (dark blue dots) are on left side of the black line ($w < 0$) and most cardiomyopathy cases (red dots) are on the right ($w > 0$).

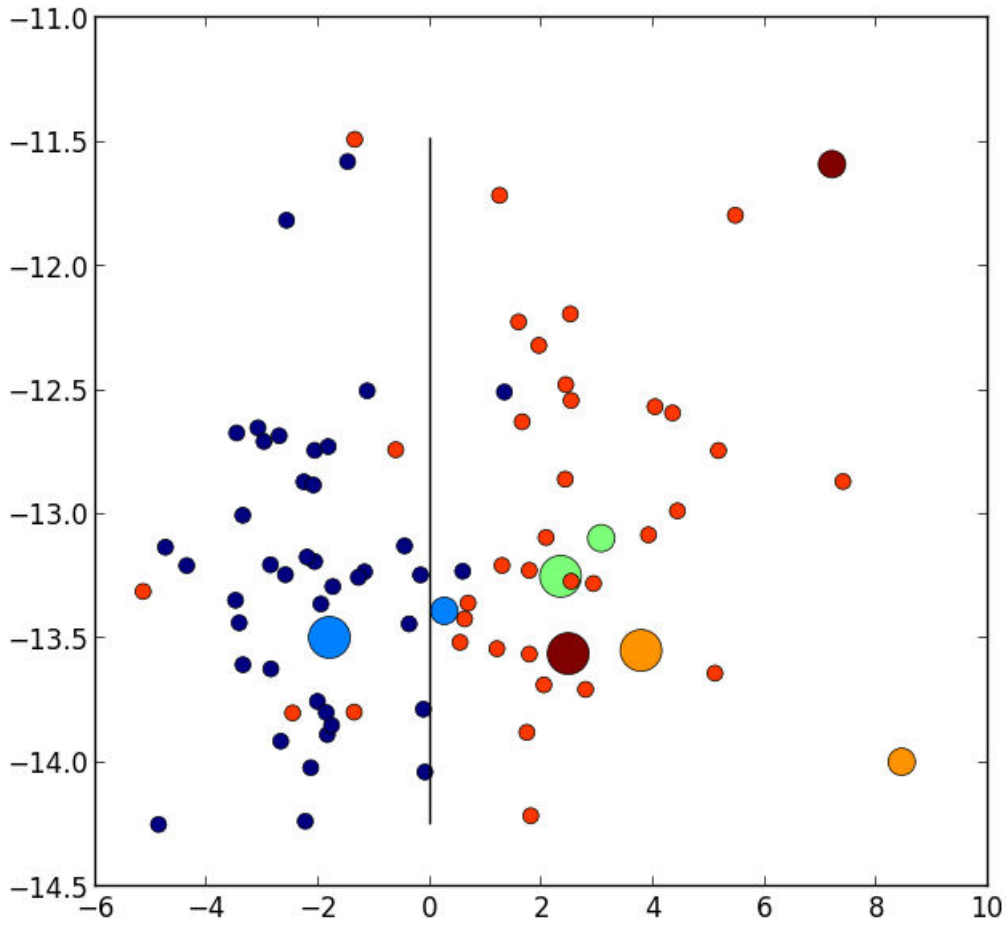

Figure 7.2: Projection of the parameter on the main direction w of a LDA classifier between the healthy cases (dark blue dots) and cardiomyopathy (other dots) cases (x-axis) and an principal orthogonal direction of this vector (y-axis). The dots in light blue, brown, orange and green correspond to 4 patients for which the data was available both at baseline (small dot) and follow-up (larger dot).

Interestingly, this could also help to quantify the evolution of the patient's heart condition under the influence of the pathology and the therapy. Indeed, for all the cardiomyopathy cases for which we have the follow up data, we can notice a decrease in the coordinates along the horizontal axis (see the pairs of brown, light blue, green and orange dots. The larger dot is the follow-up). This could be interpreted as *an*

improvement of the cardiac function with the therapy, which is at least becoming closer to the condition of an healthy heart. One of the cases (in light blue) is on the "healthy" side of the classification at follow-up.

Finally, the predictive power of such a classifier can be assessed, through a *leave-one out cross-validation*. This is done by training the classifier on all the cases but one, and predicting the diagnosis for the remaining case. If we perform the LDA over the 5 estimated parameters and the heart rate, the number of prediction errors is 11. The same classifier trained on the 3 clinical outputs (stroke volume and pressures) and the heart rate makes 9 prediction errors. However, if we train the classifier with *both the 5 estimated parameters and the 3 clinical measurements* and the heart rate, it only makes **6 classification errors**.

In this context, a possible explanation is that the estimated parameters were able to capture a complementary information on the cardiac function, different from the clinical measurements of volume and pressure only, both through the *3D personalisation* and the *comparison with the other values estimated in the population*. This information was then used by the simple linear classifier to improve its accuracy in the diagnosis of a patient.

7.5 Conclusion and Discussion

In this chapter, we presented a cardiac modeling study based on the estimation of 5 model parameters from 3 clinical measurements of stroke volume and pressures, on a large cohort of 61 patients. We used recent ideas developments in "multi-fidelity" personalisation, to drive a very fast and computationally efficient estimation of these parameters with priors. Both the personalisations with and without priors were performed simultaneously for all the patients on our cluster, and converged respectively in less than 36 and 48 hours. We showed that the use of priors during optimization reduces the variability of the estimated values in the population, leading to more consistency for further applications.

We then analyzed the estimated parameter values with respect to the clinical conditions of the patients. A linear discriminant analysis (LDA) was used to characterise the cardiac function the cases along the most discriminative axis between the two cohorts. For cardiomyoathy patients, we showed that the evolution in time along this axis suggests that their cardiac function is improving under therapy. Finally, we also demonstrated how the estimated parameter values could be complementary to clinical measurements in the context of diagnosis.

A direct extension of this study is to estimate values for more model parameters, from a larger set of measurements such as the flow or the myocardial strain. On the cardiomyopathy point of view, this could help to further discriminate between the various types of cardiomyopathy, with applications in risk stratification of heart failure. Another interesting direction of study is the further analysis of longitudinal data in order to better understand both the short-term and long-term variabilities in cardiac function, with applications on the prediction of disease evolution and

therapy planning.

Chapter 8

Population-Based Priors in Cardiac Model Personalisation.

Contents

After partially tackling the problem of parameter non-observability in personalisation with the use of priors in ***Chapter 7*** *and the corresponding study [Molléro 2017c], we propose in this chapter a general approach to answer the following questions:*

- *Given a database of cases and measurements, which parameters or parameter directions can be estimated (i.e. are observable)?*
- *Can we select a reduced and fully observable parameter subspace for personalisation, which also makes sense from a modeling point of view?*
- *Can we use population-based statistics on personalised parameter values to constrain cases with a different set of measurements in this subspace?*

We introduce a method called ***Iteratively Updated Priors*** *which performs successive personalisations of all the cases in a population, where the prior probability distribution at each iteration is set from the distribution of personalised parameters in the previous iteration. With this method, parameter values in unobservable directions are progressively "gathered" and "grouped" to values which are closer to the prior mean, which simultaneously makes the penalty stronger in these directions. At convergence, parameters in the population lie on a linear subspace of reduced dimension (with less* unobservable directions*) and the prior distribution, which we call* ***population-based****, correspond to the distribution of parameters in the population.*

Applied to the personalisation of the 137 complete acquisitions *with the 0D model, we extract from an initial space of 6 parameters, a linear subspace of dimension 4 based on 5 parameters. This space is coherent from a modeling point of view and* sufficient *in the sense that there is a unique set of parameter values for each complete acquisition in our database. We then use the resulting* ***population-based priors*** *in this subspace to personalise a database of 811 acquisitions with missing and heterogeneous measurements, and we observe that the use of priors leads to a form of imputation in the parameter space in cases where measurements are missing. We argue that because our priors are estimated from personalised parameters of 137 complete acquisitions, in a reduced and sufficient subspace, we achieved one of the most consistent parameter estimation possible in this dataset.*

Finally we believe that through the selection of a subspace of sufficient dimension, the algorithm also helps find a subspace of maximal dimension *in which parameters are completely observable from this specific dataset. In this context we believe that the proposed approach, though it requires supervision for the selection of parameters with physiological relevance, possibly provides a complete framework to tackle the problem of observability in personalisation from large databases.*

8.1 Introduction

Personalised cardiac models are of increasing interest for clinical applications. To that end, parameter values of a cardiac model are estimated to get a *personalised* simulation which reproduces the available measurements for a clinical case. Then the parameter values are used for analysis, for example comparing values between personalised hearts could help classify between pathologies and predict evolution.

Most cardiac models depend on many parameters, especially in 3D models where each parameter can take a different value at each node of the mesh. The number

of parameters can be up to hundreds of thousands while on the other hand for an individual patient, the available clinical data is usually sparse and typically consists of a set of global measurements (such as ejection fraction, systolic and diastolic pressure) and possibly some imaging data with a considerable degree of noise or blurriness. Consequently, many sets of parameter values can lead to a simulation which can reproduce the available clinical data. The parameter estimation problem is an *ill-posed inverse problem* and all the parameters cannot be uniquely estimated from the measurements only.

A classical technique to estimate relevant parameters in this context is the use of *prior probabilities* over the parameter values in Bayesian inference. In this framework, parameters values come from a (usually Gaussian) *prior* probability distribution, which represents some knowledge or beliefs about the distribution of parameters. Then, given a set of measurements, a vector of *Maximum A Posteriori* (MAP) parameter values is estimated, which realises an optimal trade-off between its likelihood in the prior probability distribution and the error of fit of the simulation. The set of *Maximum A Posteriori* values is usually smaller than the set of values for which the simulation fits the measurements and possibly unique. A challenge to estimate relevant parameters is then to define accurately the *prior probability distribution*, which should be ideally as close as possible to the "true" distribution of parameters.

Here we explore an original approach, which we name **Iteratively Updated Priors** (IUP), which consists in performing successive personalisations with priors, where the priors distribution is set from the distribution of personalised parameters in the previous personalisation. The rationale is twofold: first, if the algorithm converges, all the cases are personalised through a MAP where the prior distribution is the distribution of the population parameters itself. Intuitively this opens the possibility, for some cases where the value of a parameter is unobservable from the available measurements, to guide the estimation of this parameter value from other cases in the database where the value was observable. Secondly, when there are directions in the parameter space in which the simulated measurements do not vary (i.e. an *unobservable* parameter direction), the use of priors promotes the estimation of parameter values which are closer to the prior mean, which in turn makes the penalty (from the prior) stronger in this direction at the next personalisation. Intuitively, this process will tend to group parameters onto directions which are observable, and reduce the spread into directions which are not. In practice, we will see this algorithm leads the parameters to lie on a *linear subspace* of smaller dimension (See Figure 8.1).

In the first section we present the IUP algorithm in relation to two different mathematical frameworks. First, we express the Maximum A Posteriori (MAP) parameter estimation in the context of Bayesian inference. Secondly, we use the *Iteratively Reweighted Least Square (IRLS)* algorithm from sparse regression to show that the IUP algorithm, when it converges, performs the minimisation of a *population-wide cost function* with a sparse regulariser on the *number of dimensions of the parameter space*. We introduce two types of updates of the parameters of the (Gaussian) prior

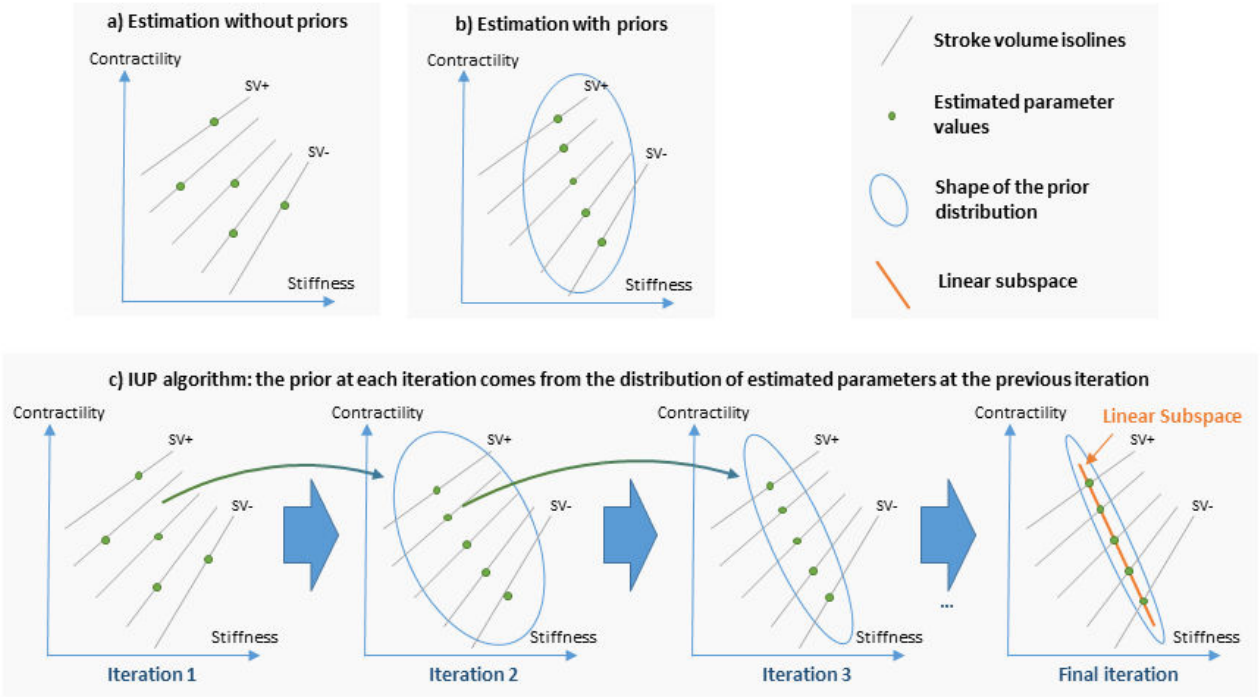

Figure 8.1: Schematic representation of parameter estimation when the problem is ill-posed. In this toy example, both the contractility and the stiffness are estimated from values of the *stroke volume* (SV). Both have an influence on the *stroke volume* (SV) so there are *isolines* of stroke volume (in grey) on which the value of the stroke volume is the same. **Image a:** estimation without priors, the estimated values (green) for each case can be anywhere on an *isoline* (grey). **Image b:** the estimation is performed with a (gaussian) prior (the gaussian covariance is in blue), the estimated values are grouped closer to the prior mean. **Image c:** the **Iteratively Updated Priors** (IUP) algorithm performs successive estimations where the prior is set from the distribution of estimated parameters at the previous iteration. This leads the parameters to lie on a *reduced linear subspace* (orange).

probability: **"Full Matrix"**, where no assumption is made on the distribution and the covariance matrix, and **"Diagonal Matrix"** where the covariance matrix is supposed diagonal, which assumes independence of parameters in the distribution of the population. We demonstrate that in the first case the algorithm leads to the automatic selection of *parameter directions* in which parameter values are set to a constant value in the population, and in the second case to the automatic selection of *parameters* which are set constant.

In the second section we present results of the IUP algorithm on the database of 137 *complete acquisitions* where the same 4 measurements are available. We perform the estimation of 6 parameters of the 0D model likely to vary in this population, which also makes the problem ill-conditioned. We observe that the IUP algorithm leads to a trade-off between the number of dimensions of the final parameter set,

and the mean error of fit of the 4 measurements across the whole database of personalised simulations. Then we show that if we impose a high goodness of fit of the personalised simulations, the algorithm leads to the selection of a *linear subspace of minimal dimension* in which *for each case of the database* there is parameter values where the simulation fits exactly the measurements. We discuss how this algorithm can be used to find a relevant subspace for personalisation from the modeling point of view. Finally we extract a relevant subspace of dimension 4, based on 5 parameters out of the original 6, in which there is a unique set of parameter values for each case of the database.

In the last section we use the reduced subspace extracted in Section 2 and the *population-based priors* built in this subspace to perform personalisation of a larger database of 811 hearts. In this database, measurements reported by the clinicians can be missing or heterogeneous. Because we use priors, estimated parameters are well conditioned, and when measurements are missing, the algorithm performs a form of imputation in the parameter space by selecting the *most likely* parameter set according to the priors. Since the priors are computed from the population of 137 cases where all the measurements are available, in a space of *minimal dimension* for the personalisation of these 137 cases, we believe that the parameter estimation presented in this section is one of the most consistent personalisation which was possible to achieve on such heterogeneous dataset.

8.2 Population-Based Priors

In this section we introduce the personalisation framework, based on the estimation of a *Maximum A Posteriori (MAP)* with prior probabilities. In order to get relevant values for each case through MAP estimation, the prior probability has to be relevant. Ideally, it should be the "true" underlying probability distribution of parameters in the population. We introduce here the *Iteratively Updated Priors (IUP)* algorithm, which performs successive personalisations of the whole population, where the prior at each step is set from the distribution of the personalised parameters at the previous step.

First we present the MAP estimation of personalised parameters or a single case (Section 8.2.1). Then we formulate the *Iteratively Updated Priors* algorithm as successive maximization of the personalised parameter probabilities under two different set of variables (Section 8.2.2). We explicit the equations of the prior parameter update in two different cases with different assumptions on the shape of the distribution (Section 8.2.3) and the actual equations which are minimised within our optimisation framework with the genetic algorithm CMA-ES (Section 8.2.4). Finally we present a link between the IUP algorithm and the *Iteratively Reweighted Least Square* algorithm for sparse regularisation, and show that the IUP algorithm performs the minimisation of a *population-wide* cost function with a penalty on the *rank* of the set of personalised parameters. We explicit the cost function and illustrate its interpretations for the two different updates (Section 8.2.5).

8.2.1 Maximum A Posterior Estimation of Personalised Parameters

We consider a cardiac model M and a set of simulated quantities called the *outputs* $\mathscr{O}$, such as the ejected volume, the mean ventricular pressure. We then consider a subset $\mathscr{P}_{\mathrm{M}}$ of varying parameters (such as the contractility, the aortic resistance) of the model, while the other model parameters $\mathscr{P}'_{\mathrm{M}}$ are supposed fixed. Given a vector $x \in \Omega_{\mathrm{M}}$ of values of the parameters $\mathscr{P}_{\mathrm{M}}$, we note $\mathscr{O}_{\mathrm{M}}(x)$ the values of the outputs $\mathscr{O}$ in the simulation of M.

With this notations, personalisation consists in estimating parameter values $X \in \Omega_M$ for which the outputs values $\mathscr{O}_{\mathrm{M}}(X)$ are consistent with some observed values $\widehat{\mathscr{O}}$ of these outputs. This is an inverse problem, which can be tackled by different methods (see the review of [Chabiniok 2016]).

We formulate the problem as the estimation of a *Maximum A Posteriori* in Bayesian inference. With Bayes' theorem, the *posterior probability* $P(x|\widehat{\mathscr{O}})$ of parameter values considering the observed output values $\widehat{\mathscr{O}}$ is proportional to the product of the *conditional likelihood* $P(\widehat{\mathscr{O}}|x)$ and the *prior probability* $P(x)$:

$$P(x|\widehat{O}) \propto P(\widehat{\mathscr{O}}|x)P(x) \tag{8.1}$$

In this work, we use Gaussian distributions for both the likelihood and the prior probability:

$$\begin{cases} P(\widehat{\mathscr{O}}|x) \propto e^{-\frac{1}{2}(O(x)-\widehat{O})^T\Sigma^{-1}(O(x)-\widehat{O})}, \\ P(x) \propto e^{-\frac{1}{2}(x-\mu)^T\Delta^{-1}(x-\mu)}, \end{cases} \tag{8.2}$$

which correspond to the assumptions that first, the observed values $\widehat{O}$ are the sum of the outputs values $O(x)$ and a Gaussian noise with covariance Σ. Second, the underlying probablity distribution of the model parameters is a Gaussian with mean μ and covariance Δ. Finding a *Maximum A Posteriori* (MAP) consists in finding (one of) the parameter values which has the highest posterior probability:

$$X = argmax_x P(x|\widehat{O}). \tag{8.3}$$

This can also be interpreted as finding a maximum of the joint probability $P(x, \widehat{O})$ of x and $\widehat{O}$ with a uniform prior P($\widehat{O}$) on $\widehat{O}$, thanks to the formula:

$$P(x, \widehat{O}) = P(x|\widehat{O})P(\widehat{O}). \tag{8.4}$$

8.2.2 Iteratively Updated Priors (IUP)

In the following we consider a population of $i = 1..n$ cases to be personalised, we note $\widehat{\mathscr{O}} = (\widehat{O}_1, ..., \widehat{O}_n)$ and $\mathscr{X} = (x_1, ..., x_n)$. We introduce the algorithm called *Iteratively Updated Priors* (IUP) which consists in successively estimating personalised parameters X_i with the MAP estimation, and re-estimating the prior parameters (μ, Δ) as the maximum likelihood of these parameters considering the estimated personalised parameters X_i:

- **Step 1: Personalisation**

  For each case i, find $X_i = argmax_x P(x_i, \widehat{O}_i|\mu, \Delta)$. This consists in performing the MAP estimation in Equation 8.3 for each case with current μ and Δ, which is the estimation of personalised parameters with a given prior.

- **Step 2: Re-estimation of the Prior**

  Find $(\mu, \Delta) = argmax_{(\mu,\Delta)} P(\mathscr{X}|\mu, \Delta)$.
  This consists in finding the most likely values (maximum likelihood estimation) of μ and Δ given a set of personalised parameters $\mathscr{X}$.

When the algorithm converges, the prior probability distribution with the resulting parameters (μ^*, Δ^*) is called a *population-based prior* based on the $\widehat{O}_i$.

8.2.3 Explicit updates formulas for μ and Δ in two cases.

We explicit here the update in the **Step 2** of the IUP algorithm in which μ and Δ are set to the solutions of $(\mu, \Delta) = argmax_{(\mu,\Delta)} P(\mathscr{X}|\mu, \Delta)$. We consider two formulations of the Gaussian prior probability:

- First, a case (**Full Matrix**) where no assumptions are made on the covariance matrix Δ of the Gaussian distribution.

- Second, a case (**Diagonal Matrix**) where we suppose that Δ is diagonal. This is equivalent to the (simplifying) assumption that parameter values are independent from each other in the population.

The solutions of the maximum likelihood estimation of μ and Δ in the two cases are[1]:

- **Update of μ:** In both cases, μ is set to the mean of personalised parameters x_i:

$$\mu^k = \frac{1}{n} \sum_{i=1}^{n} X_i^{k-1}. \tag{8.5}$$

- **"Full Matrix" update of Δ:** In this case the minimisation leads to set Δ to the covariance matrix of the personalised parameters:

$$\Delta^k = \frac{1}{n} \sum_{i=1}^{n} (X_i^{k-1} - \mu^k)(X_i^{k-1} - \mu^k)^T \tag{8.6}$$

[1] A practical derivation of the maximum likelihood estimation of the covariance matrix can be found in https://people.eecs.berkeley.edu/~jordan/courses/260-spring10/other-readings/chapter13.pdf

- **"Diagonal Matrix" update of Δ:** In this case the minimisation leads to set Δ to the *diagonal part* of the covariance matrix of the personalised parameters:

$$\Delta^k = Diag(\frac{1}{n}\sum_{i=1}^{n}(X_i^{k-1} - \mu^k)(X_i^{k-1} - \mu^k)^T) \tag{8.7}$$

8.2.4 Practical Implementation of the MAP Estimation.

In the following, we use a constant $\Sigma = \gamma diag(\mathscr{N})$ for the noise model in 8.2, where $\mathscr{N}$ is a normalisation vector whose coefficients are explicited later.

We find the MAP of Equation 8.3 through the minimization of the *negative log-likelihood* $-log(P(x|\widehat{O}), \mu, \Delta)$. It is equivalent to minimizing the following *regularized cost-function* $\widehat{S}$:

$$\widehat{S}(x, \widehat{O}, \mu, \Delta) = S(x, \widehat{O}) + \gamma R(x) \tag{8.8}$$

with

$$\begin{cases} R(x) = (x-\mu)^T \Delta^{-1}(x-\mu), \\ S(x, \widehat{O}) = ||(O(x) - \widehat{O}) \oslash \mathscr{N}||^2, \end{cases} \tag{8.9}$$

where $\oslash$ is the Hadamard (coordinate-by-coordinate) division. We call $S(x, \widehat{O})$ the *data-fit term* and $R(x)$ the *regularisation term.*

We perform optimisation of this function with a derivative-free algorithm called *CMA-ES*, which stands for Covariance Matrix Adaptation Evolution Strategy. It asks at each iteration n for the scores of m points $x_i \in \Omega_{\mathrm{M}}$ (a *generation*), drawn from a multivariate distribution with covariance I_n^c and mean I_n^m. Then, it combines Bayesian principles of *maximum likelihood* with *natural gradient descent* on the ranks of the points scores in the generation to update both I_n^c and I_n^m.

For each MAP estimation, we perform from 50 to (maximum) 250 iterations of CMA-ES with a population size of 20, and the algorithm also stops if all the values of $\sqrt{\widehat{S}}$, (which we call the *data-fit term*) within the search space are in an interval smaller than 0.01.

The algorithm is stochastic (because the parameter values of the generation samples are drawn randomly). It iteratively enlarges its search space until it contains a minimal solution, then reduces the search space according to the best members of each generation (drawn randomly). As a consequence it does not converge to the same solution when the possible solutions are not unique. Because of this it can be used to give an (empirical) evaluation of the "non-uniqueness variability" by repeating the personalisation process multiple times.

Finally for practical reasons, since all the parameters of our model are positive, we always consider in the following the logarithm of parameter values instead of their values. This enables in particular to not have the optimisation algorithm test negative (non-physical) values in this step.

8.2.5 Link with Sparse Regularization

Beside the Bayesian interpretation, the IUP algorithm has also strong links with the *Iteratively Reweighted Least Squares (IRLS)* algorithm in sparse regression. When the IUP converges, we can show (see a more complete derivation in APPENDIX) that it performs the minimization of a *population-wide cost function*, with a penalty on the *rank of the set of personalised parameters*:

$$\mathscr{S}(\mathscr{X}, \widehat{\mathscr{O}}) = \frac{1}{n}\sum_{i=1}^{n} S(x_i, \widehat{O_i}) + \gamma D \tag{8.10}$$

Where D is the rank (number of non-zero eigenvalues) of Δ^*, which is the covariance of the set of personalised parameters at convergence. The minimisation of D thus correspond to the minimisation of the *number of dimensions of the set of personalised parameters*. With the **Diagonal Matrix** assumption, the covariance matrix eigenvectors are aligned with the coordinate axes so in this case, the IUP algorithm minimises the *number of parameters which do not have a constant value in the population of personalised parameters*. In order to illustrate the difference between the two types of updates, we display in Figure 8.2 a schematic representation of the two different behaviours on the toy example presented in Figure 8.1.

8.3 Results on the 137 Complete Acquistions and Application to Parameter Selection.

In this section we present results on the personalisation of the 137 *complete acquisitions*, with the 0D cardiac model. We consider a set $\mathscr{P}_{\text{0D}}$ of 6 parameters of the model, and a set of 4 outputs $\mathscr{O}$ listed in Table 8.1 for which the values are available for all the acquisitions.

The normalisation coefficients for this problem (in the vector $\mathscr{N}$ defined in Section 8.2.4) are **10 ml** for the Maximal Volume (MV) and the Stroke Volume (SV), **200 Pa** for the Diastolic Aortic Pressure (DP) and the Mean Aortic Pressure (DP). With this normalisation, an *error of fit* $\sqrt{S}(x, \widehat{O})$ lower than 1 (resp 0.1), means a personalised simulation matches volume measurements within 10 ml (resp 1 ml) and pressure measurements within 200 Pa (resp 20 Pa), which can qualitatively be considered as *acceptable* (*very good*).

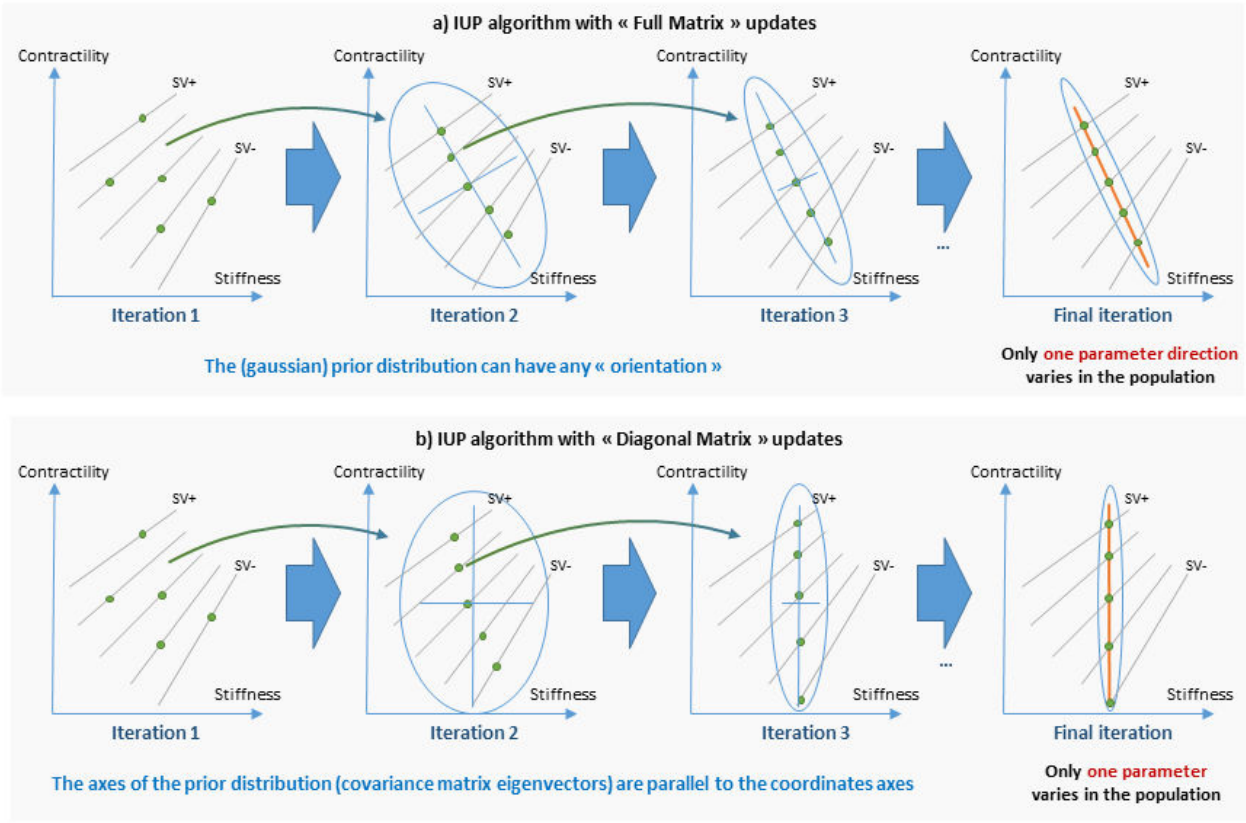

Figure 8.2: Behaviour of the algorithm for the two different updates (See legend in Figure 8.1). **Image a:** with the **Full Matrix** updates, there is no assumption on the covariance matrix so the prior distribution at the next iteration is the closest gaussian distribution (in terms of *maximum likelihood*) to the estimated parameters distribution. **Image b:** with the **Diagonal Matrix** updates, the prior distribution at each iteration is the closest gaussian distribution *with the axes parallel to the coordinate axes*. In the final population of personalised parameters, this leads some *parameters* to have a constant value (here the stiffness).

Table 8.1: Sets of *0D model parameters* and *outputs* in the example.

Personalised Parameters $\mathscr{P}$
Contractility σ_0
Resting Radius R_0
Stiffness c_1
Peripheral Resistance R_p
Windkessel Characteristic Time τ
Venous Pressure $P_{\mathbf{ve}}$

Global outputs $\mathscr{O}$
Maximal Volume MV
Stroke Volume SV
Mean Aortic Pressure MP
Diastolic Aortic Pressure DP

8.3.1 Trade-off between Data-fit, Regularisation and Dimension of the Set of Personalised Parameters

We provide results the IUP algorithm for at least 20 iterations, with both the *Diagonal Matrix* and the *Full Matrix* assumptions for values of γ of 0.5, 0.1, 0.05 (see names of the run in Table 8.2).

Name	γ	Update
FULL-IUP-005	0.05	**Full Matrix**
FULL-IUP-01	0.1	
FULL-IUP-05	0.5	
DIAG-IUP-005	0.05	**Diagonal Matrix**
DIAG-IUP-01	0.1	
DIAG-IUP-05	0.5	

Table 8.2: Names and parameters of the 6 runs of the IUP algorithm

In Figure 8.3, we report for each run the mean value $\bar{S}(\mathscr{X}, \widehat{\mathscr{O}})$ of the *data-fit term* $S(x, \widehat{O})$ and the mean value $\bar{R}(\mathscr{X})$ of the *regularization term* $\gamma R(x)$ at convergence of the MAP estimations (bottom). We also perform the Singular Value Decomposition (SVD) of the set of personalised parameters and report the eigenvalues (Figure 8.3, top). Then we report (rows of Table 8.3) the eigenvectors at the last iteration $(e_i, i = 1..6)$, and their corresponding eigenvalue $(\lambda_i, i = 1..6)$. The eigenvectors coordinates are reported as 0 in bold when the value was below 0.01.

First we observe the classic phenomenon that the higher γ is, the higher the *data-fit term* (which characterizes the distance between simulated and measured values) is (Figure 8.3, bottom, blue). A higher γ means that the noise (i.e. uncertainty on the measurements) is considered bigger in Equation 8.2 so estimated parameters values then tend to be closer to the prior mean than from a value which perfectly fits the measurements.

Second, that in every run of the algorithm, there is one or more eigenvalue which converges to 0 and is under 10^{-4} at convergence. When the value is zero, this means that the parameters lie on a subspace of lower dimension. Here for each run, we report in Table 8.4 the number of eigenvectors with a eigenvalue above 10^{-4}, the mean value $\bar{S}(\mathscr{X}, \widehat{\mathscr{O}})$ of the data-fit term across all cases and the mean value $\bar{R}(\mathscr{X})$ of the regularization term.

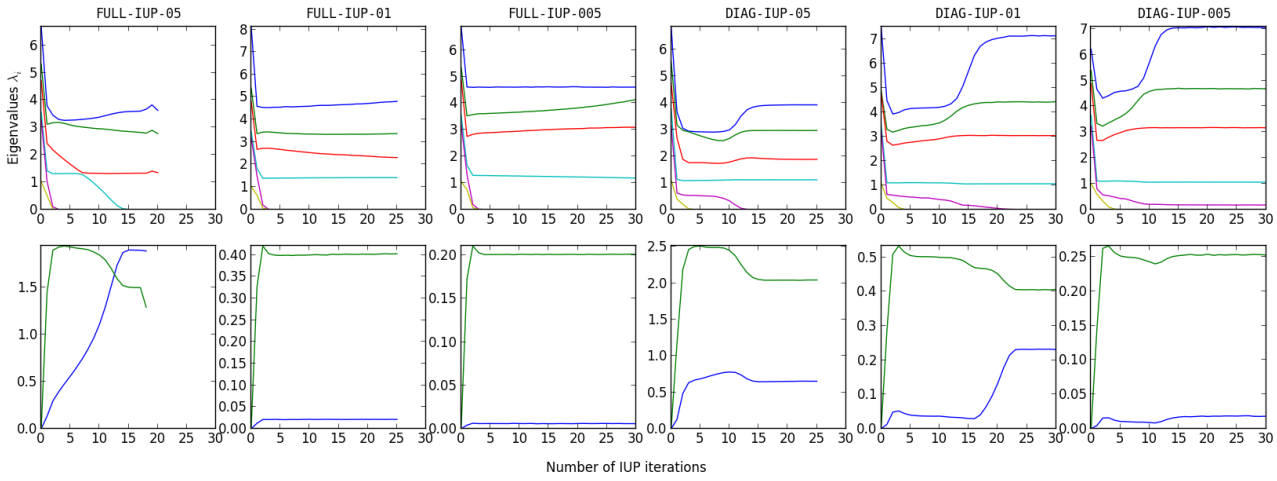

Figure 8.3: **Top:** value of the eigenvalues of the SVD of personalised parameters at each IUP iteration. **Bottom:** mean values $\bar{S}(\mathscr{X}, \widehat{\mathscr{O}})$ and $\bar{R}(\mathscr{X})$ of the *data-fit term* $S(x, \widehat{O})$ (blue) and the *regularization term* $\gamma R(x)$ (green) across the population at each IUP iteration.

FULL-IUP-05

	σ_0	R_0	c_1	P_{ve}	R_p	τ	λ_i
e_1	0.54	-0.31	-0.26	0.13	0.53	-0.50	3.62
e_2	-0.12	0.16	0.06	-0.74	-0.17	-0.62	2.73
e_3	-0.45	-0.69	-0.47	-0.25	0.03	0.15	1.34
e_4	-0.21	0.63	-0.66	-0.03	0.34	0.08	**7.42e-5**
e_5	-0.49	**0**	-0.05	0.61	-0.22	-0.58	**5.42e-6**
e_6	-0.45	**0**	0.51	-0.05	0.73	**0**	**2.87e-9**

DIAG-IUP-05

	σ_0	R_0	c_1	P_{ve}	R_p	τ	λ_i
e_1	0.16	-0.18	**0**	-0.35	0.90	**0**	3.91
e_2	-0.22	0.23	**0**	-0.91	-0.27	**0**	2.96
e_3	-0.92	0.20	**0**	0.20	0.28	**0**	1.88
e_4	-0.28	-0.93	**0**	-0.11	-0.18	**0**	1.11
e_5	**0**	**0**	1.00	**0**	**0**	0.04	**2.08e-13**
e_6	**0**	**0**	-0.04	**0**	**0**	1.00	**3.71e-30**

FULL-IUP-01

	σ_0	R_0	c_1	P_{ve}	R_p	τ	λ_i
e_1	0.38	0.09	-0.04	0.02	-0.55	0.74	4.80
e_2	0.68	-0.30	-0.41	0.33	0.42	-0.04	3.37
e_3	0.55	0.17	0.07	-0.64	-0.23	-0.45	2.31
e_4	0.08	0.69	-0.14	0.57	-0.25	-0.34	1.41
e_5	0.03	0.63	-0.06	-0.29	0.61	0.37	**6.65e-5**
e_6	0.30	**0**	0.90	0.27	0.19	0.02	**3.13e-7**

DIAG-IUP-01

	σ_0	R_0	c_1	P_{ve}	R_p	τ	λ_i
e_1	0.12	-0.08	**0**	**0**	0.54	0.83	7.15
e_2	-0.46	-0.14	**0**	**0**	0.76	-0.44	4.44
e_3	0.86	-0.24	**0**	**0**	0.29	-0.33	3.04
e_4	-0.16	-0.96	**0**	**0**	-0.23	0.08	1.06
e_5	**0**	**0**	-0.31	-0.95	**0**	**0**	**3.06e-13**
e_6	**0**	**0**	-0.95	0.31	**0**	**0**	**3.64e-17**

FULL-IUP-005

	σ_0	R_0	c_1	P_{ve}	R_p	τ	λ_i
e_1	0.09	0.15	0.37	-0.68	-0.37	-0.49	5.03
e_2	0.46	0.11	-0.27	-0.06	-0.67	0.50	4.49
e_3	-0.72	0.29	0.38	0.11	-0.34	0.36	2.99
e_4	0.31	0.74	0.20	-0.14	0.47	0.27	1.12
e_5	0.14	-0.57	0.51	-0.31	0.21	0.50	**5.73e-5**
e_6	-0.39	**0**	-0.59	-0.64	0.20	0.23	**1.10e-6**

DIAG-IUP-005

	σ_0	R_0	c_1	P_{ve}	R_p	τ	λ_i
e_1	0.13	-0.08	**0**	0.02	0.50	0.85	7.06
e_2	0.51	0.13	**0**	**0**	-0.76	0.39	4.69
e_3	0.84	-0.24	**0**	-0.01	0.34	-0.35	3.18
e_4	0.16	0.96	**0**	**0**	0.23	-0.07	1.06
e_5	**0**	**0**	**0**	**-1**	0.01	0.01	0.17
e_6	**0**	**0**	-1.00	**0**	**0**	**0**	**5.21e-14**

Table 8.3: For each run of the IUP algorithm, final eigenvectors of the SVD of personalised parameters (e_i) and their corresponding eigenvalue λ_i. In bold we emphasize the coordinates of eigenvectors which are lower than 10^{-3} and the eigenvalues which are lower than 10^{-4}.

Run	γ	$\lambda \geq 10^{-4}$	$\bar{S}(\mathscr{X}, \widehat{\mathscr{O}})$	$\bar{R}(\mathscr{X})$
FULL-IUP-05	0.5	3	1.85	1.5
FULL-IUP-01	0.1	4	2.15e-2	0.40
FULL-IUP-005	0.05	4	6.18e-3	0.20
DIAG-IUP-05	0.5	4	0.65	2.04
DIAG-IUP-01	0.1	4	0.23	0.41
DIAG-IUP-005	0.05	5	1.96e-2	0.25

Table 8.4: For each run at the final iteration : number of eigenvectors for each run with a eigenvalue above 10^{-4} (column '$\lambda \geq 10^{-4}$'), mean *data-fit* value $\bar{S}(\mathscr{X}, \widehat{\mathscr{O}})$ across all cases and mean value $\bar{R}(\mathscr{X})$ of the regularization term.

From this table, we first observe that the mean of the *regularization term* is very close to γD where D is the number of eigenvectors which do not have a value close to 0 (we use $\lambda \geq 10^{-4}$ as the threshold for *close to 0*), which is consistent with Equation 8.10 of a cost function with a sparse regulariser on the dimensionality of the set of personalised parameters. We also observe that for the same γ, the data-fit term is lower for the runs with the **Full Matrix** updates than the **Diagonal Matrix** while having a lower number of non-zero eigenvalues.

More interestingly, we can observe the shape of the eigenvectors at convergence of the algorithm. In every run with **Diagonal Matrix** updates, we observe that the smaller the eigenvalue associated to eigenvector is, the more it is aligned to a coordinate (a vector with shape **(0,...,1,...0)**). This means that for these runs, the parameters associated with these coordinates have a constant values in the final set of personalised parameters. In particular, the contractility c_1 has always a constant value, and either τ (in DIAG-IUP-05) or P_{ve} (in DIAG-IUP-01) is constant as well. On the other hand, there is no such phenomenon in the runs with **Full Matrix**.

The behaviour of the algorithm can be understood from the sparse formulation explicited in 8.2.5 and the cost functions which is minimised. The algorithm indeed tries to find a prior for which there is an optimal trade-off between the number of dimensions of the set of personalised parameters, and the mean value $\bar{S}(\mathscr{X}, \widehat{\mathscr{O}})$ of the *data-fit term*. Given a specific γ, the "cost" of lowering the dimension is an increase of γ in $\bar{S}(\mathscr{X}, \widehat{\mathscr{O}})$. With the **Diagonal Matrix** updates, this is done with a constraint on the prior covariance matrix to be diagonal so having a lower dimension means fixing the value of a parameter. On the other hand, with the **Full Matrix** updates, the algorithm can find any direction.

In particular we can observe than for $\gamma = 0.1$, both algorithms find a parameter subspace of dimension 4, but the data-fit $\bar{S}(\mathscr{X}, \widehat{\mathscr{O}})$ is higher with **Diagonal Matrix** updates ($0.23 \geq$ 2.15e-2), where both c_1 and P_{ve} are fixed. By comparing to the DIAG-IUP-005 where only the c_1 is fixed, we can interpret that the "cost" of fixing P_{ve} is a loss of around 0.23 on $\bar{S}(\mathscr{X}, \widehat{\mathscr{O}})$, which also means that the quality of some personalisations in the database is impacted.

Indeed, for the final personalisation of DIAG-IUP-01 there are at least 3 cases

for which the personalisation is highly impacted ($\sqrt{S} \geq 3.5$) because of the fixed value of P_{ve}. These cases have an *aortic diastolic pressure* which is particularly low compared to the rest of the database $DP \leq 5400Pa$. To fit this measurement, P_{ve} (which is the asymptotic and minimal value of the aortic pressure in the blood flow model) needs to be at least below this value (in particular in `DIAG-IUP-005` and `FULL-IUP-01`, all measurements of these cases are almost perfectly fitted and the estimated P_{ve} for theses cases is $\leq 5380Pa$), but at this step the prior value of P_{ve} in `DIAG-IUP-01` (which is thus the fixed constant value) is $5873Pa$, which makes the fitting of the Diastolic Pressure impossible in these cases.

8.3.2 Parameter Existence and Uniqueness in the Resulting Hyperplanes

A classical question in modeling and inverse problems, is to determine which parameters are *observable* with respect to a specific set of measurements. For example, here we estimate 6 parameters from 4 observed outputs. If there is a linear relationship between the parameters and the outputs (i.e there exist a matrix M such as $\mathscr{O}(x) = Mx$), the size of the kernel of the matrix is at least 2. Considering some measurements $\mathscr{O}$, some parameters x such as such as $\mathscr{O} = Mx$, then for any vector y in the kernel $\mathscr{O} = M(x + y)$ as well. This means that there are at least two orthogonal parameter directions in which the parameter values are *unobservable*. With a non linear-model (such as cardiac models), a similar phenomenon of non-uniqueness exists locally around some personalised parameters, to the extent that the model can be approximated by its gradient. In general, there is an entire manifold of parameters for which the outputs are the same.

Using Gaussian priors on such underconstrained linear models leads to promote a unique solution to the inverse problem, because in this case, the cost function 8.8 is strictly convex. To a certain extent, this can be locally true for a non-linear model and a unique specific value is promoted within the manifold of parameters for which the outputs are the same.

Finding a (possibly unique) value which is *the most consistent* considering a *prior knowledge* on the distribution of parameters is then the most interesting consideration of the MAP estimation, but this supposes to have an accurate prior. Since we are deriving the prior probability distribution from successive personalisations over the dataset itself, it is thus not possible to rely on its interpretation as a "prior knowledge" to set parameter values in the unobservable directions *of this dataset*.

On the other hand when no information on the statistics of the parameters is available, the only possibility is to perform a reduction of the parameter space, by forcing some parameter or parameter directions to have a fixed value. This can be done through PCA, PLS ([Rohé 2016]) or sensitivity analysis ([Marchesseau 2013a]) on the parameters with respect to the clinical data, and estimate coordinates of the first modes only. This also leads to a few questions regarding the reduced space of parameters, particulary on the existence and uniqueness of parameter values for which the simulation fits the target data.

Here our parameters converge into a reduced subspace in all runs of the algorithm. In particular in the `FULL-IUP-005`, `FULL-IUP-01`, `DIAG-IUP-005` run, there is also a very low data-fit term across the cases. This suggests that among the parameter space in which there are undetermined directions, **with a small enough prior, the algorithm selects an hyperplane of minimal dimension in which for each case, there is at least a set of parameter values which fits exactly the measurements**.

We demonstrate this claim by analysing the resulting parameter subspaces, in these terms of parameter existence and uniqueness. To that end we perform multiple personalisations without priors (i.e. an uniform prior, which is equivalent to solving Equation 8.8 without regulariser, or setting $\gamma = 0$) where parameter are taken from within these subspaces. Because the CMA-ES algorithm is stochastic, it usually converges toward different values of the parameters at each run if there are multiple set of parameter values which minimise the cost function. We compare the following parameter subspaces:

1. The complete space $\mathscr{H}_0$ of 6 parameters.
2. The subspace $\mathscr{H}_{c_1}$ of 5 parameters of all parameters except the stiffness c_1, which is set to its final (constant) in the `DIAG-IUP-005` run.
3. The 5 subspaces $\mathscr{H}_{(c_1,\sigma_0)}, \mathscr{H}_{(c_1,R_0)}, \mathscr{H}_{(c_1,R_p)}, \mathscr{H}_{(c_1,\tau)}$ and $\mathscr{H}_{(c_1,P_{\text{ve}})}$ of 4 parameters where both the stiffness and another parameter are set to the final prior mean value in the `DIAG-IUP-005` run.
4. The 4 subspaces $\mathscr{H}_5, \mathscr{H}_4, \mathscr{H}_3, \mathscr{H}_2$ of dimensions respectively 5,4,3 and 2, which are the hyperplanes defined by their center at the prior mean of the `FULL-IUP-01`, and the l largest eigenvectors of the prior covariance for respectively l=5,4,3,2.

We then report both the mean *error of fit* $\overline{\sqrt{S}(\mathscr{X}, \widehat{\mathscr{O}})}$ across all cases in the database, and the *variability* of estimated parameters across different personalisations, estimated by averaging across all cases the standard deviation of the 5 estimated values in the 5 personalisations.

We first observe that **the mean error of fit is 0 (lower than 10^{-3}) for only four parameter spaces**: the original space $\mathscr{H}_0$, the parameter space $\mathscr{H}_{c_1}$ with all the parameters except c_1, and the two parameter spaces $\mathscr{H}_4$ and $\mathscr{H}_5$ with respectively the 4 and 5 largest eigenvectors of the `Full-IUP-01` run. This shows that they are the only subspaces which contain parameter values which fit the measurements for all cases.

Then among these subspaces, we observe that **the only subspace for which both the mean error of fit and the variability of all parameters is 0 (lower than 10^{-3}) is** $\mathscr{H}_4$, the hyperplane with the 4 largest eigenvectors of `Full-IUP-01`. In the other subspaces there is a variability from one personalisation to the other for at least the haemodynamic parameters P_{ve}, R_p and τ showing that the parameters are not unique.

Table 8.5: Mean error of fit and variability of personalised parameters in 5 personalisations for the parameter subspaces. The value is reported as 0 if it is lower than 10^{-3}.

	$\overline{\sqrt{S}}$	σ_0	R_0	c_1	P_{ve}	R_p	τ
$\mathscr{H}_0$	**0**	0.03	0	0.13	0.02	0.03	0.04
$\mathscr{H}_{c_1}$	**0**	0	0	-	0.02	0.02	0.03
$\mathscr{H}_{(c_1,\sigma_0)}$	0.99	-	0	-	0.02	0.02	0.14
$\mathscr{H}_{(c_1,R_0)}$	3.90	0	-	-	0.05	0.02	0.04
$\mathscr{H}_{(c_1,P_{\text{ve}})}$	0.06	0	0	-	-	0	0.06
$\mathscr{H}_{(c_1,R_p)}$	0.07	0	0	-	0.07	-	0
$\mathscr{H}_{(c_1,\tau)}$	0.01	0	0	-	0.02	0	-
$\mathscr{H}_5$	**0**	0	0	0	0.015	0.017	0.03
$\mathscr{H}_4$	**0**	**0**	**0**	**0**	**0**	**0**	**0**
$\mathscr{H}_3$	1.99	0.03	0	0.002	0	0.004	0.01
$\mathscr{H}_2$	3.03	0	0	0	0	0	0

This shows that around the prior which was found in the `DIAG-IUP-005` run, c_1 was the only parameter which is possible to set to a constant value without the personalisation of some cases being impacted (such as the 3 cases described in the previous section). However, once c_1 is set, the variability in $\mathscr{H}_1$ show that there is still an unobservable direction (especially in the haemodynamic parameters), but it is then necessarily a *combination of parameters* which is unobservable.

Finally, because of the possibility to find subspaces which are not necessarily aligned with the coordinates, the `Full-IUP-01` run was able to find a subspace of lower dimension, 4, in which there are parameters fitting all the cases and no variability, thus reducing the space in both directions of uncertainty.

8.3.3 Selection of a Parameter Subspace for Personalisation

The resulting parameter subspaces in the previous section exhibit interesting properties in terms of existence and unicity of parameters for personalisation, so a question is *how relevant are they in the context of personalisation?* First, it is important to observe that there is no guarantee of uniqueness of the parameter directions which are selected by the algorithm (and the personalised parameter either). Indeed, in addition of the model being non-linear (which makes the data-fit term not convex, thus the whole Equation 8.8), sparse regularisations are usually not convex and have many possible solutions. In particular here, there are possibly multiple parameter subspaces on which the algorithm could converge. Visually, this can be observed in the schema of Figure 8.2, where two different subspaces can be selected, each containing a unique set of parameter values for each of the 5 cases.

Secondly, there are no guarantees that the parameter spaces selected by the algorithm are relevant from a modeling or physiological point of view. In particular,

when two parameters are not completely observable from some measurements in a database, their 'actual' value (if they correspond to physical parameters) in a population is likely variable. In addition, a drawback of fixing a parameter to a specific value, is that it might force other estimated parameters to vary more within the population to account for variations which would have come from the fixed parameter.

Parameter selection in the sense of setting a specific parameter direction to a constant value is then an imperfect approach in modeling, but it is unavoidable to not have variability in the estimation when no other information or statistics is available on this specific parameter direction. In this context, though the selection of relevant parameters for personalisation cannot be performed entirely automatically (because the physical meaning of parameters is ignored by the algorithms), we believe that our algorithm can help the modeler by revealing unobservable parameter and parameter directions. To that end, we recommend the following general approach, considering a set of clinical data for which observable parameters are unclear:

1. First, perform one (or multiple) runs of IUP with **Diagonal Matrix** updates. This is because the resulting subspace is easier to analyze, since the parameters usually have a physical meaning in the context of modeling. Then analyze the parameters which end up with a eigenvalue close to 0, and set them to a constant value if it is not incompatible with physiological considerations.

2. Second, perform one (or multiple) IUP with **Full Matrix** updates to further select a lower dimensional subspace.

We apply this approach to the current problem. First it seems physically likely that we do not have so much information on the stiffness c_1 from only the 4 measurements in Table 8.1, so we can reasonably decide to set its value to a constant, which we set at its value in `DIAG-IUP-005`. Then we perform a new run of the IUP algorithm, which we call `Final-IUP-005`, with **Full Matrix** and $\gamma = 0.05$ on the resulting parameters (thus in the hyperplane $\mathscr{H}_5$). This leads to the final eigenvectors and eigenvalues:

Table 8.6: Final eigenvectors and eigenvalues of the IUP run with **Full Matrix** and $\gamma = 0.05$ on $\mathscr{H}_5$.

`Final-IUP-005`

	σ_0	R_0	P_{ve}	R_p	τ	λ_i
e_1	0.58	0.07	0.05	-0.51	0.63	4.77467
e_2	0.46	-0.32	0.50	0.65	0.10	3.41794
e_3	0.65	-0.06	-0.44	-0.06	-0.61	2.95973
e_4	0.16	0.94	0.15	0.25	-0.05	1.03746
e_5	0.01	-0.01	0.73	-0.50	-0.47	**4.30e-6**

We then select the hyperplane $\mathscr{H}^*$ made of the 4 largest eigenvectors (e_1, e_2, e_3, e_4) at the end of the run, and test the existence and uniqueness of personalised parameters in this hyperplane, with the same method than in the previous section. Results are reported in Table 8.7.

Table 8.7: Mean error of fit and variability of personalised parameters in 5 personalisations in $\mathscr{H}^*$. The value is reported as 0 if it is lower than 10^{-3}.

	$\overline{\sqrt{S}}$	σ_0	R_0	P_{ve}	R_p	τ
$\mathscr{H}^*$	**0**	**0**	**0**	**0**	**0**	**0**

As expected, both the variability of parameters and the mean error of fit are 0 (lower than 10^{-3}). This means that for each case, the hyperplane contains a unique (to the extent that we can evaluate it through this algorithm) set of parameter values for which the simulation fits the measurements.

To conclude, we found a **minimal parameter subspace of dimension 4, based on 5 parameters**, consistent from a physiological point of view, in which to perform consistent parameter estimation. We finally point out that the final parameters μ^* and Δ^* of the prior at the end of the `Final-IUP-005` run respectively correspond to the mean and covariance of the estimated parameters, which we then call the *population-based priors*.

8.4 Consistent Parameter Estimation with Missing or Heterogeneous Data.

In this section we present the application of the proposed framework to the personalisation of a large database with missing and heterogeneous measurements in the reduced subspace $\mathscr{H}^*$, with the *population-based priors* μ^* and Δ^*.

8.4.1 A Heterogeneous Database of Cases

In addition to the 137 *complete acquisitions* for which all the measurements and the biventricular mesh were available in the database of the MD-Paedigree project, various acquisitions were also available for many patients in the various cohorts, without necessarily the imaging (which excludes the biventricular mesh) or the complete (or even the same) set of measurements.

From this data, we built a database of 811 cases from different studies, hospitals and protocols. We focused on gathering patients for which the heart rate and *at least one of the 6 following measurements in Table 8.8* was available.

Within this database, we have the following statistics:

- Pressure Measurements are available for 651 cases only.
- The Maximal Volume and Minimal Volume are both available for only 340 cases.

Measurements $\mathscr{O}$
Maximal Volume $MaxV$
Minimal Volume $MinV$
Stroke Volume SV
Ejection Fraction EF
Mean Aortic Pressure MP
Diastolic Aortic Pressure DP

Table 8.8: Measurements considered in the Heterogeneous Database

- Among the 471 other cases, either the Ejection Fraction (63 cases), Stroke Volume (386 cases) or no volume measurement (21 cases) at all are available.
- Ejection Fraction is the only measurement available in 38 cases.
- Stroke Volume is the only measurement available in 45 cases.
- 258 cases have the 'complete' set of 4 measurements: Maximal Volume, Minimal Volume, Mean Aortic Pressure and Mean Diastolic Pressure (we do not report Ejection Fraction and Stroke Volume if the Maximal Volume and Minimal Volume are already reported).

8.4.2 Personalisation in the Reduced Subspace $\mathscr{H}^*$

In order to accommodate the heterogeneous nature of the database, we need to build a *heterogeneous data-fit term.* Instead of using the fixed formulation $S(x, \widehat{O}) = ||(O(x) - \widehat{O}) \oslash \mathscr{N}||^2$ with O being the vecteur of outputs $(MaxV, MinV, MP, DP)$ and $\widehat{O}$ the corresponding measurements, we build a different vector of observations for each patient. Depending on the available measurements, we use in the order of priority, depending on the available measurements:

1. $(MaxV, MinV, MP, DP)$,
2. $(MaxV, SV, MP, DP)$,
3. $(MaxV, EF, MP, DP)$,
4. $(MinV, MP, DP)$,
5. (SV, MP, DP),
6. (EF, MP, DP),
7. $(MaxV, MinV)$,
8. $(MaxV, SV)$,
9. $(MaxV, EF)$,
10. $(MinV)$,
11. (SV),
12. (EF),

and a corresponding normalisation vector $\mathscr{N}$. The normalisation coefficient for the Ejection Fraction (EF) (which is a number between 0 and 1) is **0.05** and it is **10 ml** for the Stroke volume.

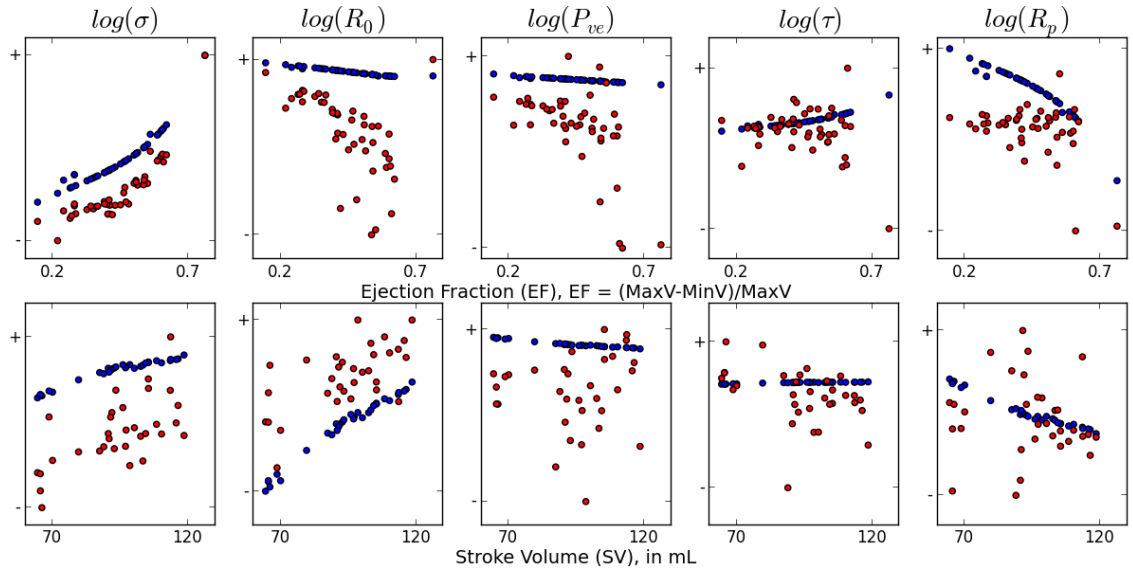

Figure 8.4: **Top:** (resp **Bottom:**) Log-value of estimated parameters value as a function of the Ejection Fraction (resp Stroke volume) for the 38 (resp 45) cases where only the Ejection Fraction (resp Stroke Volume) is available, in blue with the population-based priors μ^* and Δ^* algorithm, in red without priors.

We compare two parameter estimations for this database: first an estimation of the 5 parameters without priors, and an estimation in the space $\mathscr{H}^*$ from Section 8.3.3 with the population-based priors μ^* and Δ^* and $\gamma = 0.02$. For both estimation the mean *error of fit* across the whole database is under 0.06, which means most measurements are well fitted across the database.

The most interesting set of values to understand the impact of priors on cases where measurements are missing is the following: in Figure 8.4, we display the (log-)values of estimated parameters as a function of Ejection Fraction (resp Stroke Volume) for the cases where only the Ejection Fraction (resp Stroke Volume) is available. We observe a classic phenomenon with priors: personalised values not only have less variance with the use of priors (blue points), but because one measurement has to be fitted, they also lie onto a space of (local) dimension 1. Indeed, this space is defined (in the case of the ejection fraction) by the solution of $x(EF) = argmin_x \widehat{S}(x, \widehat{\mathscr{O}} = EF, \mu^*, \Delta^*)$. It is a space of local dimension 2 (resp 3) when 2 (resp 3) measurements have to be fitted (to the extent that the model is locally approximable to its gradient).

On an interpretative level, when some measurements are missing in our database and many parameter values are possible, the personalisation with priors in $\mathscr{H}^*$ leads to the selection of a set of parameter values which maximises its likelihood in the probability distribution of the priors (or equivalently minimizes the distance $(x_i - \mu^*)^T(\Delta^*)^{-1}(x_i - \mu^*)$). To that extent, it performs a form of imputation in the parameter space by choosing the *most likely* set of parameters according to the distribution defined by μ^* and Δ^*. Because in our case μ^* and Δ^* are computed

from a population of personalised parameter values in a space of *minimal dimension* (as explained in Section 8.3.3), we believe our population-based priors ensure one of the highest form of consistency in estimated parameters for this larger dataset.

8.5 Conclusion

We introduced a method called **Iteratively Updated Priors** which performs successive personalisations of the cases in a population, where the prior probabilities on parameter values at each iteration are set from the statistics of personalised parameters in the previous iteration. We explicited two type of updates depending on the assumptions made on the distribution of parameters in the population. We then derived a mathematical link between this algorithm and the minimisation of a *population-wide cost function* with a penalty on the *dimension of the set of personalised parameters*, with two different interpretations depending on the covariance matrix update. Depending on the type of covariance used for the updates, we see that the resulting set of personalised parameters has different properties, leading to the estimation of either *parameters* or *parameter directions* which can be set to a constant value. This led to the selection of a reduced parameter subspace and the computation of **population-based** priors in this subspace, in which we personalised a larger data set of 811 cases.

A first extension is that beside the two types of updates presented here (**Full Matrix** and **Diagonal Matrix**), many other assumptions on the probability distribution of parameters in the population could be used, resulting in different formulations of the prior parameters. For example, the assumption could be made that the contractility σ_0 is independent of the other parameters, resulting in a block matrix covariance. Similarly, if the mean of a parameter value is known, then it is also easy to change the updates to accommodate this case (the derivations of the maximum likelihood updates for parameters of Gaussian priors are easily tractable even with such constraints). Finally, in the case where external information on the patient such as the height and weight is available, this information could be included as additional parameters in the (prior) probability distribution. Preliminary results (see APPENDIX B) suggest that this could be particularly useful in cases where measurements are missing, because parameters would be partly guided by correlations to these values instead of just being attracted to the mean of the prior.

Secondly, in this work we first performed the IUP algorithm on a population where all the measurements were available, then we applied the resulting priors to the personalisation of a larger database. An interesting question is *would it be possible to do both at the same time?* This would mean simultaneously estimating a reduced parameter space, population-based priors in this space, and constrain the cases where the measurements are missing. According to preliminary results, the answer could be yes, but it needs an adaptation of the algorithm. Indeed, an IUP run on the database of 811 patients with γ as small as 0.02 leads to a parameter space of 3 directions instead of 4. Many cases with the 4 measurements available are thus

not well fitted but because cases with less measurements are well fitted, it lowers the impact on the *mean error of fit across the population*, leading the IUP algorithm to remove a direction. An approach to avoid this problem would be to progressively reduce the value of the normalisation coefficient $\mathcal{N}$ during personalisation to ensure a sufficient fit of each member of the database at each iteration. In this context, the most interesting outlook for future applications in our opinion is the possibility of using this method to simultaneously perform parameter estimation of two or multiple databases, in which parameters would only be partially constrained in each database. We believe information on observed parameters from one database could be shared to the other databases through the prior. For example, if a database only contains information on *systolic flow* and another database contains information on *diastolic flow* (such as the E and A indices in echocardiography), the values of parameters which are determined by the fitting of the systolic flow would be used as a prior to constrain the parameters in the other database, and reciprocally.

Thirdly, a last extension of this work is to apply the IUP to the 3D model to select a reduced subspace of 3D model parameters for personalisation. However in the case of the 3D model, the computational burden associated with performing a dozen or more repeated personalisations of the whole database can be too high. Even though it is usually not trivial to perform a mapping of parameter spaces between the 0D model and the 3D model, we believe a possibility, for which we show preliminary results in APPENDIX C, is to use the personalisation in a reduced subspace of 0D model parameters (such as $\mathscr{H}^*$) to influence the estimation of a 3D model. Another direction could be to investigate the use of specific 0D / 3D *multifidelity couplings* such as presented in **Chapter 5** to lower the burden of repeated personalisations.

We conclude with a general comment on priors and the relevance of parameter selection in the context of personalisation. In the ideal case where we have prior statistics on all the parameters, every parameter which has an influence on a specific measurement will likely change during inference, in accordance to the probability defined by the prior. This is why all the parameters vary at least slightly from the mean when only the ejection fraction or the stroke volume are available in our example. However if no statistics or external information is available on a set of parameters, a specific set of values of these parameters does not make *more sense* than another one that also fits the measurements. There is thus no other choice than arbitrarily choosing a direction, until more information can be given on this parameter direction from more experimental or physiological knowledge. Within these considerations, the best approach consists in our opinion in starting with a high number of parameters, and iteratively reducing the parameters space until a sufficient subspace is found in which all directions can be observed. We argue that our *Iteratively Update Prior* method, though it absolutely requires supervision for the selection of parameters with physiological relevance, gives a complete framework for consistent parameter estimation through the joint selection of a parameter subspace of reduced dimension and the creation of relevant priors on its directions.

8.6 APPENDIX: Link between the IUP algorithm and the Iteratively Reweighted Least Square (IRLS) algorithm

Here we demonstrate a link between the IUP algorithm and the *Iteratively Reweighed Least Square* in sparse regression. In particular, we exhibit a population-wide cost function with *sparse regularisation*. The sparse penalty correspond to the rank of the covariance matrix of the estimated set of personalised parameters, which has two different interpretation depending on the covariance matrix update.

For a given iteration k of the IUP algorithm, we note $\mathscr{X}_k = (x_1, ..., x_n)$ the concatenation of some vectors of parameter values $x_i, i = 1..n$ for all the n cases, and $\widehat{\mathscr{O}} = (\widehat{O}_1, ..., \widehat{O}_n)$. We define the **population-wide cost function** $\mathscr{S}(\mathscr{X}_k, \widehat{\mathscr{O}})$ as the mean of all the individual cost functions for all the $i = 1..n$ cases:

$$\mathscr{S}(\mathscr{X}_k, \widehat{\mathscr{O}}) = \frac{1}{n} \sum_{i=1}^{n} \widehat{S}(x_i, \widehat{O_i}, \mu^k, \Delta^k),$$
$$\mathscr{S}(\mathscr{X}_k, \widehat{\mathscr{O}}) = \frac{1}{n} \big(\sum_{i=1}^{n} S(x_i, \widehat{O_i}) + \gamma \sum_{i=1}^{n} R_k(x_i) \big).$$

The first sum of this expression is the sum of the data-fit terms over all the cases and is the same expression at each iteration. The second sum has a different expression at each step depending on the updates which are performed, which impact the behavior of the algorithm. We explicit here these expressions and explain the resulting behaviour of the IUP algorithm with these updates.

"Diagonal Matrix" updates.

At each iteration k we have:

$$\gamma \sum_{i=1}^{n} R_k(x_i) = \gamma \sum_{i=1}^{n} (x_i - \mu^k)^T (\Delta^k)^{-1} (x_i - \mu^k),$$

where Δ^k is a diagonal matrix computed from the personalised parameters $X_i^{\text{k-1}}$ at iteration $k-1$ with Equation 8.7. We can break down the sum along the $j = 1..N$ coordinates (corresponding to the N personalised parameters): we note Δ_{jj}^k the j-th component of the diagonal of Δ^k which formula is:

$$\Delta_{jj}^k = \frac{1}{n} \sum_{i=1}^{n} ((X_i^{\text{k-1}})_j - (\mu^{\text{k-1}})_j)^2.$$

We then have:

$$\gamma \sum_{i=1}^{n} R_k(x_i) = n\gamma \frac{1}{n} \sum_{i=1}^{n} \sum_{j=1}^{N} \frac{((x_i)_j - (\mu^k)_j)^2}{\Delta_{jj}^k},$$
$$\gamma \sum_{i=1}^{n} R_k(x_i) = n\gamma \sum_{j=1}^{N} \frac{\frac{1}{n} \sum_{i=1}^{n} ((x_i)_j - (\mu^k)_j)^2}{\Delta_{jj}^k}.$$

To understand the behaviour of our algorithm with these updates, we can look at the similarity between our updates and a classic method called *Iteratively Reweighted Least Square*, used to solve the minimisation of cost functions involving L_p norms such as

$$X^* = argmin_X ||Y - f(X)||^p = argmin_X \sum_l (Y - f(X))_l^p. \tag{8.11}$$

The IRLS algorithm works by succesively optimising the following (and usually easier) "weighted L_2" problems where in the k-th problem, each of the l coordinates are reweighted by a vector W_l^k derived from the norm of the coordinate in the solution of the previous problem:

$$\begin{cases} (X^*)^k = argmin_X \sum_l W_l^k (Y_l - f_l(X))^p, \\ \text{where } W_l^k = |Y_l - f_l((X^*)^{k-1})|^{p-2}. \end{cases} \tag{8.12}$$

In this context, the **Diagonal Matrix** updates in our algorithm are reweighting the penalty of each coordinate (or personalised parameters) j with the weight $(\Delta_{jj}^k)^{-1}$ which is inverse of the variance of the parameter in the current personalisation. To understand how the IRLS method applies in our case, we define the random vector D as the difference $(X_i^k - \mu_k)$ of the personalised parameters X_i^k to the mean of the population μ^k, for which all the cases are samples. The variance of each personalised parameter is then the (L_2) norm of the coordinate of this random vector. In this formulation, each update correspond to the IRLS formulation with p=0 for the minimisation of the L_0 norm of D.

As a consequence, if the successive μ^k and x_i^k converge, according to the IRLS method the value of regularization term converges to:

$$\gamma \sum_{i=1}^{n} R_k(x_i^*) = n\gamma ||D||_0,$$

where $||D||_0$ is the *number of coordinates of D which are non-zero*, which is also the *number of personalised parameters which do not have a unique value in the population.*

"Full Matrix" updates.

At each iteration k we have:

$$\gamma \sum_{i=1}^{n} R_k(x_i) = \gamma \sum_{i=1}^{n} (x_i - \mu^k)^T (\Delta^k)^{-1} (x_i - \mu^k).$$

As Δ^k is the covariance matrix of the X^{k-1} it can be orthogonally diagonalised and expressed as $\Delta^k = (O^k)(H^k)(O^k)^T$ with O^k an orthogonal matrix which columns are the principal directions of the set of X^{k-1}, H^k diagonal which diagonal coefficients are the variances of the X^{k-1} in these principal directions. We can write:

$$\gamma \sum_{i=1}^{n} R_k(x_i) = \gamma \sum_{i=1}^{n} (O^k(x_i - \mu^k))^T (H^k)^{-1} O^k(x_i - \mu^k),$$

and in this case, each update consists in an IRLS step in the basis b_k, defined by the principal directions of the set of X_i^{k-1} (the columns of O^k) in which the covariance matrix Δ^k is diagonal.

Each of these updates thus correspond to an optimisation step of the L_0 norm of the random vector D^k of the difference $O^k(X_i^k - \mu^k)$ of the personalised parameters X_i^k to the mean of the population μ^k, *expressed in the basis* b_k.

As a consequence, if the successive μ^k and x_i^k respectively converge to μ^* and x_i^*, and we can build a random vector D^* on a basis b^* to which the D^k and b_k respectively converge, the regularization term converges to:

$$\gamma \sum_{i=1}^{n} R_k(x_i) = n\gamma ||D^*||_0,$$

where $||D^*||_0$ is the *number of coordinates of* D^* *which are non-zero* expressed in the basis b^* (made of principal directions of the set of x^*). It is the rank of $\mathscr{X}$ or more simply the *number of principal directions in which parameters do not have a unique value in the population.*

8.7 APPENDIX B: Integration of External Parameters in the Prior Distribution for Improved Estimation of Unobserved Parameters.

The key idea behind the use of priors is to model the distribution of parameters in the population. Then with the MAP estimation, the goal is to find the *most likely parameters* according to the correlations in this distribution. Here we explore the possibility of integrating parameters which are not estimated into the prior distribution (we call them *external parameters*), to influence the value of estimated parameters.

Namely, for all the 811 cases of Section 8.4, the *height* and *weight* of the patients were available. We can also consider the *heart rate* which is not an estimated parameter. In order to add these three parameters to the prior distribution, we perform the following modifications of the method: in Equation 8.8, instead of considering a vector x which only contains the parameters to be estimated, we use the *concatenation vector* of the estimated parameters and the three *external parameters*. Formulations of the prior covariance and mean in Equations 8.2 and in the equations of Section 8.2.3 are adapted as well to accomodate this *concatenation vector*.

We then perform the following experiment: from the estimated parameters in Section 8.4, we estimate the covariance matrix and the mean of the *concatenation vector*, which we then use as a prior for a new estimation (This is equivalent to one iteration of the IUP algorithm with **Full Matrix** with this *concatenation vector*).

We report the most interesting result here in Figure 8.5. For both the estimation *without external parameters* **E1** (blue points) and *with external parameters* **E2** (red points), we display the estimated values of the *resting radius* R_0 for the cases where the Ejection Fraction is the only measurement, as a function of **a**/ the *height* of the patient (left), **b**/ the *weight* of the patient (middle) and **c**/ the *Ejection Fraction* of the patient.

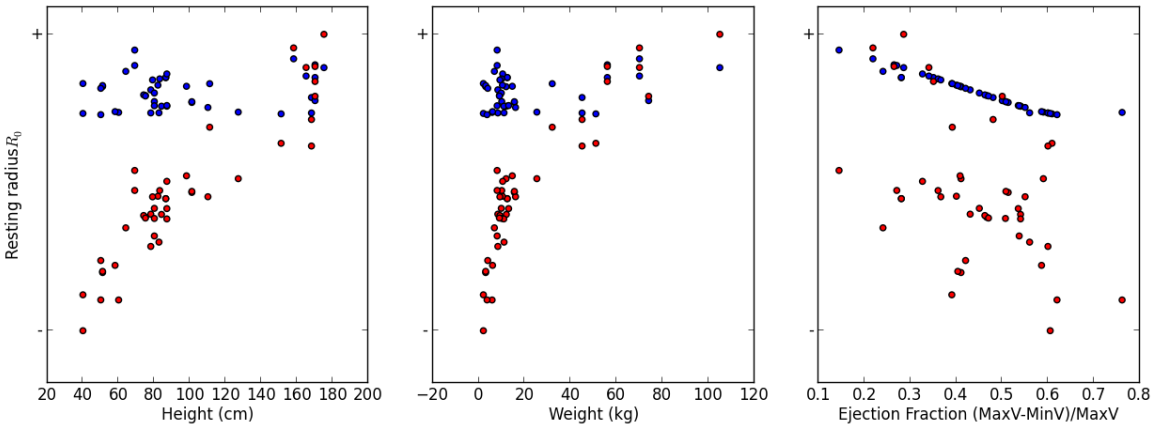

Figure 8.5: Estimated values of the *resting radius* R_0 in the estimation *without external parameters* **E1** (blue points) and *with external parameters* **E2** (red points).

The results are the following: first in both estimations the goodness of fit for the cases in the database is similar and high (a mean *error of fit* of around 0.06). For the estimation without external parameters **E1**, the resting radius is well correlated to the Ejection Fraction (this was already observed in Figure 8.4), but **not at all to the weight and the height**. However with the external parameters **E2**, the values of the resting radius is **very correlated to the height and weight of the patients**, and tends to increase with both these measurements. Since the resting radius, from a physical point of view, is related to the *size* of the heart, this correlation makes sense from a physical point of view.

The preliminary results presented here show that it is possible to add external parameters in the probability distribution of the prior, to then guide the estimation of relevant physical parameters for cases where these parameters cannot be observed (such as the cases where we only have the *ejection fraction*). An interesting extension of this work would be to investigate if it is possible to perform this step automatically within the IUP algorithm, simultaneously to the estimation of a reduced subspace of estimated parameters.

8.8 APPENDIX C: Multiscale 0D / 3D personalisation of the 137 complete acquisitions.

The IUP algorithm and parameter selection approaches presented in this chapter can be applied directly to parameter estimations with the 0D or the 3D model.

However in the case of the 3D model, the computational burden associated with performing a dozen or more repeated personalisations of the whole database (around 2.5 days per complete personalisations) is too high. Here we propose a method to use the personalisation of the 137 *complete acquisitions* in $\mathscr{H}^*$ with the 0D model (Section 8.3.3), to guide the personalisation of the same cases with the 3D model.

We focus on the estimation of the same parameters of the 3D model than in **Chapter 7**: stiffness, contractility and the 3 haemodynamics parameters. Because the stiffness was set to a constant value in the 0D model, it makes sense to set it to a constant value in the 3D model as well. The resulting sets of parameters for both model are thus the following:

Table 8.9: List of estimated 0D model parameters (in $\mathscr{H}^*$) and estimated 3D model parameters.

Estimated 0D Model Parameters	*Estimated 3D Model Parameters*
Contractility σ_0	*Contractility* σ_0
Resting Radius R_0	*Peripheral Resistance* R_p
Peripheral Resistance R_p	*Windkessel Characteristic Time* τ
Windkessel Characteristic Time τ	*Venous Pressure* $P_{\mathbf{ve}}$
Venous Pressure $P_{\mathbf{ve}}$	

The haemodynamic parameters R_p, C and P_{ve} have the same equations in both models. However as explained in **Chapter 5** the contractility σ_0 do not have the same value in both models, because of differences in mechanical assumptions and implementation. Also, we note that the *resting radius* parameter R_0 in the 0D model is not a variable in the 3D model because the biventricular mesh is an input of the mechanical model. It is thus not possible to trivially convert or perform a direct mapping of the reduced subspace $\mathscr{H}^*$ from the space of 0D parameters to the space of 3D model parameters.

A possibility would be to impose the values of the haemodynamic parameters estimated in the 0D model to the 3D model and estimating only the contractility in the 3D model. However, this leads to a very badly conditioned non-convex function for the estimation of contractility. In addition, differences in the mechanical properties of both models could possibly require haemodynamics parameters to have different values in both models to reach the same measurements. Rather, in this section, we relax this constraint and **we propose to use the estimated values of the haemodynamic parameters with the 0D model, as a prior to the haemodynamics values in the parameters estimation of the 3D model**.

We use our **Multifidelity-CMA** algorithm to personalise the whole database with this setting (which we call **P1**). We report in Figure 8.6 the (log-)values the estimated 3D parameters and the 0D as a function of the 0D parameters for all the cases, which we compare to the estimated 3D parameters of the complete database with the priors defined in Section **??** of **Chapter 7** (which we call **P2**).

The mean error of fit for **P2** is 0.07 and slightly higher (0.13) for **P1**. In both

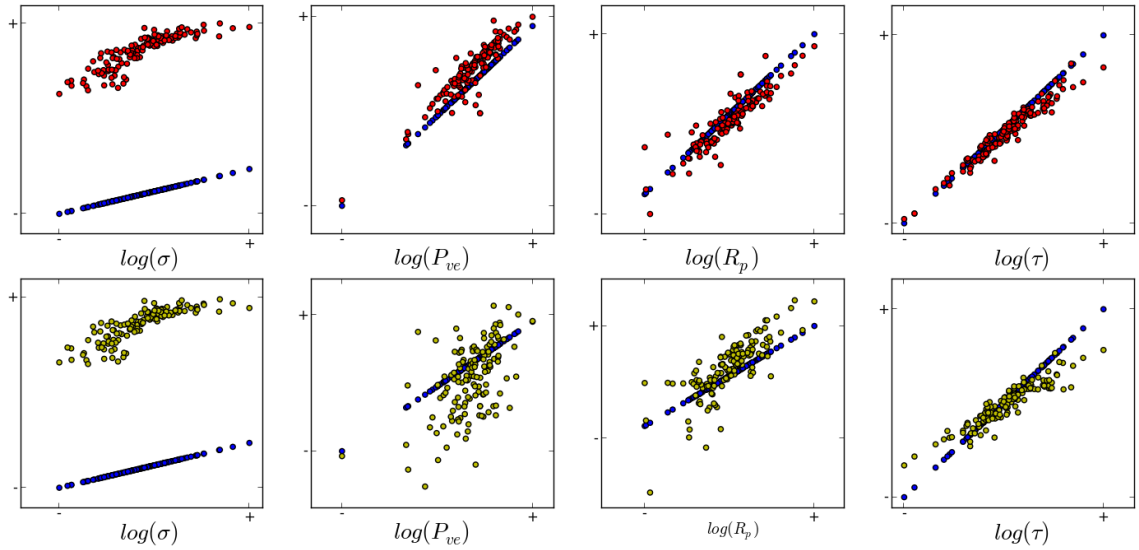

Figure 8.6: Log-value of the 3D estimated parameters as a function of the 0D estimated parameters in $\mathscr{H}^*$. **Top:** Parameters estimated in the personalisation **P1**, where the prior values for the haemodynamic parameters are their values in the estimation of 0D model parameters in $\mathscr{H}^*$. **Bottom:** Parameters estimated in the personalisation **P2**, where the prior values for the haemodynamic parameters are the one in Section **??** of **Chapter 7**.

case, most cases are fitted within 2.5ml for the stroke volume and 0.5 mmHg for the pressure measurements with few outliers. The most interesting result (which was expected), is that we observe a different spread of haemodynamic parameters in both cases: namely the estimated haemodynamic parameters in the 3D models are a lot more correlated to the 0D estimated parameters in **P1** than in **P2**, because the prior in **P1** for these parameters is their values in the parameter estimation with the 0D model.

This preliminary result shows that is possible to partially guide the personalisation of a database of cases with the 3D model from an estimation of the 0D model, instead of performing the IUP algorithm directly on the 3D model. This also exhibit a *multiscale personalisation* of the whole database, with personalised simulations in both models which have close haemodynamic parameters values.

Chapter 9

Conclusion and Perspectives

Contents

The main objective of this thesis was the consistent and efficient personalisation of a 3D electromechanical model, with the goal of using personalised parameters and simulations for the analysis of clinical databases. To that end, we first investigated a source of possible inconsistency in parameter estimation, which is the uncertainty in external (not personalised) parameters. Then, we tackled the computational burden associated with parameter estimation in 3D electromechanical models, through a 0D/3D multifidelity approach. We then built personalised 3D simulations for more than 140 cases, and explored possible uses of personalised parameters for longitudinal analysis of the cardiac function. Finally, we developed a method to tackle the problem of parameter observability in personalisation. Here we summarize the main achievements of this Ph.D. work and detail the perspectives which could be topic of future research.

9.1 Main Contributions

9.1.1 Uncertainty Quantification in Myocardial Fibre Directions and Personalisation

In **Chapter 4** and the corresponding study [Molléro 2015], we introduced an original method to quantify uncertainty in myocardial fibre orientation, by sampling a few representants of fibre variability in an atlas built from an small database of measured fibre sets. This was done by performing PCA in the atlas space, and selecting two representants in each of the 3 largest directions and the mean. We then propagated this uncertainty in a generic personalisation process, which resulted in different *personalised simulations* with different *personalised parameters values*.

This enabled a first assessment of the uncertainties which can arise in personalisation due to the uncertainty in the many parameters of a typical 3D cardiac model. In addition, the personalisation algorithm used in this study (the Unscented Transform) required a careful and manual initialisation, possibly different for each case and set of parameters. Overall, this study outlined the need for a more consistent personalisation framework (which incorporates uncertainty) as well as a more practical personalisation algorithm in order to scale to a large database of cases.

We believe that computing the modes of a PCA in an atlas of cases is a very practical way to define a data-driven *variability* of such high-dimensional vector sets, jointly with a *parametrisation* of this variability. We argue that such parametrisation is also interesting in the context of the *population-based prior probabilities* defined in **Chapter 6**, because the eigenvectors and eigenvalues of the PCA decomposition gives also a natural formulation of an Gaussian prior over this parametrisation. Finally we point out that this method could be applied to other types of high-dimensional vectors, in particular other local myocardial parameters in 3D models such as contractility or conductivity.

9.1.2 0D/3D multifidelity Coupling and Personalisation

In **Chapter 5** and the corresponding publication [Molléro 2017b], we proposed an innovative and possibly very flexible *0D/3D multifidelity approach*, in particular to tackle problems associated with the computational complexity of 3D simulations. This approach consists in three components:

- A *0D cardiac model*, which is a reduced version of our original 3D model. This model is very fast (up to 15 beats per seconds) and the equations, encoded in the CellML format, are made available from the Physiome Model Repository[1]. Efficient Python scripts to personalise this model (based on the CMA-ES genetic algorithm) will be released as well at the same location.

- A *multifidelity coupling* of the two models, which enables the fast approximation of outputs of the 3D model from 0D simulations. This coupling is based

[1] https://models.physiomeproject.org/e/470

on a parameter mapping which directly maps together parameters known to be the same in both models (such as the Windkessel model parameters), and performs en empirical quadratic mapping between parameters which have different values in both models. This enables the approximation of possibly many 3D simulations from 0D simulations and a few 3D simulations only. It is not theoretically limited to specific sets of parameters and outputs as long as the dynamics of both models are close enough for these parameters and outputs.

- **Multifidelity-CMA**, a *multifidelity personalisation algorithm* which performs successive 0D/3D couplings to approximate the objective function in many iterations of the CMA-ES genetic algorithm at once. This is done while controlling an accuracy criterion on the approximation given by the coupling, in order to determine at which iteration of CMA-ES a new coupling has to be computed to keep a good accuracy. With this algorithm, we were able to personalise 121 cases, in around 2.5 days and, more importantly, without specific manual supervision, fine-tuning of the algorithm or precomputation. We believe this be an achievement in the cardiac modeling community and was not possible with our previous approach based on the Unscented Transform. Theoretically, this algorithm is not limited to specific sets of parameters and outputs.

Beside the application to cardiac personalisation, we argue that **Multifidelity-CMA** is in itself an interesting contribution to the larger problem of *multi-objective optimisation*: indeed, the use of the **Multifidelity-CMA** with a simple quadratic approximation of the outputs (with the degree 2 hypersurface) instead of the 0D/3D coupling already leads to considerable speed-up of the optimisation and a lower computational burden. Furthermore, in the context of *multifidelity optimisation*, this algorithm could be used in other fields where models at multiple scales are available. Indeed, as long as a lower-fidelity model can help approximate the outputs of a higher-fidelity model with a direct mapping of at least some parameters, the coupling with *Multifidelity-CMA* leads to additional computational gains.

9.1.3 Personalised 3D Modeling of 137 *Complete Acquisitions*

With the **Multifidelity-CMA** method, we built *personalised 3D simulations* for 137 *complete acquisitions* in the MD-Paedigree project and demonstrated in two studies (**Chapter 6** and **7**) how they can be used for longitudinal analysis and modeling of the cardiac function:

- First in **Chapter 6** and the corresponding publication [Molléro 2017c], we built a data-driven model of cardiovascular parameter changes during digestion, from the parameters of personalised simulations at two instants (before and within 1h30 after ingestion of a high-fat high-calorie meal). From the personalised parameters, we derived a multilinear law which accurately predict changes in parameters leading to desired changes in the simulation, enabling

fast simulation of cardiovascular changes for new patients. Interestingly, this was possible despite non-uniqueness on the parameters which were not constrained with priors in this study.

- Second, in **Chapter 7** and the corresponding publication [Molléro 2017a], we tackled the problem of parameter non-observability in personalisation through the *Maximum A Posteriori* (MAP) estimation of personalised parameters for 84 different cases. We showed that the use of priors reduces considerably the variance in the population of estimated parameters (by removing the variability in non-observable directions), leading to well-conditioned parameter values whose variability in the population only reflects physiological properties of the cases. We then projected the personalised parameters onto the axis of a classifier which discriminates between a cohort of healthy and diseased cases. On this axis, we showed that the evolution of parameter values suggests an improvement of the cardiac function under therapy, since the parameters of the follow-up acquisition are closer to the *healthy side* of the classifier.

We believe that the two presented applications exhibit methodological aspects which are particularly important for the success of any study of the cardiac function with personalised simulations. First, in both cases, all the personalised simulations are built from the same set of measurements, from the same pipeline and with the same set of estimated parameters. In **Chapter 6**, this enabled the creation of a fast law of parameter changes which predict accurate changes in the simulation, which would have not necessary be possible (or with less accuracy) from personalised cases with different models and personalisation pipeline for each case.

Secondly we argue that in order to properly evaluate the cardiac function from personalised parameter values, it is very important to remove all sources of variability in the estimation which are not related to physiological properties of the cases. This was done through a MAP estimation in **Chapter 8**, which removed the variability due to the non-observability of some directions in the parameter space. In addition, we also believe that because the set of measurements can be limited and we thus cannot evaluate the true value of all parameters, it is important to evaluate personalised values *within a database* of personalised cases which includes reference cases where the cardiac function is known and also which are personalised *through the same process*.

9.1.4 Parameter Selection and Population-Based Priors

In **Chapter 8**, we developed a general approach to the problem of parameter observability in personalisation. We developed an algorithm called **Iteratively Updated Priors**, which performs successive personalisations of the database, in which the prior probability of the current personalisation is defined from the distribution of personalised parameters in the previous iteration. When the algorithm converges, it has the following properties:

- At convergence, personalised parameters lie on a linear subspace of reduced dimension. The algorithm realises a trade-off between the number of dimensions of the linear subspace and the mean error of fit of the measurements across the database, which depends on the weight of the priors (defined by γ in **Chapter 8**).

- When a high goodness of fit is imposed (small γ), the resulting subspace is a linear subspace of *minimal dimension* in which for each case of the database, there is a (possibly unique) parameter values for which the simulation fits the measurements.

- At convergence, all the cases are personalised through a MAP where the prior distribution is the distribution of the population parameters itself.

We applied to the database of 137 *complete acquisitions* for which the same 5 measurements are available. From 6 original parameters, we extracted a reduced parameter subspace of dimension 4 based on 5 parameters which makes sense from a physiological point of view and in which for each case, there is a *unique personalised value* for which the simulation fits exactly the measurements. Then we used the *population-based priors* derived from the population in this subspace to personalise 811 cases with various type of measurements. Because the parameters are estimated through a MAP where the prior comes from a larger population where all the measurements are available, we believe this ensure one of the highest form of consistency possible in our dataset.

We believe this approach can be particularly interesting for applications on larger and more heterogeneous databases: for example when the same measurements are not available in two databases, we think using the IUP algorithm on the concatenation of the two databases could lead parameters and parameter directions which are unobservable in a database to be constrained by a prior which is defined by their observed values in the other database. This theoretically enables the possibility of integrating any kind of measurement, experiment and acquisition into the same very large database, and let the algorithm jointly select relevant parameter directions, build *population-based priors* in every parameter direction and estimate a consistent population of *personalised simulations* from the data.

We also believe that by selecting of a reduced subspace of *minimal dimension for which there are parameters for each case*, the algorithm also selects a reduced subspace of *maximal dimension in which we can have a relevant statistical information from the available data*. To that extent, we think our algorithm represents a complete framework to extract the maximal statistical (and possibly physiological if parameters are well chosen) information possible from any dataset (heterogeneous or not) with a given cardiac model, while ensuring consistency of the personalisation for all cases (both in terms of goodness of fit and unicity of the parameters).

9.2 Perspectives

9.2.1 Multiscale Personalisation for the Analysis of Cardiac Pathologies

A direct extension of this work is the creation of personalised simulations with a larger number of estimated parameters, in order to reproduce a a wider variety of clinical measurements. A particularly interesting direction seems to be the personalisation of electromechanical and pressure parameters from *2D echocardiographic* measurements such as the systolic (ejection) and diastolic (filling) flows, velocities and strains of the myocardial tissue. Indeed, clinicians use these indices daily to diagnose a large variety of pathologies, so their value have a high clinical relevance. Integrating these measurements into the personalisation could drastically increase the predictive power of personalised cardiac models, possibly matching the clinicians ability to diagnose. Then with enough data we could possibly discover patterns in personalised parameters related to specific pathologies, which are not easily observable from the measurements only. This could be partially studied with the 0D model only but using the 3D model would be important to integrate specific patterns of myocardial strain in personalised simulations.

Similarly, another large (and already widely explored) area of interest for cardiac modeling and clinical applications is the personalisation of a closed-loop model of the cardiovascular circulation. Indeed, some pathologies are characterized by the dysfunction of the cardiac function at elevated heart rates and blood pressures only, during exercise for example. Modeling these effects would require to model the complete adaptation of the heart and cardiovascular system to higher cardiac outputs in order to understand the sources of dysfunction. A challenge for such studies is the simulation of many (possibly hundreds) of cardiac cycles, which could be hard with the 3D model. However we argue that a similar coupling than in **Chapter 5** could enable the speed up of the process through 0D simulations only. This could be done by finding a mapping between the outputs of 0D model and the 3D model for a specific state of the cardiac function (at rest for example) and recomputing the 0D / 3D coupling regularly every few cardiac cycles during transient effects to ensure the accuracy of the approximation (as in the **Multidelity-CMA** algorithm).

9.2.2 Prediction of Response to drugs

An application of the longitudinal modeling of short-term transient effects as described in **Chapter 6** is the prediction of a heart's response to drugs. Indeed, many drugs used in cardiology such as diuretics or beta-blockers are characterized by a rapid short-term evolution of the cardiac function, which can likely be described by rapid changes in electromechanical or cardiovascular parameters. Such changes could be quantified from the personalisation of many patients under therapy, in order to build a predictive model of the heart's response to these drugs. This could have direct applications in therapy planning, such as predicting patient-specific optimal doses to reach a specific state of the cardiac function.

9.2.3 Longitudinal Evolution of Diseases

Similarly to the longitudinal modeling of short-term effects, it should be possible, given enough data, to build models of the long-term evolution of the heart. Possible clinical application includes the prediction and cure of pathological remodeling (usually dilation) of the heart, due to hypertension for example. In some cases, we observe a *inverse remodeling* of the heart under therapy when a specific drug treatment brings the cardiovascular system in normal range of values for an extended period of time. Personalised simulations could then be used to predict the optimal treatment to stabilise the cardiovascular system and optimize the inverse remodeling process.

9.3 List of Publications

The presented work led to several published and submitted publications:

9.3.1 First Author

Journal Papers:

- [Molléro 2017b] Mollero, Roch. and Pennec, Xavier. and Delingette, Hervé. and Garny, Alan and Ayache, Nicholas. and Sermesant, Maxime. **Multifidelity-CMA: A Multifidelity Approach for Efficient Personalisation of 3D Cardiac Electromechanical Models**. *Biomechanics and Modeling in Mechanobiology*, Sep 2017.

- Mollero, Roch. and Pennec, Xavier. and Delingette, Hervé. and Ayache, Nicholas. and Sermesant, Maxime. **Population-Based Priors in Cardiac Model Personalisation for Consistent Parameter Estimation in Heterogeneous Databases**. *In preparation.*

Peer-reviewed conferences with proceedings:

- [Molléro 2015] Molléro, Roch and Neumann, Dominik and Rohé, Marc-Michel and Datar, Manasi and Lombaert, Herve and Ayache, Nicholas and Comaniciu, Dorin and Ecabert, Olivier and Chinali, Marcello and Rinelli, Gabriele and Pennec, Xavier and Sermesant, Maxime and Mansi, Tommaso. **Propagation of Myocardial Fibre Architecture Uncertainty on Electromechanical Model Parameter Estimation: A Case Study**. 8th International Conference on *Functional Imaging and Modeling of the Heart (FIMH)*, LNCS 9126, pages 448 - 456, Springer, 2015.

- [Mollero 2016] Mollero, Roch and Pennec, Xavier and Delingette, Hervé and Ayache, Nicholas and Sermesant, Maxime. **A Multiscale Cardiac Model for Fast Personalisation and Exploitation**. 19th International Conference on *Medical Image Computing and Computer Assisted Intervention (MICCAI)*, LNCS 9902, pages 174 - 182, Springer, 2016.

- [Molléro 2017c] Molléro, Roch and Hauser, Jakob and Pennec, Xavier and Datar, Manasi and Delingette, Hervé and Jones, Alexander A and Ayache, Nicholas and Heimann, Tobias and Sermesant, Maxime. **Longitudinal Parameter Estimation in 3D Electromechanical Models: Application to Cardiovascular Changes in Digestion**. 9th international conference on *Functional Imaging and Modeling of the Heart (FIMH)*, LNCS 10263, pages 432 - 440, Springer, 2017.

- [Molléro 2017a] Molléro, Roch and Neumann, Dominik and Rohé, Marc-Michel and Datar, Manasi and Lombaert, Herve and Ayache, Nicholas and Comaniciu, Dorin and Ecabert, Olivier and Chinali, Marcello and Rinelli, Gabriele and Pennec, Xavier and Sermesant, Maxime and Mansi, Tommaso. **Longitudinal Analysis using Personalised 3D Cardiac Models with Population-Based Priors: Application to Paediatric Cardiomyopathies**. 20th International Conference on *Medical Image Computing and Computer Assisted Intervention (MICCAI)*, LNCS 10434, pages 350 - 358, Springer, 2017.

9.3.2 Co-Author:

- [Rohé 2016] Rohé, Marc-Michel and Molléro, Roch and Sermesant, Maxime and Pennec, Xavier. **Highly Reduced Model of the Cardiac Function for Fast Simulation**. In *IEEE, IVMSP Workshop 2016, Image, Video, and Multidimensional Signal Processing Workshop (IVMSP)*, 12th IEEE, 2016.

- [Giffard-Roisin 2016] Roisin, Sophie and Fovargue, Lauren and Webb, Jessica and Molléro, Roch and Lee, Jack and Delingette, Hervé and Ayache, Nicholas and Razavi, Reza and Sermesant, Maxime. **Estimation of Purkinje Activation from ECG: an Intermittent Left Bundle Branch Block Study**. In 7th *International Statistical Atlases and Computational Modeling of the Heart (STACOM)* Workshop, held in Conjunction with MICCAI 2016, LNCS 10124, pages 135 - 142, Springer, 2016.

Chapter 10

Conclusion et Perspectives (French)

Contents

L'objectif principal de cette thèse était la personnalisation cohérente et efficace de modèles électromécaniques cardiaques, dans le but d'utiliser les paramètres et les simulations personnalisés pour l'analyse de cas cliniques. Nous avons d'abord démontré que l'incertitude sur les paramètres non personnalisés était potentiellement une source d'inconsistence et d'incertitude dans la personalisation. Nous avons ensuite abordé le problème du temps de calcul associé à l'estimation de paramètres dans les modèles 3D, à travers une approche multi-échelle 0D / 3D. Cela nous a permit de construire des simulations 3D personnalisées pour plus de 140 cas et d'explorer l'utilisation des paramètres personnalisés pour l'analyse longitudinale de la fonction cardiaque. Enfin, nous avons développé une méthode pour résoudre le problème de l'observabilité des paramètres dans la personnalisation. Nous résumons dans ce chapitre les principales contributions de ce doctorat et détaillons les possibles perspectives de recherche.

10.1 Contributions

10.1.1 Propagation de l'incertitude dans l'orientation des fibres myocardiques sur la personnalisation

Nous avons introduit dans le **Chapitre 4** (et l'étude correspondante [Molléro 2015]) une méthode originale pour quantifier l'incertitude dans l'orientation des fibres myocardiques, en échantillonnant quelques représentants de la variabilité dans un atlas construit à partir d'un base de données de fibres mesurées par DTI. Cela est fait via une PCA dans l'espace de l'atlas, qui permet de sélectionner deux représentants dans chacune des trois plus grandes directions plus la moyenne. Cette incertitude est ensuite propagée dans un processus de personnalisation classique, pour obtenir différentes *simulations personnalisées* avec des valeurs différentes de *paramètres personnalisés*.

Cela a permis une première évaluation des incertitudes possibles dans la personnalisation en raison de l'incertitude sur les nombreux paramètres d'un modèle cardiaque 3D. De plus, nous avons constaté que l'algorithme de personnalisation utilisé dans cette étude (Unscented Transform) nécessite une initialisation soigneuse, manuelle et possiblement différente pour chaque cas. Dans l'ensemble, cette étude a souligné la nécessité d'un cadre de personnalisation plus cohérent (qui incorpore l'incertitude) ainsi que d'un algorithme de personnalisation plus robuste et plus pratique pour personaliser des bases de données plus larges.

Enfin, nous pensons que le calcul des premiers modes d'une PCA dans un atlas est un moyen très pratique de définir une *variabilité empirique* sur de tels ensembles de vecteurs de haute dimension, conjointement avec une *paramétrisation* de cette variabilité. En particulier, une telle paramétrisation est potentiellement intéressante dans le contexte des *probabilités empiriques* définies dans le **Chapitre 6**, étant donné que les vecteurs et valeurs propres de la PCA donnent une formulation naturelle d'un a priori gaussien sur cette paramétrisation. Cette méthode peut potentiellement être appliquée à d' autres ensembles de paramètres en grande dimension, en particulier aux paramètres locaux du myocardes dans des modèles 3D tels que la contractilité ou la conductivité.

10.1.2 Couplage et personnalisation multi-échelle

Dans le **Chapitre 5** et la publication correspondante [Molléro 2017b], nous avons proposé une approche *0D / 3D multi-échelle* innovante et très flexible, en particulier pour résoudre les problèmes associé à la complexité de calcul des simulations 3D. Cette approche contient trois composants:

- Un *modèle cardiaque 0D*, qui est une version réduite de notre modèle 3D original. Ce modèle est très rapide (jusqu'à 15 battements par seconde) et les équations, encodées au format CellML, sont disponibles dans sur le site du Physiome Model Repository [1]. Des scripts Python pour personnaliser ce

[1] https://models.physiomeproject.org/e/470

modèle (basé sur l'algorithme génétique CMA-ES) seront également publiés au même endroit.

- Un *couplage multi-échelle* des deux modèles, qui permet une approximation rapide des sorties du modèle 3D à partir de simulations du modèle 0D. Ce couplage est basé sur un mapping des paramètres qui relie directement les paramètres communs aux deux modèles (tels que les paramètres du modèle haemodynamique de Windkessel) et effectue une régression polynomiale de degré 2 entre les paramètres comportant des différences dans les deux modèles. Cela permet d'obtenir une approximation de nombreuses simulations 3D à partir de simulations 0D (et de quelques simulations 3D). Ce couplage n'est pas limité théoriquement à des ensembles spécifiques de paramètres et de sorties.

- **Multifidelity-CMA**, un algorithme de *personnalisation multi-échelle* qui effectue des couplages 0D / 3D successifs pour approximer la fonction de coût dans des itérations successive de l'algorithme CMA-ES. Ceci est effectué en contrôlant simultanément un critère de précision sur l'approximation donnée par le couplage, afin de déterminer à quelle itération un nouveau couplage doit être calculé pour conserver une précision suffisante. Avec cet algorithme, nous avons pu personnaliser 121 cas en environ 2,5 jours avec le modèle 3D, sans supervision, intialisation ou précomputation manuelle de l'algorithme. Nous pensons que c'est un résultat majeur dans la communauté de la modélisation cardiaque, qui était en particulier impossible avec l'approche précédente basée sur l'algorithme "Unscented Transform". Finalement, cet algorithme n'est pas limité non plus à des ensembles spécifiques de paramètres et de sorties.

En plus de l'application à la personnalisation cardiaque, nous soutenons que **Multifidelity-CMA** est en soi une contribution intéressante au problème plus large de l'*optimisation multi-objectif*: en effet, l'utilisation de l'algorithme **Multifidelity-CMA** avec une simple approximation quadratique des sorties (au lieu du couplage des modèles 0D / 3D) conduit déjà à une accélération considérable de l'optimisation et à une charge de calcul plus faible. Ensuite, dans un contexte d'*optimisation multi-échelle*, cet algorithme pourrait être utile sur d'autres cas où des modèles à plusieurs échelles sont disponibles: en pratique, tant qu'un modèle de faible précision peut aider à approximer les sorties d'un modèle de plus grande précision et que les deux modèles partagent des paramètres communs, le couplage des deux modèles avec *Multifidelity-CMA* conduit a des gains en temps de calcul supplémentaires.

10.1.3 Création de simulations 3D personnalisée pour 137 cas

Avec la méthode **Multifidelity-CMA**, nous avons construit 137 *simulations 3D personnalisées* dans le cadre du projet MD-Paedigree, que nous avons exploitées dans deux études (**Chapitres 6** et **7**) sur l'analyse et la modélisation longitudinale de la fonction cardiaque:

- Dans le **Chapitre 6** et la publication correspondante [Molléro 2017c], nous avons construit un modèle empirique de l'évolution des paramètres cardiovasculaires durant la digestion, à partir de simulations personnalisées à deux instants (avant et dans 1h30 après l'ingestion d'un repas hypercalorique) pour 21 cas. A partir des paramètres personnalisés, nous avons dérivé une loi multilinéaire qui prédit avec précision les changements de paramètres conduisant aux changements souhaités dans la simulation, permettant une simulation rapide de nouveaux patients. Fait intéressant, cela a été possible malgré la non-unicité sur les paramètres qui n'étaient pas contraints avec des probabilités a priori dans cette étude.

- Deuxièmement, dans le **Chapitre 7** et la publication correspondante [Molléro 2017a], nous avons abordé le problème de la non-observabilité des paramètres dans la personnalisation, à travers l'estimation d'un *Maximum A Posteriori* (MAP) pour 84 cas différents. Nous avons montré que l'utilisation des probailités a priori réduit considérablement la variance de la population des paramètres estimés, en supprimant la variabilité dans les directions non observables. Cela conduit à des paramètres mieux conditionnés, dont la variabilité dans la population ne reflète que la variabilité des propriétés physiologiques des cas. Nous avons ensuite projeté les paramètres personnalisés sur l'axe d'un classifieur entre une cohorte de cas sains et de cas malades. Sur cet axe, l'évolution des valeurs des paramètres suggère une amélioration de la fonction cardiaque sous thérapie.

Nous pensons que ces deux études présentent des aspects méthodologiques particulièrement importants pour une bonne analyse de la fonction cardiaque avec des simulations personnalisées. Tout d'abord, dans les deux cas, toutes les simulations personnalisées sont construites à partir du même ensemble de mesures, à partir du même processus de traitement des données et avec le même ensemble de paramètres estimés. En particulier dans le **Chapitre 6**, cela a permis la création d'une loi d'évolution des paramètres précise, ce qui n'aurait pas été possible (ou avec moins de précision) si différents modèles ou algorithmes de personnalisation avaient été utilisés pour les différents cas.

Deuxièmement, nous soutenons que pour évaluer correctement la fonction cardiaque à partir de valeurs de paramètres personnalisés, il est très important d'éliminer toutes les sources de variabilité dans l'estimation qui ne sont pas liées aux propriétés physiologiques des cas. Cela a été fait dans le **Chapitre 8** via une estimation "MAP", qui a permis de supprimer la variabilité due à la non-observabilité de certaines directions de l'espace des paramètres. Nous pensons également que parce que nous ne pouvons pas généralement évaluer la vraie valeur de tous les paramètres (par exemple si les mesures disponibles sont limitées), il est important d'étudier les valeurs des paramètres personnalisées *en relation avec d'autres cas dans une base de données* dont la fonction cardiaque est si possible connue, et qui ont été personnalisés *avec le même processus*.

10.1.4 Sélection de paramètres et probabilités a priori empiriques

Dans le **Chapitre 8**, nous avons développé une approche générale pour répondre au problème de l'observabilité des paramètres. Celle-ci se base sur un algorithme appelé **Iteratively Updated Priors**, qui effectue des personnalisations successives de la base de données dans laquelle la probabilité a priori de la personnalisation courante est définie à partir de la distribution des paramètres personnalisés dans l'itération précédente. Lorsque l'algorithme converge, il a les propriétés suivantes:

- Les paramètres personnalisés se trouvent sur un sous-espace linéaire de dimension réduite. L'algorithme réalise un compromis entre le nombre de dimensions du sous-espace linéaire et l'erreur moyenne d'ajustement des mesures dans la base de données, qui dépend du poids de l'a priori (défini par γ in **Chapitre 8**).
- Quand une faible erreur d'ajustement est imposée (petit γ), le sous-espace résultant est un sous-espace linéaire de *dimension minimale* qui contient, pour chaque cas de la base de données, un vecteur de paramètres pour lequel la simulation correspond aux mesures.
- Tous les cas sont personnalisés à travers un MAP où la distribution a priori est la distribution des paramètres de population lui-même.

Nous avons appliqué cet algorithme à aux 137 cas pour lesquelles 5 mesures sont toutes disponibles. A partir de 6 paramètres originaux, nous avons extrait un sous-espace de paramètres de dimension 4 basé sur 5 paramètres qui a un sens d'un point de vue physiologique et qui contient pour chaque cas un unique vecteur de parametres. Nous avons ensuite utilisé les *probabilités empiriques* construites dans ce sous-espace pour personnaliser 811 cas avec différents types de mesures. Comme les paramètres sont estimés à travers un MAP où les probabilités a priori viennent d'une population plus large où toutes les mesures sont disponibles, nous pensons que cela assure une des meilleures cohérence possibles sur cet ensemble de données.

Nous pensons que cette approche peut être particulièrement intéressante pour des bases de données plus volumineuses et hétérogènes. En particulier lorsque les mêmes mesures ne sont pas disponibles dans deux bases de données, nous pensons que l'algorithme IUP appliqué aux deux bases de données en même temps peut permettre de contraindre des paramètres inobservables dans une base de données par leur valeurs observées dans l'autre base de données (via les probabilités a priori). Cela permettrait théoriquement d'intégrer n'importe quel type de mesure, d'expérience et d'acquisition dans la même (et très grande) base de données, et de sélectionner simultanément un sous-espace de paramètres pertinent, construire des *probabilités empiriques* dans chaque direction de ce sous-espace ainsi que les *simulations personnalisées*.

Enfin nous pensons qu'en sélectionnant un sous-espace réduit de *dimension minimale* dans lequel il y a un vecteur de paramètres pour chaque cas, l'algorithme sélectionne un sous-espace réduit de *dimension maximale dans laquelle on peut extraire*

une information statistique pertinente à partir données. Dans ce contexte, nous pensons que notre approche représente un cadre complet pour extraire l'information statistique (et possiblement physiologique) maximale de tout ensemble de données avec un modèle cardiaque donné, tout en créant des simulations personalisées cohérentes.

10.2 Perspectives

10.2.1 Personnalisation multi-échelle pour l'analyse des pathologies cardiaques

Une extension directe de ce travail de thèse est la création de simulations personnalisées avec un plus grand nombre de paramètres estimés, afin de reproduire une plus grande variété de mesures cliniques. Une direction particulièrement intéressante semble être la personnalisation à partir de mesures *échocardiographiques 2D*, telles que les flux systolique (éjection) et diastolique (remplissage), les vitesses et les déformations du tissu myocardique. En effet, les cliniciens utilisent quotidiennement ces indices pour diagnostiquer une grande variété de pathologies, ce qui signifie que leur valeur contient beaucoup d'information clinique. L'intégration de ces mesures dans la personnalisation pourrait considérablement augmenter le pouvoir prédictif des modèles cardiaques personnalisés, et rivaliser avec la capacité diagnostique des cliniciens. Ensuite, avec suffisamment de données, certaines pathologies pourraient être reliées a des valeurs spécifiques de paramètres personalisés, qui ne sont pas facilement observables à partir des mesures ou des images seulement. Cela pourrait être partiellement étudié avec le modèle 0D, mais l'utilisation du modèle 3D semble nécessaire pour intégrer des données comme la déformation myocardique.

Un autre domaine d'intérêt (et déjà largement exploré) avec des applications cliniques est la personnalisation d'un modèle de la circulation cardiovasculaire. En effet, certaines pathologies sont caractérisées par le dysfonctionnement de la fonction cardiaque à des rythmes cardiaques élevés uniquement, pendant un exercice par exemple. La modélisation de ces effets nécessiterait de modéliser l'adaptation complète du cœur et du système cardiovasculaire à des débits cardiaques plus élevés afin de comprendre les sources de dysfonctionnement. Un défi pour de telles études serait la simulation de plusieurs (peut-être centaines) de cycles cardiaques, ce qui pourrait être difficile avec le modèle 3D. Cependant, nous pensons qu'un couplage similaire à celui du **Chapitre 5** pourrait permettre l'accélération du processus, par exemple en trouvant d'abord un couplage entre les sorties du modèle 0D et le modèle 3D pour un état spécifique de la fonction cardiaque (au repos par exemple). Ensuite, le couplage 0D / 3D serait recalculé régulièrement après quelques cycles cardiaques pendant les effets transitoires pour assurer le précision de l'approximation.

10.2.2 Prédiction de la réponse aux médicaments

Une application de la modélisation longitudinale des effets transitoires à court terme décrits dans le **Chapitre 6** est la prédiction de la réponse du cœur aux médicaments. En effet, de nombreux médicaments utilisés en cardiologie tels que les diurétiques ou les bêta-bloquants se caractérisent par une évolution rapide à court terme de la fonction cardiaque, susceptible d'être décrite par des modifications rapides des paramètres électromécaniques ou cardiovasculaires. Ces changements pourraient être quantifiés à partir de la personnalisation de plusieurs patients sous traitement, afin de construire un modèle prédictif de la réponse du cœur à ces médicaments. Cela pourrait avoir des applications dans la planification de la thérapie, comme la prévision de doses optimales pour chaque patient pour atteindre un état spécifique de la fonction cardiaque.

10.2.3 Evolution longitudinale des maladies

De même que pour la modélisation longitudinale des effets à court terme, il devrait être possible, avec suffisamment de données, de construire des modèles de l'évolution à long terme du cœur. Une application clinique possible pourrait être la prédiction et le soin du *remodelage* de la géométrie cardiaque du cœur, dû à l'hypertension par exemple. Dans certains cas, un *remodelage inverse* du cœur sous traitement est observé, lorsque le traitement amène le système cardiovasculaire dans un état stable et normal pendant une période prolongée. Des simulations personnalisées pourraient alors être utilisées pour prédire le traitement optimal pour stabiliser le système cardiovasculaire et optimiser le processus de remodelage inverse.

10.3 Publications

Ce travail de thèse a conduit à plusieurs papiers soumis et publiés:

10.3.1 Premier Auteur:

Articles de revues:

- [Molléro 2017b] Molléro, Roch. and Pennec, Xavier. and Delingette, Hervé. and Garny, Alan and Ayache, Nicholas. and Sermesant, Maxime. **Multifidelity-CMA: A Multifidelity Approach for Efficient Personalisation of 3D Cardiac Electromechanical Models**. *Biomechanics and Modeling in Mechanobiology*, Sep 2017.

- Molléro, Roch. and Pennec, Xavier. and Delingette, Hervé. and Ayache, Nicholas. and Sermesant, Maxime. **Population-Based Priors in Cardiac Model Personalisation for Consistent Parameter Estimation in Heterogeneous Databases**. *In preparation.*

Papiers de conférence avec actes, évalués par les pairs:

- [Molléro 2015] Molléro, Roch and Neumann, Dominik and Rohé, Marc-Michel and Datar, Manasi and Lombaert, Herve and Ayache, Nicholas and Comaniciu, Dorin and Ecabert, Olivier and Chinali, Marcello and Rinelli, Gabriele and Pennec, Xavier and Sermesant, Maxime and Mansi, Tommaso. **Propagation of Myocardial Fibre Architecture Uncertainty on Electromechanical Model Parameter Estimation: A Case Study**. 8th International Conference on *Functional Imaging and Modeling of the Heart (FIMH)*, LNCS 9126, pages 448 - 456, Springer, 2015.

- [Mollero 2016] Molléro, Roch and Pennec, Xavier and Delingette, Hervé and Ayache, Nicholas and Sermesant, Maxime. **A Multiscale Cardiac Model for Fast Personalisation and Exploitation**. 19th International Conference on *Medical Image Computing and Computer Assisted Intervention (MICCAI)*, LNCS 9902, pages 174 - 182, Springer, 2016.

- [Molléro 2017c] Molléro, Roch and Hauser, Jakob and Pennec, Xavier and Datar, Manasi and Delingette, Hervé and Jones, Alexander A and Ayache, Nicholas and Heimann, Tobias and Sermesant, Maxime. **Longitudinal Parameter Estimation in 3D Electromechanical Models: Application to Cardiovascular Changes in Digestion**. 9th international conference on *Functional Imaging and Modeling of the Heart (FIMH)*, LNCS 10263, pages 432 - 440, Springer, 2017.

- [Molléro 2017a] Molléro, Roch and Neumann, Dominik and Rohé, Marc-Michel and Datar, Manasi and Lombaert, Herve and Ayache, Nicholas and Comaniciu, Dorin and Ecabert, Olivier and Chinali, Marcello and Rinelli, Gabriele and Pennec, Xavier and Sermesant, Maxime and Mansi, Tommaso. **Longitudinal Analysis using Personalised 3D Cardiac Models with Population-Based Priors: Application to Paediatric Cardiomyopathies**. 20th International Conference on *Medical Image Computing and Computer Assisted Intervention (MICCAI)*, LNCS 10434, pages 350 - 358, Springer, 2017.

10.3.2 Co-Auteur:

- [Rohé 2016] Rohé, Marc-Michel and Molléro, Roch and Sermesant, Maxime and Pennec, Xavier. **Highly Reduced Model of the Cardiac Function for Fast Simulation**. In *IEEE, IVMSP Workshop 2016, Image, Video, and Multidimensional Signal Processing Workshop (IVMSP)*, 12th IEEE, 2016.

- [Giffard-Roisin 2016] Roisin, Sophie and Fovargue, Lauren and Webb, Jessica and Molléro, Roch and Lee, Jack and Delingette, Hervé and Ayache, Nicholas and Razavi, Reza and Sermesant, Maxime. **Estimation of Purkinje Activation from ECG: an Intermittent Left Bundle Branch Block Study**. In 7th *International Statistical Atlases and Computational Modeling of the Heart (STACOM)* Workshop, held in Conjunction with MICCAI 2016, LNCS 10124, pages 135 - 142, Springer, 2016.

Bibliography

[Albert 1952] Roy E Albert*et al.* *The response of the peripheral venous pressure to exercise in congestive heart failure.* American heart journal, vol. 43, no. 3, pages 395–400, 1952. (Cited on pages 62 and 67.)

[Aliev 1996] Rubin R Aliev and Alexander V Panfilov. *A simple two-variable model of cardiac excitation.* Chaos, Solitons & Fractals, vol. 7, no. 3, pages 293–301, 1996. (Cited on page 17.)

[Arsigny 2009] Vincent Arsigny, Olivier Commowick, Nicholas Ayache and Xavier Pennec. *A Fast and Log-Euclidean Polyaffine Framework for Locally Linear Registration.* Journal of Mathematical Imaging and Vision, vol. 33, no. 2, pages 222–238, 2009. (Cited on page 31.)

[Arts 2005] Theo Arts, Tammo Delhaas, Peter Bovendeerd, Xander Verbeek and Frits W Prinzen. *Adaptation to mechanical load determines shape and properties of heart and circulation: the CircAdapt model.* American Journal of Physiology-Heart and Circulatory Physiology, vol. 288, no. 4, pages H1943–H1954, 2005. (Cited on page 17.)

[Baillargeon 2014] Brian Baillargeon, Nuno Rebelo, David D Fox, Robert L Taylor and Ellen Kuhl. *The living heart project: a robust and integrative simulator for human heart function.* European Journal of Mechanics-A/Solids, vol. 48, pages 38–47, 2014. (Cited on page 38.)

[Bestel 2001] Julie Bestel, Frédérique Clément and Michel Sorine. *A biomechanical model of muscle contraction.* In International Conference on Medical Image Computing and Computer-Assisted Intervention, pages 1159–1161. Springer, 2001. (Cited on page 17.)

[Boulakia 2011] Muriel Boulakia and Jean-Frédéric Gerbeau. *Parameter identification in cardiac electrophysiology using proper orthogonal decomposition method.* In International Conference on Functional Imaging and Modeling of the Heart, pages 315–322. Springer, 2011. (Cited on page 19.)

[Caruel 2014] Matthieu Caruel, Radomir Chabiniok, Philippe Moireau, Yves Lecarpentier and Dominique Chapelle. *Dimensional reductions of a cardiac model for effective validation and calibration.* Biomechanics and modeling in mechanobiology, vol. 13, no. 4, pages 897–914, 2014. (Cited on pages 24, 25, 39, 42 and 59.)

[Chabiniok 2012] Radomir Chabiniok, Philippe Moireau, P-F Lesault, Alain Rahmouni, J-F Deux and Dominique Chapelle. *Estimation of tissue contractility from cardiac cine-MRI using a biomechanical heart model.* Biomechanics and

modeling in mechanobiology, vol. 11, no. 5, pages 609–630, 2012. (Cited on pages 38 and 70.)

[Chabiniok 2016] Radomir Chabiniok, Vicky Y. Wang, Myrianthi Hadjicharalambous, Liya Asner, Jack Lee, Maxime Sermesant, Ellen Kuhl, Alistair A. Young, Philippe Moireau, Martyn P. Nash, Dominique Chapelle and David A. Nordsletten. *Multiphysics and multiscale modelling, data–model fusion and integration of organ physiology in the clinic: ventricular cardiac mechanics.* Interface Focus, vol. 6, no. 2, 2016. (Cited on pages 17, 39, 43, 62 and 84.)

[Chapelle 2012] D. Chapelle, P. Le Tallec, P. Moireau and M. Sorine. *Energy-preserving muscle tissue model: formulation and compatible discretizations.* International Journal for Multiscale Computational Engineering, 10(2), 2012. (Cited on pages 21, 24, 26, 30, 41 and 63.)

[Chen 2016] Zhong Chen, Rocio Cabrera-Lozoya, Jatin Relan, Manav Sohal, Anoop Shetty, Rashed Karim, Herve Delingette, Jaswinder Gill, Kawal Rhode, Nicholas Ayache, Peter Taggart, Christopher Aldo Rinaldi, Maxime Sermesant and Reza Razavi. *Biophysical modelling predicts ventricular tachycardia inducibility and circuit morphology: A combined clinical validation and computer modelling approach.* Journal of Cardiovascular Electrophysiology, vol. 27, no. 7, pages 851–860, 2016. (Cited on page 38.)

[Clayton 2008] RH Clayton and AV Panfilov. *A guide to modelling cardiac electrical activity in anatomically detailed ventricles.* Progress in biophysics and molecular biology, vol. 96, no. 1, pages 19–43, 2008. (Cited on page 17.)

[Clayton 2011] RH Clayton, Olivier Bernus, EM Cherry, Hans Dierckx, FH Fenton, L Mirabella, AV Panfilov, Frank B Sachse, G Seemann and H Zhang. *Models of cardiac tissue electrophysiology: progress, challenges and open questions.* Progress in biophysics and molecular biology, vol. 104, no. 1, pages 22–48, 2011. (Cited on pages 17 and 39.)

[Costa 2001] Kevin D Costa, Jeffrey W Holmes and Andrew D McCulloch. *Modelling cardiac mechanical properties in three dimensions.* Philosophical Transactions of the Royal Society of London A: Mathematical, Physical and Engineering Sciences, vol. 359, no. 1783, pages 1233–1250, 2001. (Cited on page 17.)

[Crozier 2015] William Andrew Crozier. *Personalised electromechanical modelling of cardiac resynchronisation therapy.* PhD thesis, King's College London, 2015. (Cited on page 70.)

[Cuellar 2003] Autumn A. Cuellar, Catherine M. Lloyd, Poul F. Nielsen, David P. Bullivant, David P. Nickerson and Peter J. Hunter. *An Overview of CellML*

1.1, a Biological Model Description Language. SIMULATION, vol. 79, no. 12, pages 740–747, 2003. (Cited on pages 41 and 42.)

[Delingette 2012] Herve Delingette, Florence Billet, Ken CL Wong, Maxime Sermesant, Kawal Rhode, Matthew Ginks, C Aldo Rinaldi, Reza Razavi and Nicholas Ayache. *Personalization of cardiac motion and contractility from images using variational data assimilation*. IEEE transactions on biomedical engineering, vol. 59, no. 1, pages 20–24, 2012. (Cited on page 18.)

[Duchateau 2016] Nicolas Duchateau, Mathieu De Craene, Pascal Allain, Eric Saloux and Maxime Sermesant. *Infarct localization from myocardial deformation: Prediction and uncertainty quantification by regression from a low-dimensional space*. Transactions on Medical Imaging, 2016. (Cited on page 38.)

[Esmaily Moghadam 2013] Mahdi Esmaily Moghadam, Irene E. Vignon-Clementel, Richard Figliola and Alison L. Marsden. *A Modular Numerical Method for Implicit 0D/3D Coupling in Cardiovascular Finite Element Simulations*. J. Comput. Phys., vol. 244, pages 63–79, July 2013. (Cited on page 17.)

[Feigin 2016] V Feigin*et al.* *Global, regional, and national life expectancy, all-cause mortality, and cause-specific mortality for 249 causes of death, 1980-2015: a systematic analysis for the Global Burden of Disease Study 2015*. The lancet, vol. 388, no. 10053, pages 1459–1544, 2016. (Cited on pages 1 and 7.)

[FitzHugh 1961] Richard FitzHugh. *Impulses and physiological states in theoretical models of nerve membrane*. Biophysical journal, vol. 1, no. 6, pages 445–466, 1961. (Cited on page 17.)

[Frangi 2002] Alejandro F Frangi, Daniel Rueckert, Julia A Schnabel and Wiro J Niessen. *Automatic construction of multiple-object three-dimensional statistical shape models: Application to cardiac modeling*. IEEE transactions on medical imaging, vol. 21, no. 9, pages 1151–1166, 2002. (Cited on page 17.)

[Garny 2015] Alan Garny and Peter J Hunter. *OpenCOR: a modular and interoperable approach to computational biology*. Frontiers in Physiology, vol. 6, no. 26, 2015. (Cited on page 42.)

[Geijtenbeek 2013] Thomas Geijtenbeek, Michiel van de Panne and A Frank van der Stappen. *Flexible muscle-based locomotion for bipedal creatures*. ACM Transactions on Graphics (TOG), vol. 32, no. 6, page 206, 2013. (Cited on page 43.)

[Giffard-Roisin 2016] Sophie Giffard-Roisin, Lauren Fovargue, Jessica Webb, Roch Molléro, Jack Lee, Hervé Delingette, Nicholas Ayache, Reza Razavi and Maxime Sermesant. *Estimation of Purkinje Activation from ECG: an Intermittent Left Bundle Branch Block Study*. In 7th International Statistical Atlases and Computational Modeling of the Heart (STACOM) Workshop,

Held in Conjunction with MICCAI 2016, Lecture Notes in Computer Science, Athens, Greece, October 2016. In press. (Cited on pages 114 and 122.)

[Gray 1995] Richard A Gray, José Jalife, Alexandre Panfilov, William T Baxter, Cándido Cabo, Jorge M Davidenko and Arkady M Pertsov. *Nonstationary vortexlike reentrant activity as a mechanism of polymorphic ventricular tachycardia in the isolated rabbit heart.* Circulation, vol. 91, no. 9, pages 2454–2469, 1995. (Cited on page 17.)

[Gray 1998] RA Gray and J Jalife. *Ventricular fibrillation and atrial fibrillation are two different beasts.* Chaos: An Interdisciplinary Journal of Nonlinear Science, vol. 8, no. 1, pages 65–78, 1998. (Cited on page 17.)

[Guccione 1991] Julius M Guccione, Andrew D McCulloch, LK Waldman*et al. Passive material properties of intact ventricular myocardium determined from a cylindrical model.* J Biomech Eng, vol. 113, no. 1, pages 42–55, 1991. (Cited on page 17.)

[Hansen 2006] Nikolaus Hansen. *The CMA evolution strategy: a comparing review.* In Towards a new evolutionary computation, pages 75–102. Springer Berlin Heidelberg, 2006. (Cited on pages 39 and 43.)

[Hauser 2016] Jakob A Hauser*et al. Comprehensive assessment of the global and regional vascular responses to food ingestion in humans using novel rapid MRI.* Am. J. Physiol. Regul. Integr. Comp. Physiol., vol. 310, no. 6, pages R541–R545, 2016. (Cited on pages 23, 62, 66 and 71.)

[Helm 2005] Patrick A. Helm, Hsiang-Jer Tseng, Laurent Younes, Elliot R. McVeigh and Raimond L. Winslow. *Ex Vivo 3D Diffusion Tensor Imaging and Quantification of Cardiac Laminar Structure.* Magnetic Resonance in Medicine, 2005. (Cited on page 31.)

[Hodgkin 1952] Alan L Hodgkin and Andrew F Huxley. *A quantitative description of membrane current and its application to conduction and excitation in nerve.* The Journal of physiology, vol. 117, no. 4, pages 500–544, 1952. (Cited on page 17.)

[Holzapfel 2001] Gerhard A Holzapfel and Thomas C Gasser. *A viscoelastic model for fiber-reinforced composites at finite strains: Continuum basis, computational aspects and applications.* Computer methods in applied mechanics and engineering, vol. 190, no. 34, pages 4379–4403, 2001. (Cited on page 17.)

[Hsu 2009] Daphne T. Hsu*et al. Heart Failure in Children.* Circ. Heart. Fail., vol. 2, no. 1, pages 63–70, 2009. (Cited on page 71.)

[Humphrey 1990] JD Humphrey, RK Strumpf and FCP Yin. *Determination of a constitutive relation for passive myocardium: I. A new functional form.*

Journal of biomechanical engineering, vol. 112, no. 3, pages 333–339, 1990. (Cited on page 17.)

[Huxley 1957] A Huxley. *Muscle structure and theories of contraction.* Progress in biophyics and biophysical chemistry, vol. 7, pages 255–318, 1957. (Cited on page 24.)

[Huyghe 1991] Jacques M Huyghe, Dick H van Campen, Theo Arts and Robert M Heethaar. *The constitutive behaviour of passive heart muscle tissue: a quasi-linear viscoelastic formulation.* Journal of biomechanics, vol. 24, no. 9, pages 841–849, 1991. (Cited on page 17.)

[Jolly 2011] Marie-Pierre Jolly, Christoph Guetter, Xiaoguang Lu, Hui Xue and Jens Guehring. *Automatic segmentation of the myocardium in cine MR images using deformable registration.* In International Workshop on Statistical Atlases and Computational Models of the Heart, pages 98–108. Springer, 2011. (Cited on pages 20 and 56.)

[Julier 1997] Simon J Julier and Jeffrey K Uhlmann. *A new extension of the Kalman filter to nonlinear systems.* In Int. symp. aerospace/defense sensing, simul. and controls, volume 3, pages 3–2. Orlando, FL, 1997. (Cited on page 30.)

[Kayvanpour 2015] Elham Kayvanpour, Tommaso Mansi, Farbod Sedaghat-Hamedani, Ali Amr, Dominik Neumann, Bogdan Georgescu, Philipp Seegerer, Ali Kamen, Jan Haas, Karen S Frese, Maria Irawati, Emil Wirsz, Vanessa King, Sebastian Buss, Derliz Mereles, Edgar Zitron, Andreas Keller, Hugo A Katus, Dorin Comaniciu and Benjamin Meder. *Towards Personalized Cardiology: Multi-Scale Modeling of the Failing Heart.* PLoS ONE, vol. 10, no. 7, 2015. (Cited on pages 38 and 42.)

[Kennedy 2000] Marc C Kennedy and Anthony O'Hagan. *Predicting the output from a complex computer code when fast approximations are available.* Biometrika, vol. 87, no. 1, pages 1–13, 2000. (Cited on pages 39 and 58.)

[Kerckhoffs 2003] RCP Kerckhoffs, PHM Bovendeerd, JCS Kotte, FW Prinzen, K Smits and T Arts. *Homogeneity of cardiac contraction despite physiological asynchrony of depolarization: a model study.* Annals of biomedical engineering, vol. 31, no. 5, pages 536–547, 2003. (Cited on page 17.)

[Kerckhoffs 2007] Roy C. P. Kerckhoffs, Maxwell L. Neal, Quan Gu, James B. Bassingthwaighte, Jeff H. Omens and Andrew D. McCulloch. *Coupling of a 3D Finite Element Model of Cardiac Ventricular Mechanics to Lumped Systems Models of the Systemic and Pulmonic Circulation.* Annals of Biomedical Engineering, vol. 35, no. 1, pages 1–18, Jan 2007. (Cited on page 17.)

[Khalil 2006] Ahmad S Khalil, Brett E Bouma and Mohammad R Kaazempur Mofrad. *A combined FEM/genetic algorithm for vascular soft tissue elas-*

ticity estimation. Cardiovascular Engineering, vol. 6, no. 3, pages 93–102, 2006. (Cited on page 19.)

[Konukoglu 2011] E. Konukoglu, J. Relan, U. Cilingir, B. Menze, P. Chinchapatnam, A. Jadidi, H. Cochet, M. Hocini, H. Delingette, P. Jaïs, M. Haïssaguerre, N. Ayache and M. Sermesant. *Efficient Probabilistic Model Personalization Integrating Uncertainty on Data and Parameters: Application to Eikonal-Diffusion Models in Cardiac Electrophysiology.* Progress in Biophysics and Molecular Biology, vol. 107, no. 1, pages 134–146, Oct 2011. (Cited on pages 19 and 28.)

[Laskey 1990] W. K. Laskey*et al. Estimation of total systemic arterial compliance in humans.* J Appl Physiol, vol. 69, no. 1, pages 112–119, 1990. (Cited on page 73.)

[Laughlin 1999] M Harold Laughlin. *Cardiovascular response to exercise.* American Journal Physiology, vol. 277, no. 6 Pt 2, pages S244–S259, 1999. (Cited on page 62.)

[Liu 2009] Huafeng Liu, Pengcheng Shi*et al. Maximum a posteriori strategy for the simultaneous motion and material property estimation of the heart.* IEEE Transactions on Biomedical Engineering, vol. 56, no. 2, pages 378–389, 2009. (Cited on page 18.)

[Lluch 2017] Eric Lluch, Rubén Doste, Sophie Giffard-Roisin, Alexandre This, Maxime Sermesant, Oscar Camara, Mathieu De Craene and Hernán G Morales. *Smoothed Particle Hydrodynamics for Electrophysiological Modeling: An Alternative to Finite Element Methods.* In International Conference on Functional Imaging and Modeling of the Heart, pages 333–343. Springer, 2017. (Cited on page 17.)

[Lombaert 2011] Herve Lombaert, Jean-Marc Peyrat, Pierre Croisille, Stanislas Rapacchi, Laurent Fanton, Patrick Clarysse, Hervé Delingette and Nicholas Ayache. *Statistical Analysis of the Human Cardiac Fiber Architecture from DT-MRI.* In Leon Axel and Dimitris Metaxas, editors, Proceedings of FIMH Conference 2011, volume 6666 of *LNCS*, pages 171–179. Springer, May 2011. Best Paper Award. (Cited on page 31.)

[Lopez-Perez 2015] Alejandro Lopez-Perez, Rafael Sebastian and Jose M Ferrero. *Three-dimensional cardiac computational modelling: methods, features and applications.* Biomedical engineering online, vol. 14, no. 1, page 35, 2015. (Cited on page 17.)

[Marchesseau 2010] Stéphanie Marchesseau, Tobias Heimann, Simon Chatelin, Rémy Willinger and Hervé Delingette. *Multiplicative jacobian energy decomposition method for fast porous visco-hyperelastic soft tissue model.* In International Conference on Medical Image Computing and Computer-Assisted

Intervention, pages 235–242. Springer, 2010. (Cited on pages 17, 21, 22, 26 and 41.)

[Marchesseau 2013a] S. Marchesseau, H. Delingette, M. Sermesant and N. Ayache. *Fast parameter calibration of a cardiac electromechanical model from medical images based on the unscented transform.* Biomechanics and modeling in mechanobiology, 12(4), 815-831, 2013. (Cited on pages 21, 22, 23, 24, 26, 28, 30, 41, 72 and 92.)

[Marchesseau 2013b] Stéphanie Marchesseau. *Simulation of patient-specific cardiac models for therapy planning.* Thesis, Ecole Nationale Supérieure des Mines de Paris, 2013. (Cited on pages 18 and 64.)

[Marchesseau 2013c] Stéphanie Marchesseau, Hervé Delingette, Maxime Sermesant, Rocío Cabrera Lozoya, Catalina Tobon-Gomez, Philippe Moireau, Rosa M. Figueras i Ventura, Karim Lekadir, Alfredo I. Hernández, Mireille Garreau, Erwan Donal, Christophe Leclercq, Simon G. Duckett, Kawal S. Rhode, C. Aldo Rinaldi, Alejandro F. Frangi, Reza Razavi, Dominique Chapelle and Nicholas Ayache. *Personalization of a cardiac electromechanical model using reduced order unscented Kalman filtering from regional volumes.* Medical Image Analysis, vol. 17, no. 7, pages 816–829, 2013. (Cited on pages 18, 38 and 42.)

[McLeod 2013] Kristin McLeod, Tommaso Mansi, Maxime Sermesant, Giacomo Pongiglione and Xavier Pennec. *Statistical shape analysis of surfaces in medical images applied to the Tetralogy of Fallot heart.* In Modeling in Computational Biology and Biomedicine, pages 165–191. Springer, 2013. (Cited on page 17.)

[Mihalef 2017] Viorel Mihalef, Lucian Itu, Tommaso Mansi and Puneet Sharma. *Lumped Parameter Whole Body Circulation Modelling.* In Patient-specific Hemodynamic Computations: Application to Personalized Diagnosis of Cardiovascular Pathologies, pages 111–152. Springer, 2017. (Cited on page 17.)

[Mitchell 2003] Colleen C Mitchell and David G Schaeffer. *A two-current model for the dynamics of cardiac membrane.* Bulletin of mathematical biology, vol. 65, no. 5, pages 767–793, 2003. (Cited on page 17.)

[Moireau 2008] Philippe Moireau. *Assimilation de données par filtrage pour les systèmes hyperboliques du second ordre-Applications à la mécanique cardiaque.* PhD thesis, Ecole Polytechnique X, 2008. (Cited on page 18.)

[Moireau 2011] Philippe Moireau and Dominique Chapelle. *Reduced-order Unscented Kalman Filtering with application to parameter identification in large-dimensional systems.* ESAIM: Control, Optimisation and Calculus of Variations, vol. 17, no. 2, pages 380–405, 2011. (Cited on page 18.)

[Molléro 2015] Roch Molléro, Dominik Neumann, Marc-Michel Rohé, Manasi Datar, Herve Lombaert, Nicholas Ayache, Dorin Comaniciu, Olivier Ecabert, Marcello Chinali, Gabriele Rinelli, Xavier Pennec, Maxime Sermesant and Tommaso Mansi. *Propagation of Myocardial Fibre Architecture Uncertainty on Electromechanical Model Parameter Estimation: A Case Study.* In Functional Imaging and Modeling of the Heart, LNCS., 8th International Conference, FIMH 2015, Maastricht, The Netherlands, June 25-27, 2015. Proceedings, pages 448–456, Maastricht, Netherlands, June 2015. (Cited on pages 3, 9, 28, 38, 63, 108, 113, 116 and 122.)

[Mollero 2016] Roch Mollero, Xavier Pennec, Hervé Delingette, Nicholas Ayache and Maxime Sermesant. *A Multiscale Cardiac Model for Fast Personalisation and Exploitation.* In International Conference on Medical Image Computing and Computer-Assisted Intervention, pages 174–182. Springer, 2016. (Cited on pages 38, 39, 41, 52, 65, 73, 113 and 122.)

[Molléro 2017a] Roch Molléro, Hervé Delingette, Manasi Datar, Tobias Heimann, Jakob Hauser, Dilveer Panesar, Alexander Jones, Andrew Taylor, Kelm Marcus, Titus Kuehne, Marcello Chinali, Gabriele Rinelli, Nicholas Ayache, Xavier Pennec and Maxime Sermesant. *Longitudinal Analysis using Personalised 3D Cardiac Models with Population-Based Priors: Application to Paediatric Cardiomyopathies.* In Medical Image Computing and Computer Assisted Intervention (MICCAI), MICCAI 2017, Lecture Notes in Computer Science, Québec City, Canada, September 2017. (Cited on pages 4, 10, 69, 110, 114, 118 and 122.)

[Molléro 2017b] Roch Molléro, Xavier Pennec, Hervé Delingette, Alan Garny, Nicholas Ayache and Maxime Sermesant. *Multifidelity-CMA: a multifidelity approach for efficient personalisation of 3D cardiac electromechanical models.* Biomechanics and Modeling in Mechanobiology, Sep 2017. (Cited on pages 3, 9, 38, 108, 113, 116 and 121.)

[Molléro 2017c] Roch A Molléro, Jakob Hauser, Xavier Pennec, Manasi Datar, Hervé Delingette, Alexander A Jones, Nicholas Ayache, Tobias Heimann and Maxime Sermesant. *Longitudinal Parameter Estimation in 3D Electromechanical Models: Application to Cardiovascular Changes in Digestion.* In FIMH 2017 - 9th international conference on Functional Imaging and Modeling of the Heart, Toronto, Canada, June 2017. Springer. (Cited on pages 4, 10, 61, 79, 109, 114, 118 and 122.)

[Nash 2000] Martyn P Nash and Peter J Hunter. *Computational mechanics of the heart.* Journal of elasticity and the physical science of solids, vol. 61, no. 1-3, pages 113–141, 2000. (Cited on page 17.)

[Nash 2004] Martyn P Nash and Alexander V Panfilov. *Electromechanical model of excitable tissue to study reentrant cardiac arrhythmias.* Progress in biophysics and molecular biology, vol. 85, no. 2, pages 501–522, 2004. (Cited on page 17.)

[Neumann 2014a] Dominik Neumann, Tommaso Mansi, Bogdan Georgescu, Ali Kamen, Elham Kayvanpour, Ali Amr, Farbod Sedaghat-Hamedani, Jan Haas, Hugo Katus, Benjamin Meder*et al. Robust Image-Based Estimation of Cardiac Tissue Parameters and Their Uncertainty from Noisy Data.* In Medical Image Computing and Computer-Assisted Intervention–MICCAI 2014, pages 9–16. Springer, 2014. (Cited on pages 19 and 28.)

[Neumann 2014b] Dominik Neumann, Tommaso Mansi, Sasa Grbic, Ingmar Voigt, Bogdan Georgescu, Elham Kayvanpour, Ali Amr, Farbod Sedaghat-Hamedani, Jan Haas, Hugo Katus*et al. Automatic image-to-model framework for patient-specific electromechanical modeling of the heart.* In Biomedical Imaging (ISBI), 2014 IEEE 11th International Symposium on, pages 935–938. IEEE, 2014. (Cited on pages 21 and 29.)

[Neumann 2016] Dominik Neumann, Tommaso Mansi, Lucian Mihai Itu, Bogdan Georgescu, Elham Kayvanpour, Farbod Sedaghat-Hamedani, Ali Amr, Jan Haas, Hugo A. Katus, Benjamin Meder, Stefan Steidl, Joachim Hornegger and Dorin Comaniciu. *A Self-Taught Artificial Agent for Multi-Physics Computational Model Personalization.* CoRR, vol. abs/1605.00303, 2016. (Cited on pages 19 and 55.)

[Nickerson 2005] David Nickerson, Nicolas Smith and Peter Hunter. *New developments in a strongly coupled cardiac electromechanical model.* EP Europace, vol. 7, no. s2, pages S118–S127, 2005. (Cited on page 17.)

[Nordsletten 2011] D Nordsletten, M McCormick, PJ Kilner, Peter Hunter, D Kay and NP Smith. *Fluid–solid coupling for the investigation of diastolic and systolic human left ventricular function.* International Journal for Numerical Methods in Biomedical Engineering, vol. 27, no. 7, pages 1017–1039, 2011. (Cited on page 17.)

[Oertel 2011] Herbert Oertel and Sebastian Krittian. Modelling the human cardiac fluid mechanics. KIT Scientific Publishing, 2011. (Cited on page 17.)

[Otsuki 2006] T Otsuki*et al. Contribution of systemic arterial compliance and systemic vascular resistance to effective arterial elastance changes during exercise in humans.* Acta physiologica, vol. 188, no. 1, pages 15–20, 2006. (Cited on pages 62 and 67.)

[Panfilov 1998] Alexandre V Panfilov. *Spiral breakup as a model of ventricular fibrillation.* Chaos: An Interdisciplinary Journal of Nonlinear Science, vol. 8, no. 1, pages 57–64, 1998. (Cited on page 17.)

[Pant 2016] Sanjay Pant, Chiara Corsini, Catriona Baker, Tain-Yen Hsia, Giancarlo Pennati and Irene E. Vignon-Clementel. *Data assimilation and modelling of patient-specific single-ventricle physiology with and without valve regurgitation.* Journal of Biomechanics, vol. 49, no. 11, pages 2162 – 2173, 2016.

Selected Articles from the International Conference on CFD in Medicine and Biology (Albufeira, Portugal â August 30th - September 4th, 2015). (Cited on page 17.)

[Pant 2017] Sanjay Pant, Chiara Corsini, Catriona Baker, Tain-Yen Hsia, Giancarlo Pennati and Irene Vignon-Clementel. *Inverse problems in reduced order models of cardiovascular haemodynamics: aspects of data-assimilation and heart-rate variability.* Journal of the Royal Society Interface, 2017. (Cited on page 18.)

[Panthee 2016] Nirmal Panthee, Jun-ichi Okada, Takumi Washio, Youhei Mochizuki, Ryohei Suzuki, Hidekazu Koyama, Minoru Ono, Toshiaki Hisada and Seiryo Sugiura. *Tailor-made heart simulation predicts the effect of cardiac resynchronization therapy in a canine model of heart failure.* Medical image analysis, vol. 31, pages 46–62, 2016. (Cited on page 39.)

[Peherstorfer 2016] Benjamin Peherstorfer, Karen Willcox and Max Gunzburger. *Survey of multifidelity methods in uncertainty propagation, inference, and optimization.* 2016. (Cited on pages 39, 58, 65 and 73.)

[Peng 2016] Peng Peng, Karim Lekadir, Ali Gooya, Ling Shao, Steffen E Petersen and Alejandro F Frangi. *A review of heart chamber segmentation for structural and functional analysis using cardiac magnetic resonance imaging.* Magnetic Resonance Materials in Physics, Biology and Medicine, vol. 29, no. 2, pages 155–195, 2016. (Cited on page 18.)

[Pernod 2011] E. Pernod*et al.* *A multi-front eikonal model of cardiac electrophysiology for interactive simulation of radio-frequency ablation.* Computers & Graphics, vol. 35, no. 2, pages 431–440, 2011. (Cited on pages 21 and 63.)

[Petitjean 2011] Caroline Petitjean and Jean-Nicolas Dacher. *A review of segmentation methods in short axis cardiac MR images.* Medical image analysis, vol. 15, no. 2, pages 169–184, 2011. (Cited on page 18.)

[Peyrat 2007] Jean-Marc Peyrat, Maxime Sermesant, Xavier Pennec, Hervé Delingette, Chenyang Xu, Eliot R. McVeigh and Nicholas Ayache. *A Computational Framework for the Statistical Analysis of Cardiac Diffusion Tensors: Application to a Small Database of Canine Hearts.* IEEE Transactions on Medical Imaging, vol. 26, no. 11, pages 1500–1514, November 2007. (Cited on page 31.)

[Powell 2009] Michael JD Powell. *The BOBYQA algorithm for bound constrained optimization without derivatives.* Cambridge NA Report NA2009/06, University of Cambridge, Cambridge, 2009. (Cited on page 41.)

[Relan 2010] Jatin Relan, Mihaela Pop, Hervé Delingette, Graham Wright, Nicholas Ayache and Maxime Sermesant. *Estimation of Reaction, Diffusion and Restitution Parameters for a 3D Myocardial Model Using Optical Mapping and*

MRI. In Oscar Camara, Mihaela Pop, Kawal Rhode, Maxime Sermesant, Nic Smith and Alistair Young, editors, MICCAI Workshop on Statistical Atlases and Computational Models of the Heart: Mapping Structure and Function (STACOM) and a Cardiac Electrophysiological Simulation Challenge (CESC'10), volume 6364 of *Lecture Notes in Computer Science*, pages 270–280, Beijing, China, 2010. Springer. (Cited on page 17.)

[Rohé 2016] Marc-Michel Rohé, Roch Molléro, Maxime Sermesant and Xavier Pennec. *Highly Reduced Model of the Cardiac Function for Fast Simulation*. In IEEE - IVMSP Workshop 2016, Image, Video, and Multidimensional Signal Processing Workshop (IVMSP), 2016 IEEE 12th, page 5, Bordeaux, France, July 2016. IEEE. (Cited on pages 92, 114 and 122.)

[Schaerer 2006] Joël Schaerer, Zhen Qian, Patrick Clarysse, Dimitris Metaxas, Leon Axel and Isabelle E Magnin. *Fast and automated creation of patient-specific 3D heart model from Tagged MRI*. In Proceedings of the MICCAI 2006 SA2PM Workshop, 2006. (Cited on page 38.)

[Schmid 2008] Holger Schmid, P OâCallaghan, MP Nash, W Lin, IJ LeGrice, BH Smaill, AA Young and PJ Hunter. *Myocardial material parameter estimation*. Biomechanics and modeling in mechanobiology, vol. 7, no. 3, pages 161–173, 2008. (Cited on page 19.)

[Seegerer 2015] Philipp Seegerer, Tommaso Mansi, Marie-Pierre Jolly, Dominik Neumann, Bogdan Georgescu, Ali Kamen, Elham Kayvanpour, Ali Amr, Farbod Sedaghat-Hamedani, Jan Haas*et al. Estimation of Regional Electrical Properties of the Heart from 12-Lead ECG and Images*. volume 8896 of *LNCS*, 2015. (Cited on pages 19, 21, 29 and 55.)

[Sermesant 2006] Maxime Sermesant, Hervé Delingette and Nicholas Ayache. *An electromechanical model of the heart for image analysis and simulation*. IEEE transactions on medical imaging, vol. 25, no. 5, pages 612–625, 2006. (Cited on page 17.)

[Sermesant 2007] M. Sermesant*et al. An anisotropic multi-front fast marching method for real-time simulation of cardiac electrophysiology*. In FIMH 2007, pages 160–169. Springer, 2007. (Cited on pages 17, 21 and 63.)

[Sermesant 2012] Maxime Sermesant, Radomir Chabiniok, Phani Chinchapatnam, Tommaso Mansi, Florence Billet, Philippe Moireau, Jean-Marc Peyrat, Ken C.L. Wong, Jatin Relan, Kawal S. Rhode, Matt Ginks, Pier Lambiase, Hervé Delingette, Michel Sorine, C. Aldo Rinaldi, Dominique Chapelle, Reza Razavi and Nicholas Ayache. *Patient-Specific Electromechanical Models of the Heart for Prediction of the Acute Effects of Pacing in CRT: a First Validation*. Medical Image Analysis, vol. 16, no. 1, pages 201–215, January 2012. (Cited on pages 38 and 42.)

[Smith 2011] Nic Smith, Adelaide de Vecchi, Matthew McCormick, David Nordsletten, Oscar Camara, Alejandro F. Frangi, Hervé Delingette, Maxime Sermesant, Jatin Relan, Nicholas Ayache, Martin W. Krueger, Walther H. W. Schulze, Rod Hose, Israel Valverde, Philipp Beerbaum, Cristina Staicu, Maria Siebes, Jos Spaan, Peter Hunter, Juergen Weese, Helko Lehmann, Dominique Chapelle and Reza Rezavi. *euHeart: personalized and integrated cardiac care using patient-specific cardiovascular modelling.* Interface Focus, vol. 1, no. 3, pages 349–364, 2011. (Cited on page 38.)

[Streeter 1979] Daniel D Streeter. *Gross morphology and fiber geometry of the heart.* Handbook of physiology, pages 61–112, 1979. (Cited on pages 21 and 41.)

[Suinesiaputra 2014] Avan Suinesiaputra, Brett R Cowan, Ahmed O Al-Agamy, Mustafa A Elattar, Nicholas Ayache, Ahmed S Fahmy, Ayman M Khalifa, Pau Medrano-Gracia, Marie-Pierre Jolly, Alan H Kadish*et al. A collaborative resource to build consensus for automated left ventricular segmentation of cardiac MR images.* Medical image analysis, vol. 18, no. 1, pages 50–62, 2014. (Cited on page 18.)

[Sundar 2009] Hari Sundar, Christos Davatzikos and George Biros. *Biomechanically-constrained 4D estimation of myocardial motion.* In International Conference on Medical Image Computing and Computer-Assisted Intervention, pages 257–265. Springer, 2009. (Cited on page 18.)

[Ten Tusscher 2004] KHWJ Ten Tusscher, D Noble, PJ Noble and Alexander V Panfilov. *A model for human ventricular tissue.* American Journal of Physiology-Heart and Circulatory Physiology, vol. 286, no. 4, pages H1573–H1589, 2004. (Cited on page 17.)

[Thomas 1992] James D Thomas and Arthur E Weyman. *Numerical modeling of ventricular filling.* Annals of biomedical engineering, vol. 20, no. 1, pages 19–39, 1992. (Cited on page 17.)

[Trayanova 2011] Natalia A Trayanova. *Whole-heart modeling.* Circulation research, vol. 108, no. 1, pages 113–128, 2011. (Cited on page 17.)

[Vercauteren 2009] Tom Vercauteren, Xavier Pennec, Aymeric Perchant and Nicholas Ayache. *Diffeomorphic Demons: Efficient Non-parametric Image Registration.* NeuroImage, vol. 45, no. 1, Supp.1, pages S61–S72, March 2009. (Cited on page 31.)

[Vignon-Clementel 2006] Irene E Vignon-Clementel, C Alberto Figueroa, Kenneth E Jansen and Charles A Taylor. *Outflow boundary conditions for three-dimensional finite element modeling of blood flow and pressure in arteries.* Computer methods in applied mechanics and engineering, vol. 195, no. 29, pages 3776–3796, 2006. (Cited on page 17.)

[Wang 2009] Vicky Y Wang, HI Lam, Daniel B Ennis, Brett R Cowan, Alistair A Young and Martyn P Nash. *Modelling passive diastolic mechanics with quantitative MRI of cardiac structure and function.* Medical image analysis, vol. 13, no. 5, pages 773–784, 2009. (Cited on page 19.)

[Wang 2012] Vicky Y Wang, Corné Hoogendoorn, Alejandro F Frangi, Brett R Cowan, Peter J Hunter, Alistair A Young and Martyn P Nash. *Automated personalised human left ventricular FE models to investigate heart failure mechanics.* In International Workshop on Statistical Atlases and Computational Models of the Heart, pages 307–316. Springer, 2012. (Cited on page 38.)

[Wang 2013a] Y Wang, B Georgescu, T Chen, W Wu, P Wang, X Lu, R Ionasec, Y Zheng and D Comaniciu. *Learning-Based Detection and Tracking in Medical Imaging: A Probabilistic Approach.* In LNCVB, volume 7, pages 209–235. 2013. (Cited on pages 20 and 29.)

[Wang 2013b] Yang Wang, Bogdan Georgescu, Terrence Chen, Wen Wu, Peng Wang, Xiaoguang Lu, Razvan Ionasec, Yefeng Zheng and Dorin Comaniciu. *Learning-based detection and tracking in medical imaging: a probabilistic approach.* In Deformation Models, pages 209–235. Springer, 2013. (Cited on pages 56 and 72.)

[Westerhof 1969] Nicolaas Westerhof, Frederik Bosman, Cornelis J De Vries and Abraham Noordergraaf. *Analog studies of the human systemic arterial tree.* Journal of biomechanics, vol. 2, no. 2, 1969. (Cited on pages 17 and 26.)

[Westerhof 2009] Nico Westerhof*et al.* *The arterial windkessel.* Med Biol Eng Comput, vol. 47, no. 2, pages 131–141, 2009. (Cited on pages 22, 64 and 72.)

[Xi 2011] Jiahe Xi, Pablo Lamata, Jack Lee, Philippe Moireau, Dominique Chapelle and Nic Smith. *Myocardial transversely isotropic material parameter estimation from in-silico measurements based on a reduced-order unscented Kalman filter.* Journal of the mechanical behavior of biomedical materials, vol. 4, no. 7, pages 1090–1102, 2011. (Cited on pages 18 and 38.)

[Yang 1991] Ming Yang and Larry A Taber. *The possible role of poroelasticity in the apparent viscoelastic behavior of passive cardiac muscle.* Journal of biomechanics, vol. 24, no. 7, pages 587–597, 1991. (Cited on page 17.)

[Yang 2017] Huanhuan Yang and Alessandro Veneziani. *Efficient estimation of cardiac conductivities via POD-DEIM model order reduction.* Applied Numerical Mathematics, vol. 115, pages 180–199, 2017. (Cited on page 19.)

[Yu 2011] Tommy Yu, Catherine M. Lloyd, David P. Nickerson, Michael T. Cooling, Andrew K. Miller, Alan Garny, Jonna R. Terkildsen, James Lawson, Randall D. Britten, Peter J. Hunter and Poul M. F. Nielsen. *The Physiome Model Repository 2.* Bioinformatics, vol. 27, no. 5, page 743, 2011. (Cited on page 41.)

[Zettinig 2014] Oliver Zettinig, Tommaso Mansi, Dominik Neumann, Bogdan Georgescu, Saikiran Rapaka, Philipp Seegerer, Elham Kayvanpour, Farbod Sedaghat-Hamedani, Ali Amr, Jan Haas, Henning Steen, Hugo Katus, Benjamin Meder, Nassir Navab, Ali Kamen and Dorin Comaniciu. *Data-driven estimation of cardiac electrical diffusivity from 12-lead ECG signals.* Medical Image Analysis, vol. 18, no. 8, pages 1361 – 1376, 2014. (Cited on pages 19, 21, 28, 29 and 34.)

Robust Personalisation of 3D Electromechanical Cardiac Models. Application to Heterogeneous and Longitudinal Clinical Databases

Abstract: Personalised cardiac modeling consists in creating virtual 3D simulations of real clinical cases with an electromechanical cardiac model through the estimation of biophysical parameter values for which the simulation match the clinical data. The goal of this modeling is to help clinicians in patient care by predicting the behaviour of the heart, but also improve the understanding of some pathologies from the estimated values of these biophysical parameters, which are hard to quantify from the imaging only.

We introduce this thesis by quantifying and propagating uncertainty in myocardial fibres orientation from a fibre atlas into a generic personalisation process. We show that the resulting uncertainty in the estimated parameters is extremely large compared to the physical variability of these parameters. This underlines the need for a more robust personalisation process which includes the uncertainty in parameter values, as an a priori for a possible clinical analysis.

In order to build a practical approach to parameter estimation, we first tackle the computational complexity of 3D models. To that end we introduce an original multiscale 0D/3D approach for cardiac models. We first build a multiscale coupling to approximate outputs of a 3D model with a reduced "0D" version of the same model. Then we derive from this coupling an efficient multifidelity optimisation algorithm for the 3D model.

In a second step, this algorithm is used to build more than 140 personalised 3D simulations, in the context of two studies involving the longitudinal analysis of the cardiac function. On one hand the analysis of long-term cardiomyopathy evolution under therapy, on the other hand the modeling of short-term cardiovascular changes during digestion. Through these studies we outline possible use cases of personalised parameter values in clinical practice.

Finally, after demonstrating the need to constrain and possibly select parameters to get consistent values for clinical applications, we present an algorithm to automatically detect and select observable directions in the parameter space from a set of measurements. This same algorithm estimates consistent population-based priors probabilities in these directions, which can be used to constrain the parameter estimation for cases where measurements are missing. This finally enables to perform consistent parameter estimations in a large clinical database of 811 cases with the 0D model.

Keywords: Cardiac Modeling, Parameter Estimation, Multifidelity methods, Prior probabilities.

Personalisation Robuste de Modèles 3D Electromécaniques du Coeur: application à des bases de données cliniques hétérogènes et longitudinales.

Résumé: La modélisation cardiaque personnalisée consiste à créer des simulations de cas cliniques réels avec un modèle cardiaque électromécanique en estimant des valeurs de paramètres pour lesquelles la simulation correspond aux données cliniques. L'objectif de ces simulations est d'assister le clinicien dans le traitement des patients et possiblement de mieux comprendre l'évolution de certaine maladies. Un important aspect pour permettre de telles applications cliniques est l'estimation des valeurs pertinentes et cohérentes des paramètres de simulation.

D'abord nous quantifions et propageons l'incertitude sur l'orientation des fibres myocardiques, calculée à partir d'un atlas, dans un processus de personnalisation générique. Nous montrons que l'incertitude qui en résulte dans les paramètres estimés est extrêmement importante par rapport à la variabilité physique de ces paramètres. Cela montre la nécessité d'un processus de personnalisation plus robuste qui prend en compte l'incertitude sur les valeurs des paramètres.

Afin de concevoir une approche pratique de l'estimation des paramètres nous présentons ensuite une approche multi-échelle 0D / 3D originale pour les modèles cardiaques. Nous construisons un couplage multiscalaire pour approximer les sorties d'un modèle 3D à partir d'une version "0D" réduite du même modèle. Ensuite, nous dérivons de ce couplage un algorithme efficace de personalisation pour le modèle 3D.

Dans un deuxième temps, nous utilisons cet algorithme pour construire plus de 140 simulations 3D personnalisées, dans le cadre de deux études impliquant l'analyse longitudinale de la fonction cardiaque. D'une part, l'analyse de l'évolution de la cardiomyopathie à long terme sous thérapie, d'autre part, la modélisation des changements cardiovasculaires à court terme pendant la digestion. Grâce à ces études, nous décrivons des cas d'utilisation possibles de valeurs de paramètres personnalisés dans la pratique clinique.

Enfin nous présentons un algorithme pour détecter et sélectionner automatiquement les directions observables dans l'espace des paramètres à partir d'un ensemble de mesures. Ce même algorithme estime des probabilités *a priori* basées sur la population dans ces directions, qui peuvent ensuite être utilisées pour contraindre l'estimation de paramètres pour les cas où des mesures sont manquantes. Cela nous permet d'effectuer des estimations de paramètres cohérentes dans une grandes bases de données cliniques de 811 cas avec le modèle 0D.

Mots-clés: Modélisation cardiaque, Estimation de paramètres, Méthodes multi-échelles, Probabilités à priori.